

EDITORIAL BOARD

Editor-in-Chief B.E. Paton

Scientists of PWI, Kiev

S.I. Kuchuk-Yatsenko (*vice-chief ed.*),

V.N. Lipodaev (*vice-chief ed.*),

Yu.S. Borisov, G.M. Grigorenko,

A.T. Zelnichenko, V.V. Knysh,

I.V. Krivtsun, Yu.N. Lankin,

L.M. Lobanov, V.D. Poznyakov,

I.A. Ryabtsev, V.F. Khorunov,

K.A. Yushchenko

Scientists of Ukrainian Universities

M.N. Brykov, ZNTSU, Zaporozhie

V.V. Dmitrik, NTU «KhPI», Kharkov

V.F. Kvasnitsky, NUS, Nikolaev

V.D. Kuznetsov, NTUU «KPI», Kiev

Foreign Scientists

N.P. Alyoshin

N.E. Bauman MSTU, Moscow, Russia

Guan Qiao

Beijing Aeronautical Institute, China

A.S. Zubchenko

DB «Gidropress», Podolsk, Russia

M. Zinigrad

College of Judea & Samaria, Ariel, Israel

V.I. Lysak

Volgograd STU, Russia

Ya. Pilarczyk

Welding Institute, Gliwice, Poland

U. Reisgen

Welding and Joining Institute,

Aachen, Germany

O.I. Steklov

Welding Society, Moscow, Russia

G.A. Turichin

St. Petersburg SPU, Russia

Founders

E.O. Paton Electric Welding Institute, NASU

International Association «Welding»

Publisher

International Association «Welding»

Translators

A.A. Fomin, O.S. Kurochko,

I.N. Kutianova

Editor

N.A. Dmitrieva

Electron galley

D.I. Sereda, T.Yu. Snegiryova

Address

E.O. Paton Electric Welding Institute,

International Association «Welding»

11, Bozhenko Str., 03680, Kiev, Ukraine

Tel.: (38044) 200 60 16, 200 82 77

Fax: (38044) 200 82 77, 200 81 45

E-mail: journal@paton.kiev.ua

www.patonpublishinghouse.com

State Registration Certificate

KV 4790 of 09.01.2001

ISSN 0957-798X

Subscriptions

\$348, 12 issues per year,

air postage and packaging included.

Back issues available.

All rights reserved.

This publication and each of the articles contained herein are protected by copyright.

Permission to reproduce material contained in this journal must be obtained in writing from the Publisher.

CONTENTS

Interview with Prof. L.M. Lobanov, the Deputy Director of the E.O. Paton Electric Welding Institute 1

SCIENTIFIC AND TECHNICAL

Kuchuk-Yatsenko S.I., Zyakhov I.V., Chernobaj S.V., Nakonechny A.A. and Zavertanny M.S. Structure of γ -TiAl joints in resistance butt welding with application of interlayers 5

Ustinov A.I., Falchenko Yu.V., Melnichenko T.V., Petrushinets L.V., Lyapina K.V., Shishkin A.E. and Gurienko V.P. Diffusion welding of steel to tin bronze through porous interlayers of nickel and copper 13

Yushchenko K.A., Yarovitsyn A.V., Khrushchov G.D., Fomakin A.A. and Olejnik Yu.V. Analysis of process of bead shaping in cladding on narrow substrate 20

Matvienko V.N., Mazur V.A. and Leshchinsky L.K. Evaluation of shape and sizes of weld pool in surfacing using combined strip electrode 28

Ryabtsev I.A., Lankin Yu.N., Soloviov V.G., Osechkov P.P., Tishchenko V.A. and Tikhomirov A.G. Computer information-and-measuring system for investigation of arc surfacing processes 32

INDUSTRIAL

Lobanov L.M., Makhlin N.M., Smolyakov V.K., Vodolazsky V.E., Popov V.E. and Sviridenko A.A. Equipment for preparation of pipe ends to welding of position butt joints of pipeline 36

Grigorenko G.M., Puzrin A.L., Atroshenko M.G., Poleshchuk M.A., Shevtsov A.V. and Mossokovskaya I.A. Autovacuum brazing in repair of copper panels of MCCB moulds 45

Shapovalov K.P., Belinsky V.A., Kosinov S.N., Litvinenko S.N., Yushchenko K.A., Lychko I.I. and Kozulin S.M. Manufacturing large-sized beds by consumable-nozzle electroslag welding 50

Levchenko O.G., Kuleshov V.A. and Arlamov A.Yu. Noise characteristics during welding in argon-containing shielding gases 53

Interview with Prof. L.M. Lobanov, the Deputy Director of the E.O. Paton Electric Welding Institute

Over the whole period of activity of the E.O. Paton Electric Welding Institute a great attention is paid to the creation of highly-efficient welded structures. Nowadays this direction of works is headed by Prof. Leonid M. Lobanov, the academician of the NAS of Ukraine, honored worker of science and technology of Ukraine. His scientific activity is associated with the fundamental and applied research works in the field of materials science, strength of materials and welded structures. His works are devoted to investigations of behavior of materials in welding, development of theory of welding stresses and deformations and methods of investigation and regulation of stress-strain states of welded joints, creation of welded structures of new engineering, development of methods and means of their non-destructive testing and diagnostics. The research and development works, performed by L.M. Lobanov and the team under his supervision, were distinguished by a number of prizes:

1981 – the Prize of the Council of Ministers of the USSR for development and implementation of new physical methods for study and improvement of metallurgical processes and structures of new engineering;

1994 – the State Prize of Ukraine in the field of science and technology for the series of scientific works on theory of calculations of spatial structures and erections at static and dynamic loads;

2004 – the Evgeny Paton Prize for the series of works in the field of strength, diagnostics and life extension of welded structures.

L.M. Lobanov published over 700 scientific papers, including 80 authors' certificates and patents, prepared 9 Doctors of Technical Sciences and 16 Candidates of Technical Sciences, he was awarded the Orders of Merit of the First, the Second and the Third Class, as well as the Order of the Badge of Honor and was distinguished with the NAS of Ukraine Award «For Scientific Achievements».

On the eve of the 75th anniversary of the birth of L.M. Lobanov the Editorial Board of the Journal made an interview with the jubilee concerning the directions of his activity.

Prof. Lobanov, many scientists and experts in Ukraine and abroad are familiar with your publications on the topic of creating the cost-effective welded structures, testing their quality and improvement of their reliability. What are the roots of Your interest towards this direction?

Creation of the cost-effective, reliable and long-life welded structures, operating on the ground and under water at normal, high and low temperatures, under different extreme operating conditions is an essential scientific and

technical challenge. A great contribution to its solution has been brought by the scientists and specialists of the E.O. Paton Electric Welding Institute.

By possessing an extensive knowledge and extraordinary engineering insight, Evgeny Paton, the founder of our Institute, defined the main directions of works associated with the creation of reliable and cost-effective welded structures. They envisage an integrated solution of research, materials science, and engineering tasks. This approach gained a wide development due to activity of his pupils and followers. The R&D works, carried out at the PWI, provided an opportunity of manufacturing the rational welded structures at a high level of automation and mechanization of welding works. Moreover, the basic volumes of welding works are transferred to the plant conditions, providing a significant increase in efficiency of welding processes and improvement of quality of welded joints.





What are the relevant problems to be solved in the related field today?

At the present time the complex of the new investigations is carried out for evaluation of static and cyclic strength of welded joints taking into account their mechanical heterogeneity and presence of crack-like defects, resistance of welded joints to brittle and laminated fractures, development of scientific approaches to providing reliability and longevity of welded structures in implementation of requirements to reduction of their metal consumption, creation of technologies of hardening treatment of welded joints, application of mathematical methods for investigation of thermal deformation processes in welding, wide application of non-destructive testing and technical diagnostics of welded joints and structures. The new types of highly-efficient welded structures, including metal structures, bridge spans, heavily-loaded structures of high-strength steels for mining equipment and railway transport are created.

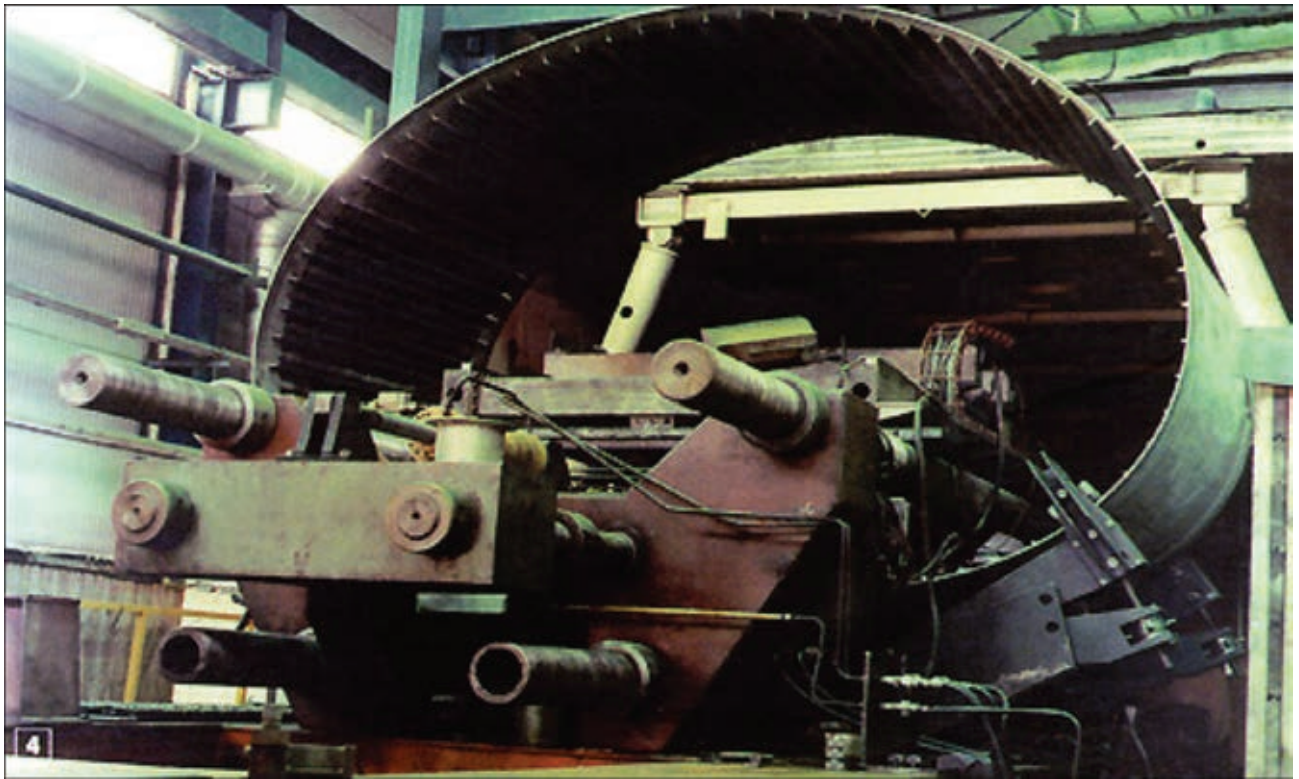
What are the practical examples of realization of the PWI developments in the field of welded structures in the recent years?

The construction of the National Sports Complex «Olimpijsky» in Kiev before the European Football Championship EURO-2012 should be noted. A team of the PWI developed and implemented the technologies of welding the load-carrying metal structures of this unique complex. The scientific and technological support of assembly and welding works was carried out in the plant conditions as well as directly at the construction site. The similar works were carried out during the construction of the International Exhibition Centre at the Brovary highway in Kiev.

The new steels S390–S690 were introduced into production of welded structures and with their application a number of unique engineering constructions was created, among which the oil storage tanks of 50,000 and 75,000 tons volume, spans of the Podolsky bridge and the Chabansky bridge in Kiev. The personnel of the PWI took an active part in the construction of the Darnitsky rail-road bridge in Kiev and was participating in the construction of the Zaporozhsky bridge. The scientific and technical support of assembly and welding works was carried out in erection of aluminium alloy metal structures of the roof of terminal «D» at the Borispol airport. A large experience of research and development works of the PWI in the fields of design and manufacture of different types of constructions, determination of their technical condition and reconstruction is summarized in the three-volume edition «Welded Constructions».

Prof. Lobanov, in your publications the term «deformation-free welding of structures» is frequently used. Could you explain the essence of such approach in production of structures?

Thanks to our developments a new scientific and technical direction, i.e. deformation-free welding of structures, was formed, which is based on creation of the preliminary stress-strain states before welding, optimized with respect to the welding stresses and deformations. For all types of welded joints the methods for determination of optimal parameters of preliminary stress-strain states were developed, which allow eliminating the residual welding deformations. This approach includes also the use of



assembly-welding units that combine distorting systems, equipment for mechanical treatment of welded edges under the conditions of preset loading and specialized welding equipment.

Could you please give some examples of its use?

It was realized at the enterprises of rocket and aerospace industry in manufacture of thin-walled structures of light alloys, to which high requirements as to the accuracy of geometric dimensions and quality of joints are specified. The unique installations were delivered to the enterprises of P.R. China under the contracts. At the moment the contract with the Design Bureau «Yuzhnoe» was concluded for the development of technology of deformation-free welding of stringer panels and, in future, of stringer shells of high-strength aluminum alloy.

What new methods of non-destructive testing would you prefer?

A significant contribution to the creation of systems for diagnostics of products of space and aircraft technology was made. A diagnostic method of electronic shearography, which is based on application of laser equipment and computer processing of optical information, was developed. Its essential advantage is contact-free measurement and the ability to perform a real-time non-destructive quality control of objects of both metal as well as composite materials. The developed technology for diagnostics and shearography equipment were implemented at the Design Bureau «Yuzhnoe». The investigations at the specimens of aircraft lining, carried out on the order of the State Enterprise «Antonov», showed that the method of electron shearography reveals corrosive damages of the elements of fuselage and wing of the aircraft without disassembly of lining and sealant.

On the basis of application of the method of electronic speckle-interferometry the technology and portable device for determination of residual stresses in welded joints of structures of new technology were created. The competition, carried out by the International Institute of Welding, confirmed that the method and equipment for its implementation developed at the PWI provide a valid evaluation of local peculiarities of residual stressed state of welded joints. This methodology and equipment are effectively used in the laboratory practice of the PWI and were delivered under the contracts to different industrial and research organizations of far abroad.

Prof. Lobanov, it is known that in the recent decades You are devoting many efforts and energy to the problem of residual life of continuously operating structures and constructions. How is the work in this direction organized in Ukraine?

In many countries the tendency of expiration of standard operation terms of a great number of structures, constructions and engineering systems is observed. This problem became of a particular importance in Ukraine. Due to the difficult economic conditions the majority of subjects of economic activity almost stopped renovation of main resources. In this regard, the issues of safe operation of the critical objects of industry, power engineering, transport, construction become every year more and more relevant. Those tasks are important, which are related to the control of operational reliability and longevity of such objects by determination of their technical condition and residual life, establishment of scientifically based service terms and regulations.

To the solution of these problems the target integrated program «Problems of Life and Safe Operation of Structures, Constructions and Machines» of the NAS of Ukraine is devoted, which has been carried out since 2004. The scientific supervisor of the Program is Prof. Boris E. Paton. The aim of the Program is the development of methodological bases for prediction of residual life, development of methods, techniques and technologies for evaluation of technical condition and life extension of technogeneous and environmentally dangerous objects.

The projects of the Program are aimed at the implementation of such important tasks as development of methods and means for non-destructive quality control and technical diagnostics of structures; creation of systems for continuous monitoring of critical objects of long-term operation using the modern information technologies; development of methods for prediction of residual life of structures with damages and technologies for restoration of their operability; creation of effective methods, mechanical means and technologies for evaluation and extension of life of equipment for heat and nuclear power engineering, chemical and petroleum industry, oil and gas pipelines, aerospace engineering, as well as bridges, building and transport constructions; preparation of standard documents, scientific and technical handbooks and manuals on evaluation and life extension of objects of long-term operation.

Are there any positive results of performance of works by the program «Resource»?

In the process of implementation of projects of the Program the significant scientific, technical and practical results were obtained. Thus, the acoustic emission systems were introduced for continuous diagnostics of equipment components at the Odessa Port Plant and the district heating plant «Kievenergo», the equipment for contact-free measurement of surfaces wear of railroad rails was created, the methodology of low-frequency ultrasonic testing of fractures at the hard-to-reach pipeline sections was developed, the technology and equipment for the formation of reinforcing structures were developed using a metal polymer wire coupling for repair of local defects of oil and gas pipelines without stopping the products transportation, the unique industrial objects and spans of railroad bridges were restored, the modern standards and standard documents for engineering practice were issued and many other.

The main results of works by each project of the Program are summarized in the final collections of papers, which are published by the Institute every three years. The specialists regard these collections as the encyclopedia on the problems of life. They make an important contribution to the formation of scientific and technical aspects of engineering culture in our country and provide the new instruments in solving the problems of resource of safe service of structures and equipment.

Thank you, Prof. Lobanov, for Your interesting and thorough coverage of the problems related to the creation of modern welded structures. We wish You a strong health and new achievements for the benefit of Ukraine.

Editorial Board of «The Paton Welding Journal»



STRUCTURE OF γ -TiAl JOINTS IN RESISTANCE BUTT WELDING WITH APPLICATION OF INTERLAYERS

S.I. KUCHUK-YATSENKO, I.V. ZYAKHOR, S.V. CHERNOBAJ,
A.A. NAKONECHNY and M.S. ZAVERTANNY
E.O. Paton Electric Welding Institute, NASU
11 Bozhenko Str., 03680, Kiev, Ukraine. E-mail: office@paton.kiev.ua

The paper deals with the features of producing joints of an alloy based on γ -TiAl intermetallics at resistance butt welding with application of interlayers in the form of foil, differing by thickness, composition and structural state. Investigations were performed on samples of Ti-47Al-2Cr-2Nb (at.%) alloy, produced by electron beam remelting, both in as-delivered (cast) condition, and after heat treatment (1250 °C, 6 h). Used as interlayer was titanium foil with microcrystalline structure 100, 200 and 400 μm thick, and nanostructured multilayered foils Ti/Al (52Ti-48Al, at.%) and Ti/Co (75Ti-25Co, at.%) of 30–160 μm thickness. Experiments were performed in K802 system, welding mode parameters were varied in the following ranges: 5–20 MPa pressure at heating, 20–100 MPa upset pressure, hand 5–15 mm upset value. Joint microstructure and composition were studied by optical and scanning electron microscopy and X-ray microprobe analysis. Metal strength properties in the joint zone were assessed by microhardness distribution and rupture testing. It is established that the zone of Ti-47Al-2Cr-2Nb alloy joints made with application of solid titanium foil demonstrates structural inhomogeneity in the form of a continuous titanium interlayer and diffusion zone between the interlayer and alloy being welded, containing linear porosity. Application of nanostructured Ti/Al and Ti/Co foils ensures formation of defect-free joints. Metal structure in the joint zone is fine-grained bimodal $\gamma/\gamma + \alpha_2$, irrespective of base metal initial structure. Remains of nanostructured foils of Ti/Al system are present in the joint zone in the form of an interlayer of dispersed γ -TiAl intermetallic, not containing any chromium or niobium. At application of foil of Ti/Co system of eutectic composition, no chemical inhomogeneity in the form of foil transformation products is found in the butt. At rupture testing of the joints, fracture runs through the base metal of Ti-47Al-2Cr-2Nb alloy. Joint region of higher hardness in all the considered cases coincides with the zone of structural changes resulting from thermodeformational impact of the welding process. 21 Ref., 11 Figures.

Keywords: resistance butt welding, titanium aluminide, interlayer, nanostructured multilayer foil, welded joint

One of the urgent problems is development of methods of technological processing and producing permanent joints of intermetallic titanium alloys, in particular, gamma-alloys based on γ -TiAl titanium aluminide. Gamma-alloys have high values of heat resistance (at 700–750 °C) and oxidation resistance at relatively low density (3850 kg/m³) [1–3]. Depending on purity and microstructure, mechanical properties of TiAl intermetallic vary in broad ranges and are equal to $\sigma_t = 350\text{--}580$ MPa, $\delta = 0.5\text{--}1.5$ %, $E = 175$ GPa, $G = 65$ GPa. It is proposed to apply gamma-alloys for manufacturing car engine valves, and aircraft engine parts operating at high temperatures [4, 5].

One of the causes, limiting application of titanium aluminides, is their poor adaptability-to-fabrication, in particular, difficulty of welding them, because of their extremely low ductility, and high sensitivity to cracking at thermode-

formational impact. Joints produced in nonconsumable arc welding [6] and electron beam welding [7] are prone to cracking, which develops along the fusion line or in the HAZ. To lower the probability of cracking in titanium aluminide joints at application of fusion welding processes, preheating of the structure being welded to high temperature is required [8].

In press welding of γ -TiAl intermetallic alloy [9], welded joints feature a low strength because of formation of brittle stringers in the joint zone. The main problems in producing sound joints of titanium aluminides in friction welding [10, 11] is microcracking in the thermomechanical impact zone (TMIZ) during deformation and at cooling. At vacuum diffusion welding (VDW) of Ti-48Al-2Nb-2Mn alloy the interface is clearly defined and defects in the form of micropores are observed in the transition zone structure [12].

Low ductility of intermetallic alloys necessitates longer heating and increasing the thermodeformational parameters of VDW process. Formation of titanium aluminide joints without metal-



lographically detectable defects at VDW is achieved through long soaking under pressure at the temperature of 1100–1200 °C and subsequent high-temperature heat treatment [12, 13].

Intermetallic alloy sensitivity to thermodeformational welding cycle is driving technologists to look for the ways to facilitate the conditions of activation of the surfaces being welded, primarily due to intensification of the process of local plastic deformation and acceleration of diffusion processes in the contact zone. The main technique in pressure welding processes is application of interlayers from various materials. For instance, at VDW the conditions for activation of the surfaces being welded are greatly facilitated at introduction of interlayers from ductile materials between them: aluminium, copper, nickel, titanium [9, 14]. A problem in the processes of pressure welding with application of an interlayer from different metals is formation of chemical inhomogeneity in the welded joint [9].

The effect of simultaneous increase of deformation intensity and acceleration of diffusion processes in the contact zone is achieved through application of interlayers from vacuum condensates based on multilayer structures, consisting from elements with a high reactivity [15–18]. It is shown that the lowest chemical inhomogeneity in the butt is provided by multilayer nanostructured foils (NF) of Ti/Al system produced by the process of electron beam evaporation and deposition of the vapour phase in vacuum [18]. So, VDW of γ -TiAl base alloy with application of NF of Ti/Al system provides formation of sound joints [16, 17] with the strength close to base material (BM) values. Positive influence of NF application at VDW is associated with intensification of mass transfer processes in the zone of contact, owing to running of the reaction of self-propagating high-temperature synthesis (SHS) [19].

VDW application is limited by the need to heat the entire item being welded up to considerable temperatures in the vacuum chamber, extremely high requirements to preparation of surfaces being welded and low efficiency of the welding process. Therefore, an urgent issue is studying the applicability of pressure welding processes providing higher efficiency and possibility of sound joining of various materials without application of shielding medium or vacuum.

Such pressure welding processes include resistance butt welding (RBW). In [20] joint formation at RBW of Ti-47Al-1.5Cr-2Nb alloy produced by electron beam remelting technology was studied. It is found that application of NF of

Ti/Al system allowed an essential improvement of joint formation, reducing sample upset value and RBW process duration. Positive effect was achieved owing to a more concentrated evolution of heat in the contact zone due to running of SHS reaction in NF. NF application allowed reducing the heat input, localizing deformation in the contact zone and avoiding cracking. However, a considerable hardness gradient is observed in the joints: microhardness value rises by 60 %, compared to BM values [20]. At mechanical testing fracture runs in the transition zone between TMIZ and BM of the cast alloy. It can be assumed that this zone features a combination of the high level of welding stresses and extremely low ductility of metal of γ -TiAl cast alloy with coarse-crystalline plate-like structure.

Obtained results show the good prospects for NF application as activators of the process of RBW of titanium intermetallic alloys. Investigations of the influence of NF composition and thickness, as well as initial structure of the alloy being welded on joint formation, are urgent for further improvement of RBW technology.

The objective of the work is to establish the features of formation of joint structure of γ -TiAl alloy in different initial condition at RBW with application of interlayers, differing by their composition, structural state and thickness.

Investigation procedure. Investigations were performed on samples of Ti-47Al-2Cr-2Nb (at.%) alloy produced by electron beam remelting (samples of square section of 10 × 10 mm). The first batch of samples was welded in as-delivered condition, and the second was annealed at the temperature in ($\alpha + \gamma$)-region (1250 °C, 6 h) before conducting RBW that resulted in coarse-crystalline plate-like structure of the cast alloy transforming into completely granular structure, differing by higher ductility values [2].

Used as interlayer at RBW were foils of three types, differing by composition and structural state: titanium foil with microcrystalline structure and nanolayered foils: Ti/Al (52Ti-48Al, at.%) and Ti/Co (75Ti-25Co, at.%) (Figure 1). Foil thickness was as follows: titanium – 100, 200 and 400 μm , Ti/Al NF – 30, 60 and 160 μm , Ti/Co NF – 100 μm . Difference in foil composition predetermines the difference in their melting temperature T_{melt} , compared to T_{melt} of the alloy being welded: higher (titanium foil with $T_{\text{melt}} = 1668$ °C), equal (Ti/Al NF transformed at heating into TiAl intermetallic with $T_{\text{melt}} = 1460$ °C) and lower (Ti/Co NF transformed into an eutectic with $T_{\text{melt}} = 1170$ °C).



Experiments on RBW were conducted in a laboratory set-up, based on K802 welding machine. Current value and compression force were regulated by computerized control system. Range of process parameter variation was optimized on the basis of preliminary experiments so as to provide the specified deformation (upset value) in welding all sample batches. RBW parameters were varied in the following ranges: 5–20 MPa pressure at heating, 20–100 MPa upset pressure, and 5–15 mm upset value.

Welding quality was assessed by a comprehensive testing procedure [21], envisaging application of computerized on-line control of welding mode parameters, techniques of welded joint NDT and metallographic examination. Welded joint microstructure and composition was studied by optical microscopy (Neophot-32), scanning electron microscopy (JEOL JSM-35SA) and X-ray microprobe analysis (EDS-analyzer INCA-450 of Oxford Instruments with probe diameter of about 1 μm). Strength properties were evaluated by microhardness distribution (LECO microhardness meter M400) at 2 N load.

Investigation results. It is established that at RBW of Ti-47Al-2Cr-2Nb cast alloy with completely lamellar structure defects such as lacks-of-penetration and linear porosity were observed in the joint zone. Defect formation at RBW without interlayer application was observed at process parameters variation in the entire studied range, and was due to high deformation resistance and low ductility of intermetallic alloy. In welding of samples after preliminary heat treatment, joint formation conditions were improved, apparently, due to higher ductility values of the alloy with completely granular structure; however, defect formation could not be avoided (Figure 2, *a*).

Figure 2, *b* shows microstructure of the zone of Ti-47Al-2Cr-2Nb alloy joint, made with application of an interlayer in the form of titanium foil. No cracks, lacks-of-penetration, or oxide films were found in the joint structure. Irrespective of applied foil thickness (in the range of 100–400 μm), however, the joint zone demonstrates chemical inhomogeneity in the form of a continuous titanium interlayer.

Presence of titanium foil in the contact zone at RBW of Ti-47Al-2Cr-2Nb alloy promotes localization of plastic deformation, activation of surfaces being welded and formation of defect-free joints. However, complete pressing out of titanium interlayer from the butt is not observed, even at maximum values of force and upset in the studied range. Performance of postweld heat treatment of the joints (1150 $^{\circ}\text{C}$, 6 h) does not completely eliminate chemical inhomogeneity.

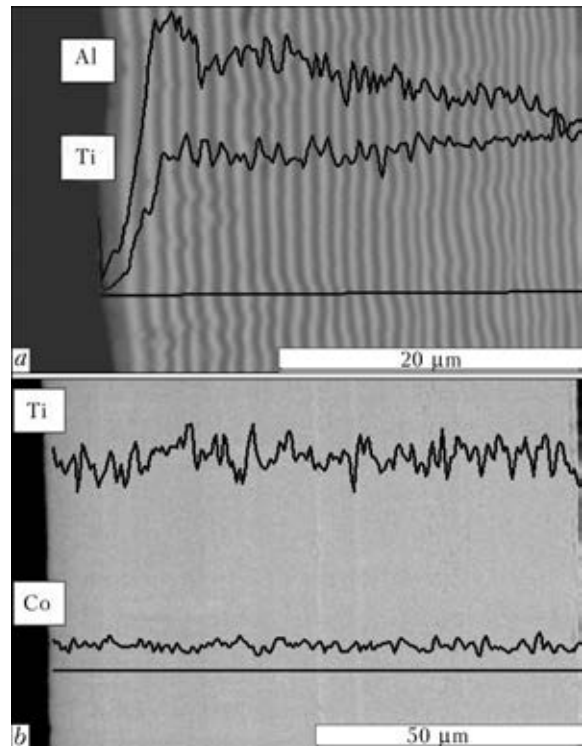


Figure 1. Microstructure of nanostructured multilayer Ti/Al (*a*) and Ti/Co (*b*) foils

Moreover, it leads to formation of a diffusion zone between titanium interlayer and γ -TiAl alloy BM (Figure 3). Width of titanium interlayer is equal to 40–50 μm , that of diffusion zone with varying concentration of Ti, Al, Cr, Nb is about 25 μm . Diffusion zone contains linear porosity (Figure 3, *a*). By the data of X-ray microprobe analysis the total width of the zone of concentrational variations is equal to about 100 μm (Figure 3, *b*). Development of chemical inhomogeneity cannot be avoided at RBW of either cast or pre-heat treated Ti-47Al-2Cr-2Nb alloy.

Microstructure of welded joint of Ti-47Al-2Cr-2Nb cast alloy (without preliminary heat treatment) made with application of Ti/Al NF of $\delta = 60 \mu\text{m}$ is given in Figure 4. No defects of any kind, including pores, were found in the joint zone. Structural changes in the joint cover a zone of total width of about 2.5 mm (Figure 4, *a*). Coarse-crystalline completely plate-like structure of BM cast alloy is transformed into fine-grained bimodal (mixed) structure in the joint zone, containing dispersed products of SHS reaction in NF. Single-phase grains of γ -phase (Figure 4, *d*) are surrounded by $\gamma + \alpha_2$ two-phase regions with plate-like structure.

Width of the zone of Ti, Al, Cr, Nb concentrational changes is about 50 μm (Figure 5, *a*) that is indicative of presence of dispersed products of SHS reaction in NF. Structure of the zone of transition from TMIZ to BM is almost plate-

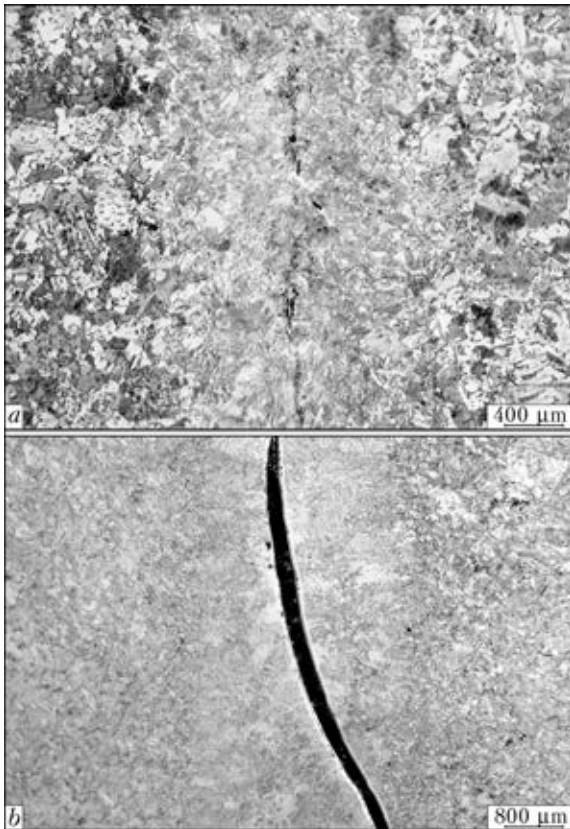


Figure 2. Microstructure of Ti-47Al-2Cr-2Nb alloy joint at RBW without an interlayer (a) and with application of titanium foil of $\delta = 400 \mu\text{m}$ (b)

like. Analysis of joint microstructure is indicative of completion of SHS reaction in NF across the entire cross-section of billets being welded and incomplete pressing-out of NF transformation products from the butt during RBW. Values of metal microhardness (Figure 5, b) in the joint zone ($HV_2-4800-5660 \text{ MPa}$) are much higher than those for BM alloy ($HV_2-3700-4300 \text{ MPa}$). Joint region of higher hardness coincides with the zone of structural changes as a result of thermodeformational impact of RBW process, that

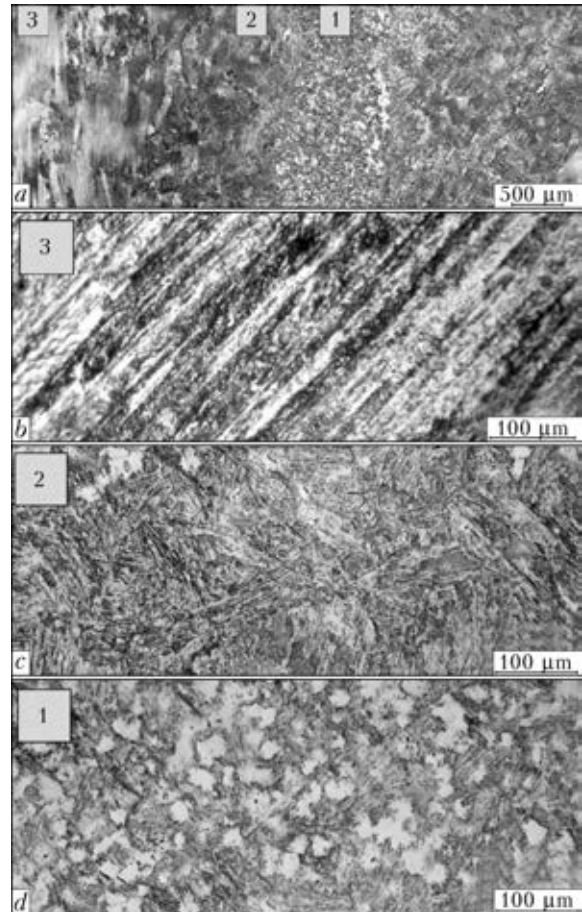


Figure 4. Microstructure of joint of Ti-47Al-2Cr-2Nb cast alloy at RBW with application of Ti/Al NF of $\delta = 60 \mu\text{m}$: a – general view; b – BM; c – transition zone; d – fine-grained zone

may be indicative of the contribution of high-temperature plastic deformation into changing of alloy mechanical properties. Thus, at RBW of Ti-47Al-2Cr-2Nb cast alloy with application of Ti/Al NF of $\delta = 60 \mu\text{m}$, formation of defect-free joints is ensured at considerable hardness gradient ($HV_2-1100-1300 \text{ MPa}$) in TMIZ.

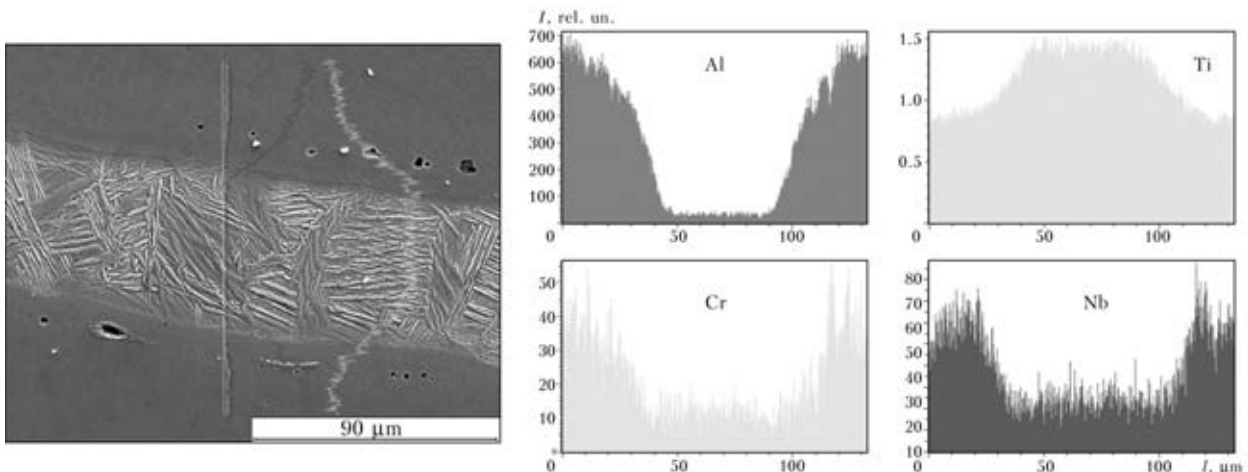


Figure 3. Microstructure and distribution of Ti, Al, Cr, Nb in the joint of Ti-47Al-2Cr-2Nb alloy at RBW with application of titanium foil of $\delta = 100 \mu\text{m}$ (SEM)



Microstructure of the joint of pre-heat treated Ti-47Al-2Cr-2Nb alloy made by RBW with application of Ti/Al NF of $\delta = 60 \mu\text{m}$ is shown in Figure 6, *a*. Nature of structural changes in the joint zone is similar to that found in the previous case with the difference that BM initial granular structure transforms into fine-grained bimodal structure (Figure 7, *a*). Width of the zone of Ti, Al, Cr, Nb concentrational changes in the joint is equal to about $40 \mu\text{m}$. Values of metal microhardness in the joint zone (HV_3 -4300–4700 MPa) are also higher than those for BM alloy (HV_3 -3500–3800 MPa). Joint region of higher hardness coincides with thermodeformational impact zone. Transition zone structure is bimodal, unlike almost plate-like structure of transition zone of cast alloy joint. Hardness gradient in the joint zone is equal to HV_2 -800–900 MPa that is somewhat lower compared to that in cast alloy welding.

Joint structure at RBW of heat-treated Ti-47Al-2Cr-2Nb alloy with application of Ti/Al NF of $\delta = 160 \mu\text{m}$ (Figure 6, *b*) is similar. Selection of such foil is due to technological considerations – application of NF of greater thickness allows lowering the requirements to preparation

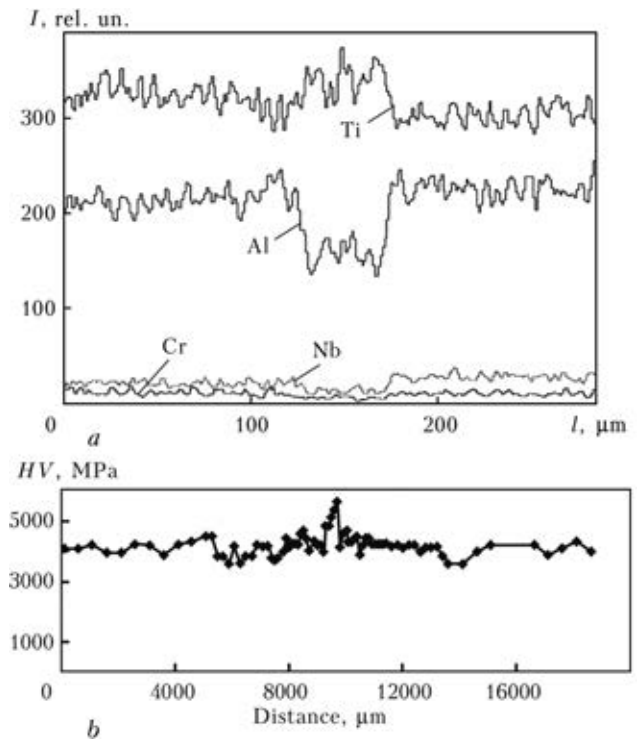


Figure 5. Distribution of Ti, Al, Cr, Nb (*a*) and metal microhardness (*b*) in the joint zone of Ti-47Al-2Cr-2Nb cast alloy produced by RBW with application of Ti/Al NF of $\delta = 60 \mu\text{m}$



Figure 6. Microstructure of heat-treated Ti-47Al-2Cr-2Nb alloy joint at RBW with application of NF of Ti/Al of $\delta = 60 \mu\text{m}$ (*a*), Ti/Al of $\delta = 160 \mu\text{m}$ (*b*) and Ti/Co of $\delta = 100 \mu\text{m}$ (*c*)

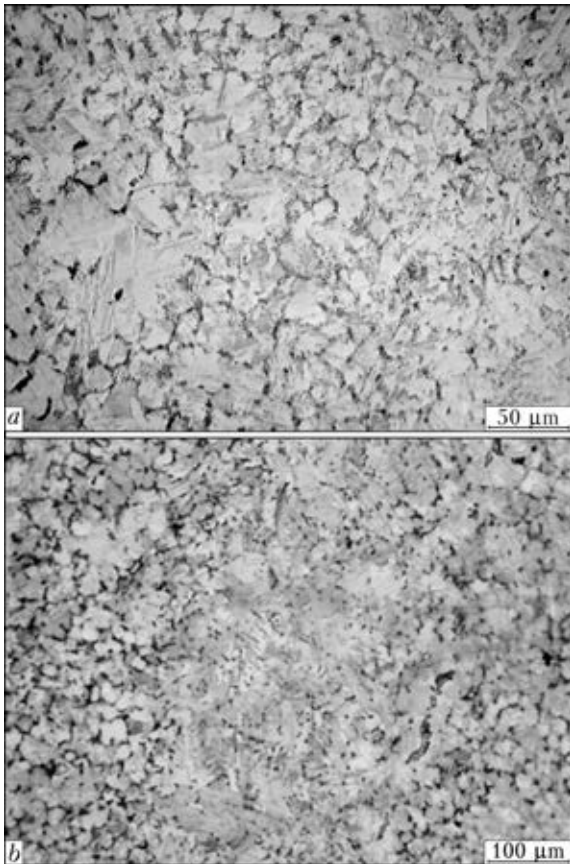


Figure 7. Metal microstructure in fine-grained zone of heat-treated Ti-47Al-2Cr-2Nb alloy joint at RBW with application of NF of Ti/Al of $\delta = 60 \mu\text{m}$ (a) and Ti/Al of $\delta = 160 \mu\text{m}$ (b)

of surfaces being welded at RBW of billets of large cross-sections. Increase of thickness of NF applied at specified RBW mode leads to greater width of the zone of Ti, Al, Cr, Nb concentrational changes, which in this case is equal to about $120 \mu\text{m}$. Nature of microhardness variation in the joint zone is similar to the previous case.

Structural changes in the joint of heat-treated Ti-47Al-2Cr-2Nb alloy, made with application of Ti/Co NF of eutectic composition, cover a zone of not more than 2 mm total width (see Figure 6, c). Metal in the joint plane, transition zone and BM has bimodal $\gamma/\gamma + \alpha_2$ structure with structural element size of about 15, 35 and $110 \mu\text{m}$, respectively (Figure 8). Unlike joints made by RBW with application of Ti/Al NF, no Ti/Co NF transformation products are found in the butt joint at X-ray microprobe analysis (Figures 9 and 10). Element concentration across and along the joint zone corresponds to this value for Ti-47Al-2Cr-2Nb BM alloy. It can be assumed that during billet deformation at RBW the forming liquid phase of eutectic composition under the conditions of compression and passage of high-power current pulses is totally pressed-

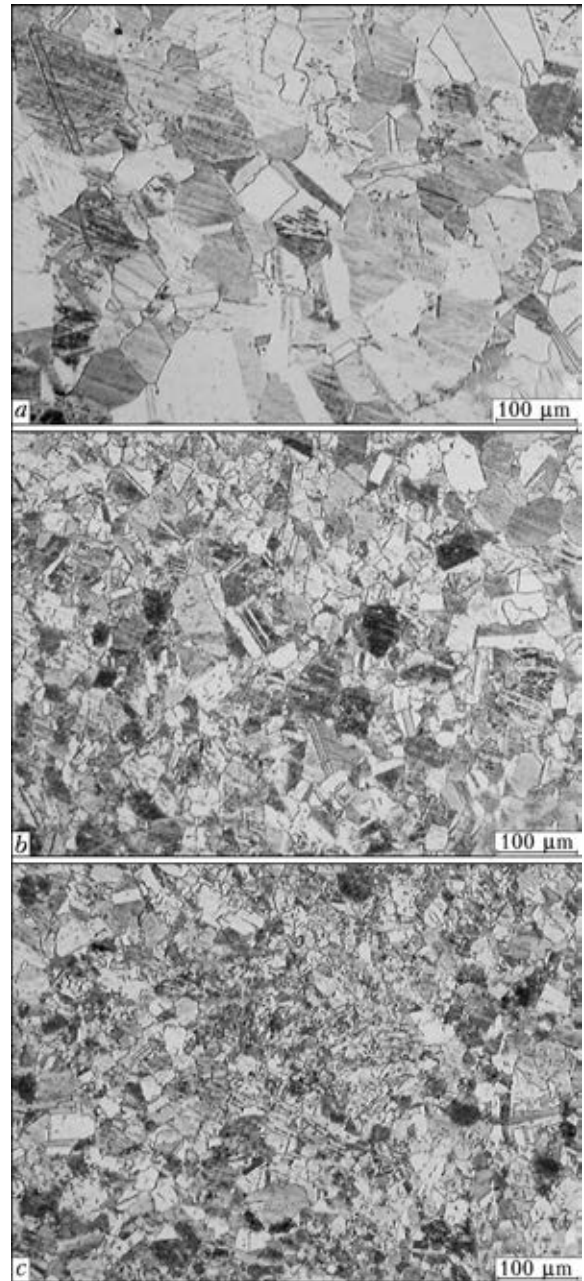


Figure 8. Microstructure of heat-treated Ti-47Al-2Cr-2Nb alloy joint at RBW with application of Ti/Co NF of $\delta = 100 \mu\text{m}$: a – BM; b – transition zone; c – fine-grained zone

out of the butt together with near-contact volumes of the alloy being welded.

Positive role of appearance of liquid phase of eutectic composition during RBW is, apparently, manifested, firstly, in local increase of specific electric resistance of metal in the contact zone that allows localization and intensification of shear plastic deformation; and, secondly, in considerable increase of mass transfer rate on liquid-solid interface. Presence of hardness gradient of $HV2-700-900 \text{ MPa}$ in the joint zone, similar to the previous cases, is indicative of the role of high-temperature plastic deformation in the

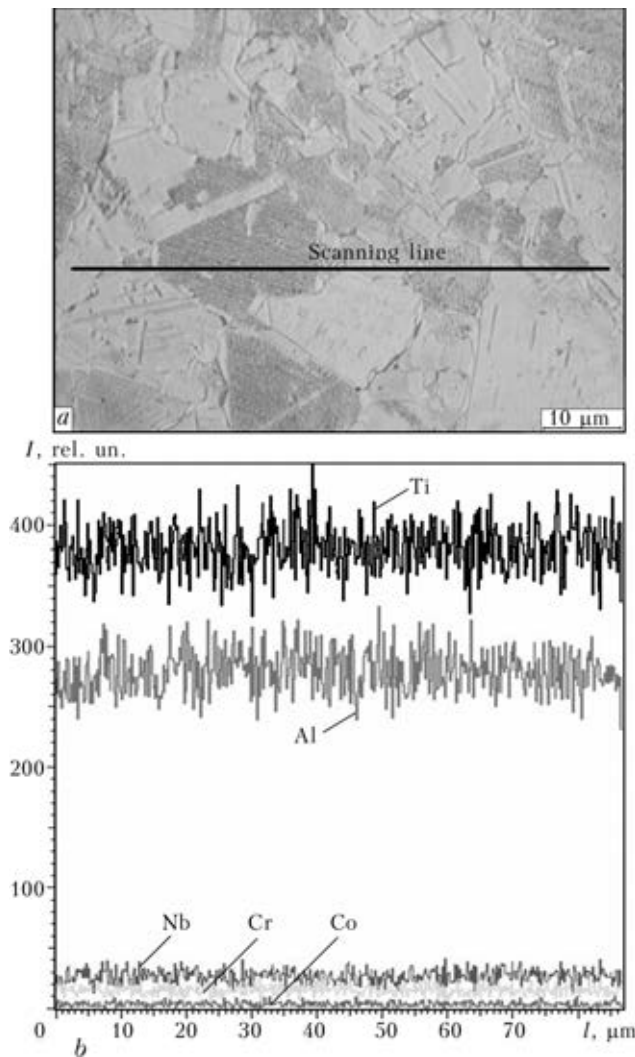
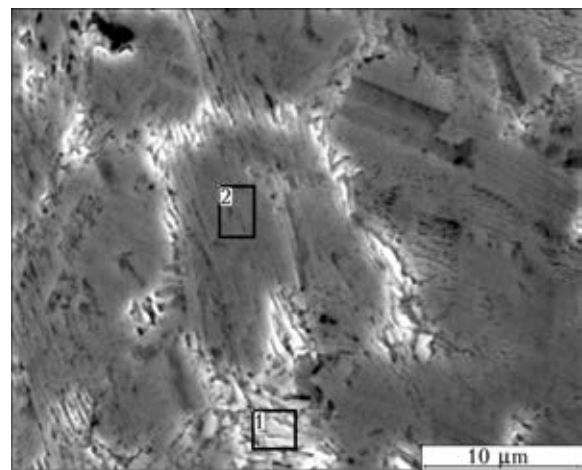


Figure 9. Microstructure (a) and Ti, Al, Cr, Nb, Co distribution (b) in metal of Ti-47Al-2Cr-2Nb alloy joint zone at RBW with application of Ti/Co NF of $\delta = 100 \mu\text{m}$

change of intermetallic alloy mechanical properties. At rupture testing of joints fracture runs through BM of Ti-47Al-2Cr-2Nb alloy (Figure 11).

Analysis of the studied joint microstructure shows that at RBW of Ti-47Al-2Cr-2Nb alloy with application of Ti/Al NF transforming into γ -TiAl intermetallic during welding, metal in the joint zone has fine-grained bimodal $\gamma/\gamma + \alpha_2$ structure, irrespective of BM initial structure. Increase of applied NF thickness at preset RBW mode leads to greater width of the zone of Ti, Al, Cr, Nb concentrational changes in the joint zone.

Joint region of higher hardness coincides with the zone of structural changes resulting from thermodeformational impact of RBW process, and is practically independent on NF thickness. Microstructure and value of hardness gradient of metal in the zone of transition from BM to fine-grained region is determined by the structure of



Spectrum	Al	Ti	Cr	Nb
1	44.51	51.05	2.22	2.22
2	45.94	50.36	1.56	2.14

Figure 10. Microstructure and results of EDS-analysis of metal on joint line of Ti-47Al-2Cr-2Nb alloy at RBW with application of Ti/Co NF of $\delta = 100 \mu\text{m}$



Figure 11. Samples of Ti-47Al-2Cr-2Nb alloy welded joints after rupture testing

billet initial metal. Performance of pre-heat treatment of samples being welded provides a slight lowering of hardness gradient in the joint zone.

To lower microhardness gradient and stabilize the structure of welded joint metal, heat treatment [17] is performed at the temperature corresponding to $(\alpha + \gamma)$ -region of Ti-Al constitutional diagram.

Conclusions

1. At RBW of Ti-47Al-2Cr-2Nb cast alloy without interlayer application, welding defects were observed in the entire studied range of technological parameter changing.

2. In the zone of Ti-47Al-2Cr-2Nb alloy joints, produced by RBW with application of monolithic titanium foil, structural inhomogeneity is found in the form of continuous titanium interlayer and diffusion zone between the



interlayer and alloy being welded, which contains linear porosity.

3. Application of multilayer NF of Ti/Al system (52Ti–48Al) 60–160 μm thick at RBW of Ti–47Al–2Cr–2Nb alloy provides formation of defect-free joints. Fine-grained bimodal $\gamma/\gamma + \alpha_2$ structure forms in the joint zone, irrespective of BM initial structure. NF remains are present in the joint zone in the form of an interlayer of disperse γ -TiAl intermetallic, not containing any chromium, or niobium.

4. Formation of defect-free joints is provided at RBW with application of NF of Ti/Co system (75Ti–25Co), and no chemical inhomogeneity in the form of foil transformation products is found in the butt. At rupture testing of joints, fracture runs through BM Ti–47Al–2Cr–2Nb alloy.

5. In all the considered cases, joint region of higher hardness coincides with the zone of structural changes, resulting from thermodeformational impact of RBW process.

1. Ivanov, V.I., Nochovnaya, V.A. (2007) Intermetallics on titanium base (analysis of state of the problem). *Titan*, **1**, 44–48.
2. Polkin, I.S., Kolachev, B.A., Iliin, A.A. (1997) Titanium aluminides and alloys on their base. *Tekhnol. Lyog. Splavov*, **3**, 32–39.
3. Dimiduk, D.M. (1995) Gamma titanium aluminides – An emerging materials technology. In: *Gamma titanium aluminides: TMS'95 Ann. Meet. Proc.* (Las Vegas), 3–20.
4. Ivanov, V.I., Yasinsky, K.K. (1996) Efficiency of application of heat-resistant alloys on the base of Ti₃Al and TiAl intermetallics for service at temperatures of 600–800 °C in aviation engineering. *Tekhnol. Lyog. Splavov*, **3**, 7–12.
5. Pavlinich, S.P., Zajtsev, M.V. (2011) Application of intermetallic titanium alloys in casting of GTE components and blades with lightweight high-strength structures for aviation engines of new generation. *Vestnik UfimGATU*, **15**(4), 200–202.
6. Arenas, M.F., Acoff, V.L. (2003) Analysis of gamma titanium aluminide welds produced by gas tungsten arc welding. *Welding J.*, **5**, 110–115.
7. Patterson, R.A. et al. (1990) Titanium aluminide: Electron beam weldability. *Ibid.*, **1**, 39–44.
8. Zamkov, V.N., Velikoivanenko, E.A., Sabokar, V.K. et al. (2001) Selection of temperature of preheating of γ -titanium aluminide in electron beam welding. *The Paton Welding J.*, **11**, 17–20.
9. Yushtin, A.N., Zamkov, V.N., Sabokar, V.K. et al. (2001) Pressure welding of intermetallic alloy γ -TiAl. *Ibid.*, **1**, 33–37.
10. Miyashita, T., Hino, H. (1994) Friction welding characteristics of TiAl intermetallic compound. *J. Japan Inst. Metals*, **58**(2), 215–220.
11. Baeslack, W.A., Threadgill, P.L., Nicholas, E.D. et al. (1996) Linear friction welding of Ti–48Al–2Cr–2Nb (at.%) titanium aluminide. In: *Proc. of Titanium-95 Conf. on Science and Technology* (Birmingham, UK, 22–26 Oct. 1995), 424–431.
12. Gam, G., Bohm, K.N., Kocak, M. (1999) Diffusionsschweissen fein gegossener Titanaluminide. *Schweißen und Schneiden*, **8**, 470–475.
13. Nakao, Y., Shinozaki, K., Hamada, M. (1992) Diffusion bonding of intermetallic compound TiAl. In: *Proc. of 3rd Int. Conf. on Trends in Welding Research* (Gattinburg, USA, June 1–5, 1992), 1057–1061.
14. Yan, P., Somekh, R.E., Wallach, E.R. (1992) Solid state bonding of TiAl with interlayers. *Ibid.*, 1063–1067.
15. Duarte, L.I., Ramos, A.S., Vieira, M.F. et al. (2006) Solid-state diffusion bonding of γ -TiAl alloys using Ti/Al thin films as interlayers. *Intermetallics*, **14**, 1151–1156.
16. Ustinov, A.I., Falchenko, Yu.V., Ishchenko, A.Ya. et al. (2009) Producing permanent joints of γ -TiAl based alloys using nanolayered Ti/Al interlayer by vacuum diffusion welding. *The Paton Welding J.*, **1**, 12–15.
17. Kharchenko, G.K., Ustinov, A.I., Falchenko, Yu.V. et al. (2011) Diffusion bonding of γ -TiAl base alloy in vacuum by using nanolayered interlayers. *Ibid.*, **3**, 2–6.
18. Ustinov, A.I., Falchenko, Yu.V., Melnichenko, T.V. et al. (2012) Multilayer Ti/Al foils: Methods of producing, properties and application in pressure welding. *Spetsselektrometallurgiya*, **1**, 30–37.
19. Kharchenko, G.K., Mazanko, V.F., Ustinov, A.I. et al. (2009) Investigation of diffusion processes in welded joints of titanium aluminides (TiAl). *Visnyk ChDTU*, Series Tekhn. Nauky, **37**, 117–119.
20. Kuchuk-Yatsenko, V.S., Shvets, V.I., Sakhatsky, A.G. et al. (2009) Features of resistance welding of titanium aluminides using nanolayered aluminium-titanium foils. *The Paton Welding J.*, **3**, 11–14.
21. Kuchuk-Yatsenko, S.I., Zyakhor, I.V., Zavertanny, M.S. (2015) Quality control of pressure welded joints using nanomaterials. *Standartyz., Sertyfikats., Yakist*, **1**, 38–41.

Received 21.04.2015



DIFFUSION WELDING OF STEEL TO TIN BRONZE THROUGH POROUS INTERLAYERS OF NICKEL AND COPPER

A.I. USTINOV, Yu.V. FALCHENKO, T.V. MELNICHENKO, L.V. PETRUSHINETS,
K.V. LYAPINA, A.E. SHISHKIN and V.P. GURIENKO

E.O. Paton Electric Welding Institute, NASU
11 Bozhenko Str., 03680, Kiev, Ukraine. E-mail: office@paton.kiev.ua

Friction assemblies based on steel and bronze are widely applied in many mechanical systems. Steel and bronze joints are produced by diffusion welding at temperatures of 750–850 °C. Defect formation in the joint zone in a number of cases is associated with high welding temperature. The paper deals with the possibility of lowering diffusion welding temperature by interlayer application in the case of making permanent joints of steel (20Kh3MVF) and bronze (BrOSN 10-2-3). Porous nickel and copper foils, produced by vacuum deposition, were used as interlayers. It is shown that application of such porous interlayers allows welding temperature to be lowered to 660–700 °C. Lowering of welding temperature prevents growth of liquation precipitates of tin and lead in the joint zone, that lowers the probability of defect formation. The thus produced joints are stable at short-time heating to 800–850 °C, that allows later on performing heat treatment of steel as part of composite material to increase its strength properties. 13 Ref., 1 Table, 5 Figures.

Keywords: *bimetal joints, steel, bronze, porous interlayers, diffusion welding, welding modes, joint structure*

Bimetal materials consisting of steel and tin bronze and produced by diffusion welding are widely applied in mechanical systems (friction assemblies). Such a composite structure of material provides a combination of high strength and low friction coefficient to the parts. Reliability and service life of parts with bimetal structure depends on the quality of joining steel and tin bronze components.

According to the data of [1], structure of tin bronze BrOSN 10-2-3 consists of α -solid solution and inclusions of $\alpha + \text{Cu}_3\text{Sn}$ (or $\alpha + \text{Cu}_{31}\text{Sn}_8$) eutectoid. Its composition further includes nickel and tin. Nickel added to bronze increases the eutectoid amount, but does not form any new phases, while being in solid solution. Lead, insoluble in copper, is present in the form of individual inclusions. Difficulties in welding steel and tin bronze alloyed by lead are associated with higher liquation susceptibility of bronze, bronze surface melting already at 760–780 °C, because of lead presence, as well as the probability of development of Rebinder effect at copper penetration into steel intercrystalline space.

Known is the technology of tin bronze welding to steel in the mode of solid-liquid state at tem-

peratures $T_w = 870\text{--}880$ °C and soaking for $t_w = 15$ min [2].

Authors of [3] developed a technology to produce joints of bronze bushing with slide bearing body. This technology envisages bushing pressing into the steel body with subsequent burnishing that ensures running of localized plastic deformation on steel-bronze interface. Then diffusion welding is performed at $T_w = 750$ °C, $t_w = 30$ min.

Known are technologies of steel to bronze welding with application of copper and nickel interlayers or electroplated nickel coatings. So, for instance, in welding 40Kh steel to bronze BrOSN 10-2-3 it is recommended to weld a copper interlayer (1 mm thick) to steel at $T_w = 900$ °C, $P_w = 10$ MPa, $t_w = 20$ min, and then to weld the assembly to bronze at $T_w = 750$ °C, $P_w = 5$ MPa, $t_w = 10$ min, that allows producing welded joints with 229 MPa pull strength [4].

Conducted analysis shows that steel and bronze joints are produced during diffusion welding at elevated temperatures that may promote increase of liquational inhomogeneities in bronze or liquid phase formation in the joint zone. This leads to lowering of joint strength and dependence of its quality on bronze initial state. Welding temperature lowering can be one of the ways to prevent development of negative processes. However, even in the case of activation of diffusion processes in the joint zone by simultaneous



deformation of samples being welded at rolling, material joining cannot be achieved at temperature below 750 °C [5].

On the other hand, it was shown in a number of studies that application of interlayers, based on ductile materials, can promote softening of the conditions of producing permanent joints [6]. Porous materials can also be used as such interlayers [7]. Taking these results into account, the possibility of lowering the temperature of diffusion welding of steel and tin bronze through nickel and copper interlayers with porous structure was considered, and the features of microstructure formation in the joint zone were studied in this work.

Materials and methods of investigation. Vacuum diffusion welding of samples of 20Kh3MVF steel (further on steel) and tin bronze BrOSN 10-2-3 (further on bronze) was conducted by the procedure, described in [8]. Welding process parameters were as follows: $T_w = 600\text{--}800$ °C, $t_w = 5\text{--}20$ min, $P_w = 10\text{--}20$ MPa, vacuum in the working chamber was kept on the level of $1.33 \cdot 10^{-3}$ Pa.

Thin foils of nickel and copper were produced by electron beam vacuum deposition by the procedure described in detail in [9].

Analysis of structural characteristics of foil and welded joints was performed in scanning electron microscope CAMSCAN 4, fitted with energy dispersive analysis system Oxford INCA Energy 200 to determine the composition on flat samples. For this purpose transverse sections of foils and welded joints were prepared by a standard procedure using grinding-polishing equipment of Struers. Deformational behaviour of thin foils during heating under the conditions of continuous tensile loads was evaluated in a dilatometric system fitted with a special device [10]. Load magnitude was selected as 1/10 of applied

pressure that is equal to about 2–4 MPa at diffusion welding under 20–40 MPa pressure.

Measurement of welded joint Vickers microhardness was performed with application of Polivarmet optical microscope, fitted with an attachment for microhardness measurement, at load on indenter of 0.098 N.

Experimental results and their discussion.

According to the data of [11], one of the methods to produce bimetal cylinder blocks of hydraulic machines is diffusion welding of parts from tin bronze and steel, which is performed at 870 ± 10 °C for 50 min at constant pressure at assembly immersion into a salt bath. After completion of welding process, the parts are subjected to oil quenching that allows increasing steel hardness to required level.

Figure 1 gives a typical microstructure of a defective steel/bronze welded joint produced by diffusion welding at $T_w = 860$ °C with subsequent quenching. High welding temperature leads to tin and lead liquation along grain boundaries with their subsequent evaporation that, alongside thermal stresses arising at joint quenching from welding temperature, promotes appearance of ruptures and discontinuities in the weld zone. In [12] we have shown in the case of stainless steel that application of porous nickel foil allows lowering diffusion welding temperature.

Porous foil characterization. Porous nickel and copper foils produced by EB PVD process were used in the work. Figure 2 gives the characteristic cross-sectional microstructure of foils. It is seen that microstructure of as-deposited foils (Figure 2, a, c) is characterized by columnar structure of grains, the cross-section of which is equal to about 2–3 μm, with elongated pores observed on their boundary, which run through the foil entire thickness.

In [12] in the case of vacuum condensates of nickel, it was shown that the conditions for producing such foils (low deposition temperature $T_d < 0.3T_{\text{melt}}$, where T_{melt} is the melting temperature of deposited metal) promote formation of structurally nonequilibrium state in them. Therefore, structural changes are observed in such foils at low heating, which are accompanied by the processes of pore coalescence and healing. These processes running results in changes in porous structure characteristics: a transition from open to closed porosity is observed, and pore shape changes from elongated to spherical one.

Investigations of deformational behaviour of porous nickel and copper foil at heating under the conditions of continuous tensile stresses (of the order of 2–4 MPa) showed that foil plastic

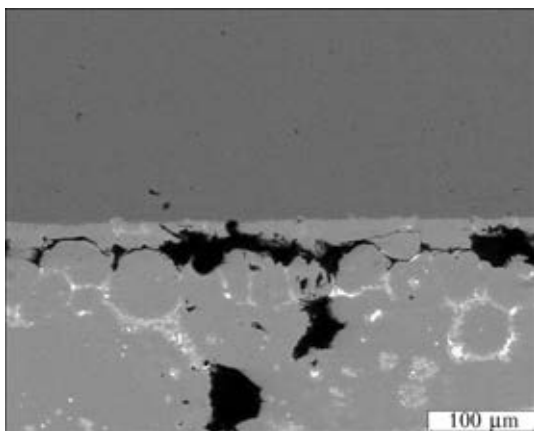


Figure 1. Microstructure of steel/bronze welded joint produced by diffusion welding at $T_w = 860$ °C + quenching

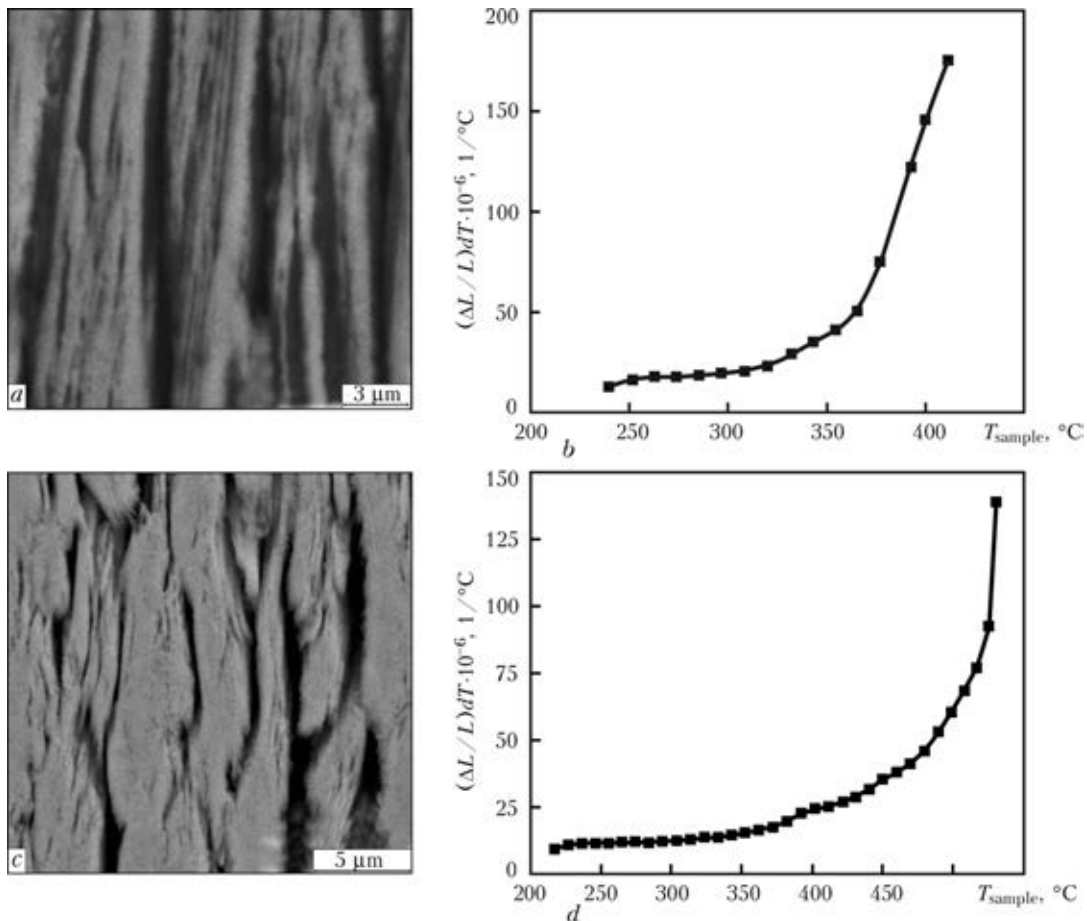


Figure 2. Microstructure and deformation rate of samples of porous foil based on copper with 30 vol.% porosity (*a, b*) and nickel with 25 vol.% porosity (*c, d*)

flow rate non-monotonically depends on temperature. As is seen from Figure 2, *b, d*, foil deformation rate at temperature increase varies as follows: up to 380 and 450 °C for copper and nickel foils, respectively, it remains on the level of metal coefficient of thermal expansion (tensile stresses below the foil yield point), and above the indicated temperatures their deformation rate rises abruptly, and acquires an exponential dependence. Such deformational behaviour of foil at heating is characteristic for materials at their transition into superplastic state, at which plastic deformation runs predominantly by the mechanism of intergranular slipping. In the case of pure metals, structural superplasticity is manifested at their heating above $0.5T_{\text{melt}}$. Plastic deformation localizing along grain boundaries during superplastic flow of materials is accompanied by pore formation that, in its turn, promotes intergranular slipping [13]. This leads to an assumption that lower temperature of porous foil transition into superplastic state, compared to monolithic materials, can be due to presence of pores in them.

Proceeding from that, it can be assumed that interlayers with porous structure will promote

development of plastic deformations in the joint zone at lower temperatures compared to those, at which running of plastic deformation of steel or bronze becomes possible, that is the prerequisite for establishing physical contact between the surfaces being joined and diffusion processes activation in them, and this, in its turn, will promote lowering of welding temperature. Moreover, welding temperature lowering can be influenced also by increased structural inhomogeneity of vacuum condensates.

Welded joint characteristics. Figure 3 shows the microstructures of steel/bronze welded joints produced through porous nickel foil with 25 vol.% porosity and 50 μm thickness at different welding modes. It is seen (Figure 3, *a*) that application of porous nickel interlayer ensures formation of steel/bronze joint already at $T_w = 660^\circ\text{C}$. It should be noted that welding temperature is somewhat higher than that of porous nickel foil transition into the superplastic state (450–500 °C). Considering that formation of permanent joints in diffusion welding requires providing the conditions for intergrowing of grains between surfaces being welded, it can be assumed that at the temperature of interlayer transition

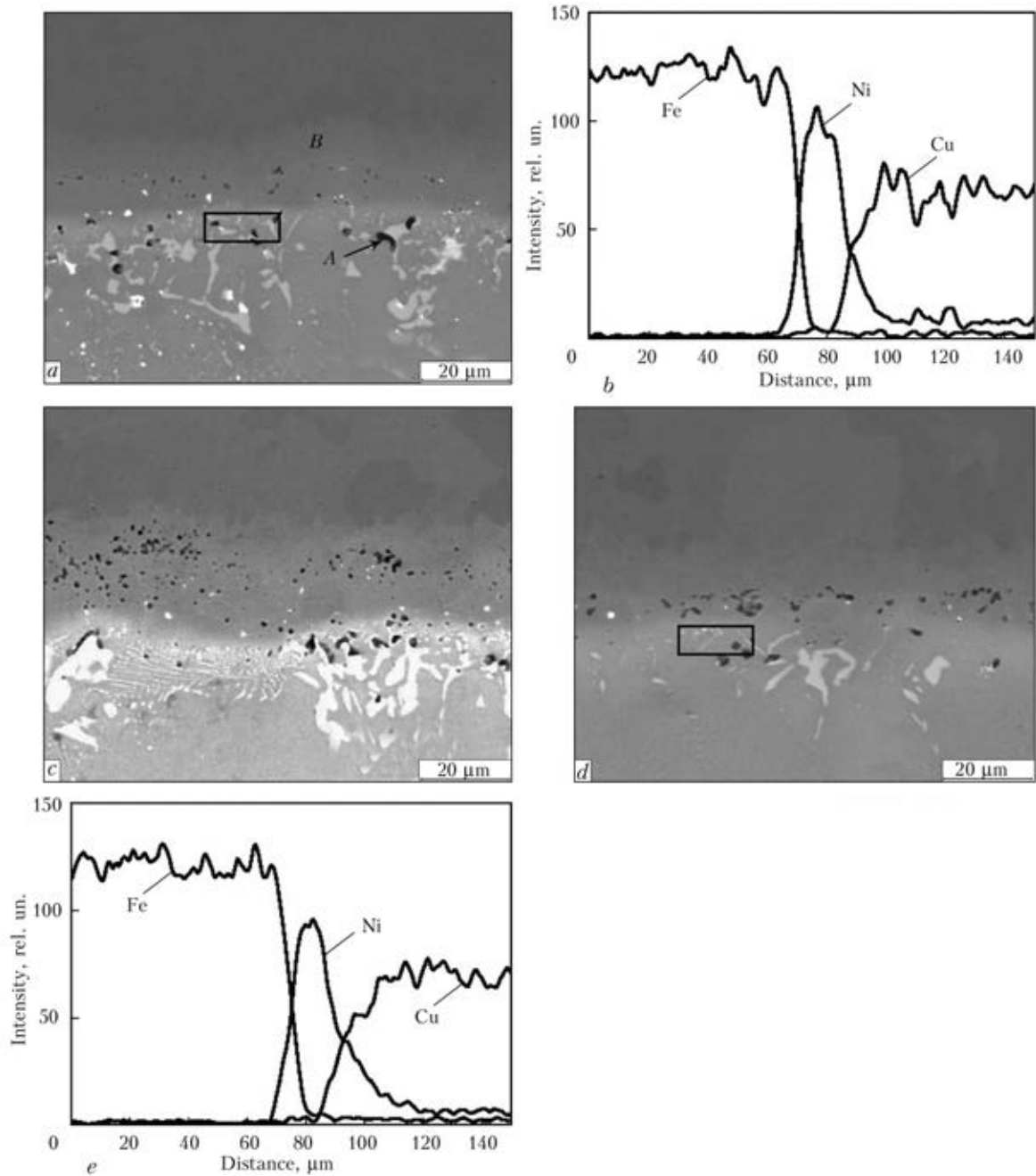


Figure 3. Microstructure of steel/bronze welded joint made by diffusion welding with application of porous nickel interlayer of 25 vol.% porosity and 50 μm thickness: *a* – $T_w = 660^\circ\text{C}$, $t_w = 30$ min; *b* – distribution of main components of materials in joint zone; *c* – $T_w = 700^\circ\text{C}$, $t_w = 5$ min; *d* – $T_w = 700^\circ\text{C}$, $t_w = 20$ min; *e* – main component distribution in the joint zone, shown in Figure 3, *d*

into superplastic state, the rate of diffusion processes running is insufficient to provide these conditions. Results of studying the joint zone microstructure also provide evidence in favour of such a conclusion.

Phase contrast in the image of joint zone microstructure shows that interdiffusion of components of samples being welded and foil occurs at welding temperature. Diffusion-induced interaction of nickel foil with surfaces being welded results in foil becoming saturated with iron atoms from the steel side, and with copper atoms –

from bronze side (Figure 3, *b*). A diffusion zone of inhomogeneous composition forms in the joint zone. More over, pores are observed in the diffusion zone.

Low welding temperature does not provide pore healing, either in nickel interlayer, or of pores in the HAZ, arising at coalescence of vacancies, which form as a result of unbalanced diffusion flows of copper atoms into nickel and those of nickel into bronze (Kirkendall effect). It should be noted that vacancy clusters (pores) form on the boundaries of copper alloy grains in



Composition of joint zone near the interlayer-bronze interface

Welding mode/Interlayer	Composition of joint zone (designated by a rectangle in microstructure image), wt.%				
	Fe	Ni	Cu	Sn	Pb
$T_w = 660\text{ }^\circ\text{C}$, $t_w = 30\text{ min}$ /Ni with 25 vol.% porosity, thickness of 50 μm	0.26	45.41	42.01	10.67	1.65
$T_w = 700\text{ }^\circ\text{C}$, $t_w = 20\text{ min}$ /Ni with 25 vol.% porosity, thickness of 50 μm	0.59	40.01	46.21	13.19	–
$T_w = 700\text{ }^\circ\text{C}$, $t_w = 20\text{ min}$ /Ni with 25 vol.% porosity, thickness of 20 μm	0.45	37.05	50.73	11.77	–
$T_w = 700\text{ }^\circ\text{C}$, $t_w = 20\text{ min}$ /Cu with 30 vol.% porosity, thickness of 30 μm	1.27	3.06	87.22	8.45	–
Bronze	–	4.01	83.38	10.23	2.38

the area of bronze/nickel foil interface (see Figure 3, *a*, point *A*). Pores are absent in the area of diffusion zone from steel side (point *B*). Pore appearance in the area of bronze/nickel foil interface is attributable to the fact that nickel diffusion into bronze stimulates formation of eutectoid component. So, chemical analysis of this zone showed (the Table) that its nickel concentration is much higher than in bronze material. Eutectoid formation results in appearance of an additional vacancy inflow which ensures pore coalescence. At welding temperature increase up to 700 °C, eutectoid volume fraction in

bronze/nickel foil diffusion zone becomes greater (Figure 3, *c*). Here, the short welding time (5 min) is insufficient for pore healing in the joint zone. It is seen that porosity of interlayer and diffusion zone in the area of bronze/nickel foil interface is more pronounced, compared to welding at 660 °C for 30 min (Figure 3, *a*, *c*). At increase of soaking time at 700 °C, porosity decreases both in the interlayer area, and in the area of bronze/nickel foil interface (Figure 3, *d*). On the one hand, bronze/nickel foil diffusion zone becomes wider, while its nickel content per a unit of volume decreases that is indicative of

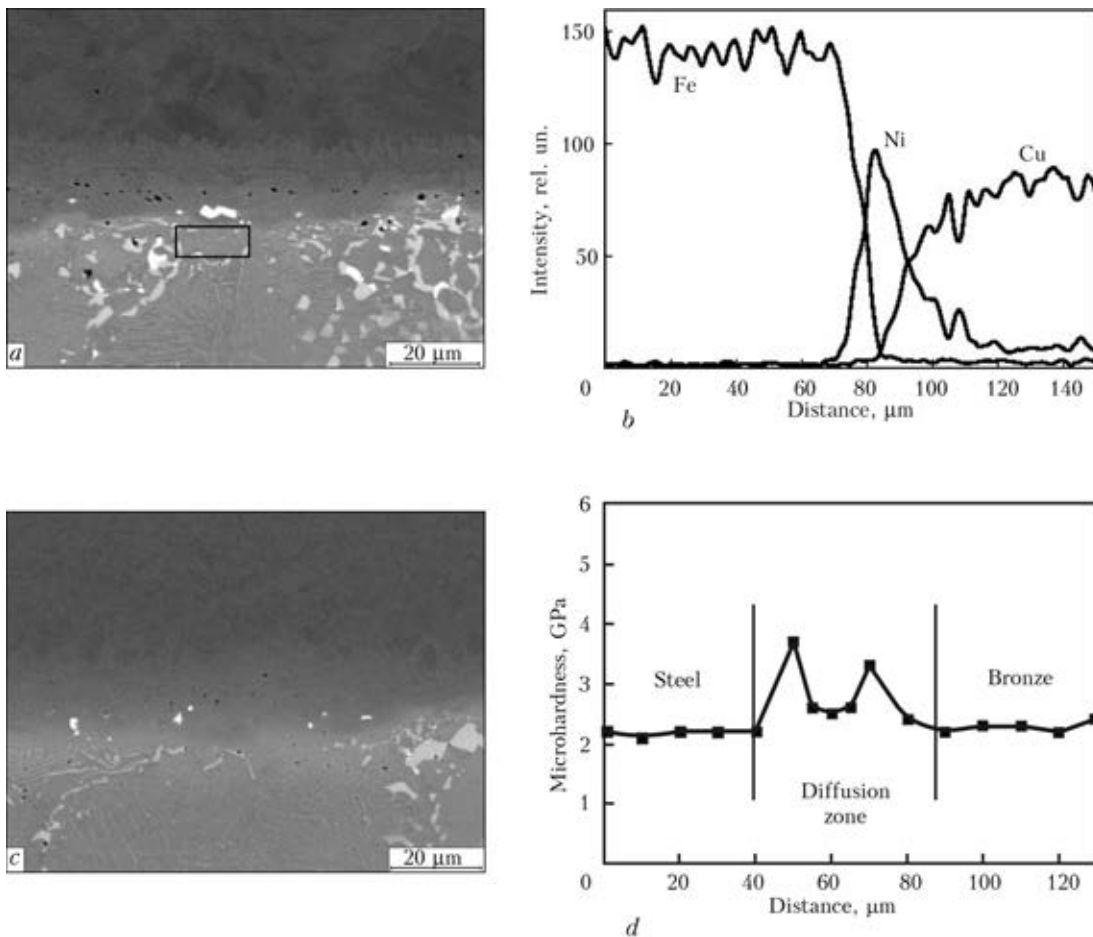


Figure 4. Microstructure of steel/bronze welded joint produced by diffusion welding with application of porous nickel interlayer at $T_w = 700\text{ }^\circ\text{C}$, $t_w = 20\text{ min}$: *a* – 25 vol.% porosity, 20 μm thickness; *b* – respective distribution of main elements in the butt area; *c* – 10 vol.% porosity, 20 μm thickness; *d* – microhardness distribution in the joint zone



lowering of nickel concentration (see the Table), that leads to decrease of eutectoid volume fraction in the area of foil/bronze interface, and, therefore, vacancy inflow due to eutectoid transformation becomes smaller. On the other hand, longer soaking time ensures partial healing of pores, but it appears to be insufficient for complete elimination of porosity.

It is obvious that to eliminate residual porosity in the joint zone, it is necessary to decrease the volume fraction of pores and vacancies, associated with presence of porous foil interlayer in the butt. This can be solved in two ways: first,

by reducing foil thickness, and, second, by reducing its porosity.

Figure 4, *a* shows the microstructure of steel/bronze welded joint, produced by diffusion welding at $T_w = 700\text{ }^\circ\text{C}$, $t_w = 20\text{ min}$, using an interlayer of nickel foil with porosity of 25 vol.% and 20 μm thickness. Application of thinner porous foil ensures reduction of residual nickel layer in the joint zone (Figure 4, *b*). Here, porosity in the foil area and in the diffusion zone from bronze side is reduced that can be the consequence of both reduction of eutectoid volume fraction, because of lowering of nickel concentration in this area (see the Table), and of pore healing. Application of interlayers with smaller porosity (of the order of 10 vol.%) and 20 μm thickness essentially lowers pore concentration both in the interlayer area, and near the nickel interlayer/bronze interface (Figure 4, *c*). Inhomogeneous composition of the diffusion zone affects microhardness distribution in the joint zone (Figure 4, *d*). It is seen that interdiffusion of the components of steel, bronze and interlayer leads to formation in the joint zone of material regions of higher microhardness than that in initial materials.

From the steel side diffusion interaction of iron and nickel leads to formation of particles of intermetallic compound FeNi_3 that ensures precipitation hardening of material. Interdiffusion of copper and nickel leads to formation in the butt of material close to Monel high-strength alloy as to its composition. Obtained results give grounds to state that application of porous nickel interlayer in diffusion welding of steel and bronze intensifies the diffusion processes in the joint zone. On the one hand, this is promoted by establishing of good physical contact of the surfaces being welded due to superplastic behaviour of porous foil, and, on the other hand – relaxation of foil non-equilibrium state through pore coalescence and healing activates diffusion interaction of material components in the joint zone. Application of porous nickel foil allows lowering welding temperature that prevents appearance of the liquid phase on bronze surface and improves joint strength.

It is known [4] that one of the methods, preventing appearance of liquid phase on bronze surface during the welding process, is welding a thin copper interlayer to steel surface. In this connection, it is of interest to apply porous copper foil as interlayer in diffusion welding of steel and bronze. Figure 5, *a* shows the microstructure of steel/bronze joint produced by diffusion welding with application of an interlayer of copper with 30 vol.% porosity and 30 μm thickness at

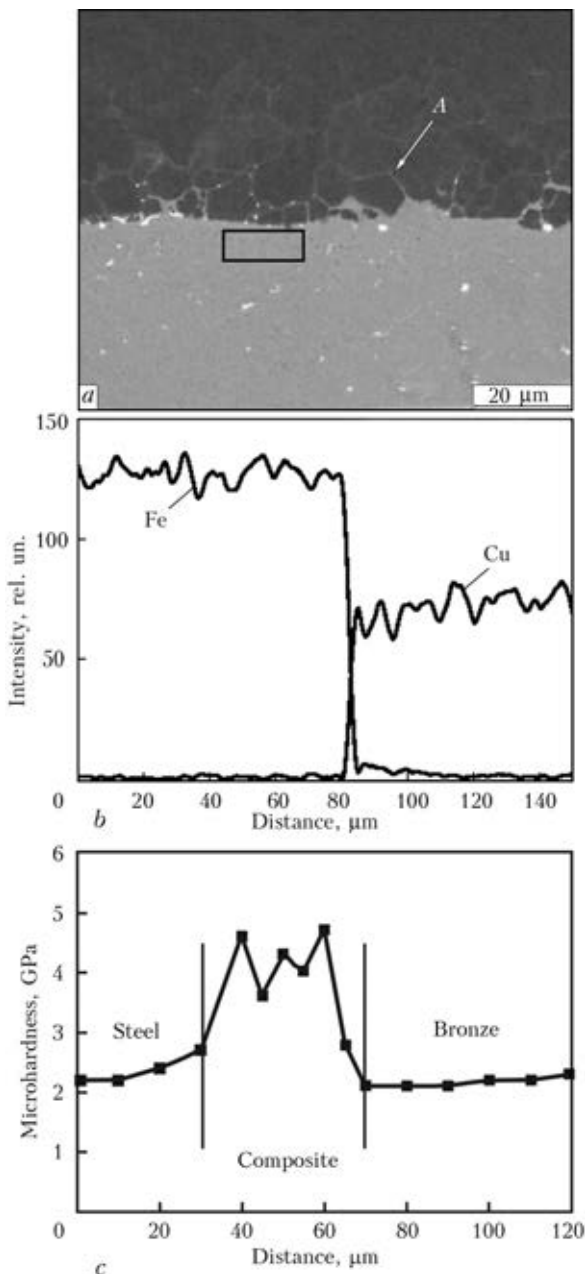


Figure 5. Microstructure of steel/bronze welded joint made by diffusion welding with application of porous copper interlayer with 30 vol.% porosity and 30 μm thickness at $T_w = 700\text{ }^\circ\text{C}$, $t_w = 20\text{ min}$ (*a*), distribution of main elements (*b*) and microhardness (*c*) in the joint zone



$T_w = 700\text{ }^\circ\text{C}$, $t_w = 20\text{ min}$. It is seen that the joint zone has no residual porosity. Absence of copper-based interlayer or clearcut interdiffusion zone in the joint zone is indicative of intensive diffusion of components of materials being joined and copper foil. Proceeding from element distribution in the joint zone (Figure 5, *b*) and data on chemical composition from bronze side (see the Table), it can be noted that in the area of copper interlayer location alloying element concentration is practically the same as in bronze, i.e. intensive redistribution of elements proceeds between porous copper interlayer and bronze during diffusion welding that promotes pore healing. At the same time, phase contrast in the image of joint microstructure (see Figure 5, *a*, point *A*) points to copper diffusion along steel grain boundaries.

Thus, performed studies lead to the conclusion that during welding diffusion interaction of porous copper interlayer on steel/copper interface is determined by grain-boundary diffusion of copper into steel, and that on the interface with bronze — by tin and nickel diffusion from bronze into copper. Diffusion redistribution of components during welding leads to formation in the joint zone of an interlayer of a steel-based composite with high microhardness. It can be assumed that such a change of mechanical properties in welded joint will promote localizing of plastic deformation under the impact of external load, chiefly, in bronze regions directly adjacent to steel. A smoother microhardness change in the area of steel/bronze joint produced with application of porous nickel interlayer will, probably, provide a more diffuse area of relaxation processes running at external loads.

Conclusions

1. Application of interlayers based on porous nickel and copper foil allows lowering the temperature of diffusion welding of steel/bronze to 660–700 °C.

2. It is shown that at diffusion welding of steel and bronze through porous nickel foil the welded joint structure forms from the steel side by interdiffusion of nickel and iron atoms, and

from bronze side — by that of nickel and copper atoms that leads to formation of material interlayers of higher microhardness in the butt area.

3. Structure of steel/bronze welded joint, made through porous copper interlayer forms by grain boundary diffusion of copper atoms into steel and by nickel and tin atoms diffusion into copper that promotes formation of a composite with higher microhardness in the joint zone.

1. Kazakov, N.F. (1976) *Diffusion welding of materials*. Moscow: Metallurgiya.
2. Malevsky, Yu.B., Nesmikh, V.S. (1981) *Pressure welding of bronze with steel*. Moscow: Metallurgiya.
3. Potekhin, B.A., Izmajlov, D.K. (2008) Peculiarities of vacuum diffusion welding without application of external pressure. *Svarochn. Proizvodstvo*, **2**, 8–13.
4. Kazakov, N.F. (1981) *Diffusion welding of materials*: Refer. Book. Moscow: Mashinostroenie.
5. Charukhina, K.E., Golovanenko, S.A., Masterov, V.E. et al. (1970) *Bimetallic joints*. Moscow: Metallurgiya.
6. Ustinov, A., Falchenko, Y., Melnichenko, T. et al. (2013) Diffusion welding of aluminium alloy strengthened by Al₂O₃ particles through an Al/Cu multilayer foil. *J. Materials Proc. Techn.*, **213**(4), 543–552.
7. Lyushinsky, A.V. (2011) Application of nanopowders of metals in diffusion welding of dissimilar materials. *The Paton Welding J.*, **5**, 31–34.
8. Kharchenko, G.K., Ustinov, A.I., Falchenko, Yu.V. et al. (2011) Diffusion bonding of γ -TiAl base alloy in vacuum by using nanolayered interlayers. *Ibid.*, **3**, 2–6.
9. Ustinov, A.I., Lyapina, K.V., Melnichenko, T.V. (2005) Regularities of stainless steel porous structure formation during its deposition from vapor phase in presence of sodium chloride vapors. *Advances in Electrometallurgy*, **4**, 19–24.
10. Ustinov, A.I., Matvienko, Ya.I., Polishchuk, S.S. et al. (2009) Investigation of phase transformations and plastic deformation at continuous heating of Al/Cu multilayer foil. *The Paton Welding J.*, **10**, 23–27.
11. Vajvod, N.I., Bykov, G.M. (1982) Diffusion welding in production of cylinder blocks of axial-plunger pumps. *Svarochn. Proizvodstvo*, **3**, 32–33.
12. Ustinov, A.I., Falchenko, Yu.V., Melnichenko, T.V. et al. (2015) Vacuum diffusion welding of stainless steel through porous nickel interlayers. *The Paton Welding J.*, **7**, 3–9.
13. Kuznetsova, R.I., Bryukhovetsky, V.V., Pojda, V.P. (1995) Mechanisms of development of grain-boundary pores and local deformation heterogeneity under conditions of superplastic flow. *Metallofizika i Nov. Tekhnologii*, **17**(8), 64–72.

Received 30.04.2015



ANALYSIS OF PROCESS OF BEAD SHAPING IN CLADDING ON NARROW SUBSTRATE

K.A. YUSHCHENKO, A.V. YAROVITSYN, G.D. KHRUSHCHOV, A.A. FOMAKIN and Yu.V. OLEJNIK

E.O. Paton Electric Welding Institute, NASU

11 Bozhenko Str., 03680, Kiev, Ukraine. E-mail: office@paton.kiev.ua

Analysis of geometry dependencies of bead shaping was carried out at full-scale modelling of technologically possible cross-sections of beads deposited on narrow substrate of 0.5–5.0 mm thickness. The tasks were specified for technological regulation of shape of single-layer bead and series of process criteria was stated, namely efficient rising of narrow substrate being deposited, optimum effective cross-section of the bead and acceptable side machining allowances. Proposed are the formulae for estimation engineering calculations determining the relationship between required height of deposited layer, bead size, mass of deposited metal and filler consumption. 16 Ref., 3 Tables, 9 Figures.

Keywords: microplasma powder cladding, nickel heat-resistant alloy, narrow substrate, full-scale modelling of bead cross-section, process criteria of bead shape

Significant scope of works in repair of parts of aircraft gas turbine engines falls at repair or strengthening of their sealing and antivibration elements of 0.5–5.0 mm width and length from 10–15 mm to 2–3 m. Argon-arc [1, 2] or microplasma powder cladding [3–5] applying nickel heat-resistant alloys as filler material are used for solving of such tasks. It is carried out under conditions of free bead formation on vertically positioned construction element of part. A bead is formed under effect of gravity force, arc pressure, internal friction of molten metal (toughness) and surface tension in processes of cladding. Its cross-section contour is approximated to circumference or ellipse (Figure 1). A special term «narrow substrate», i.e. elements of surface of base metal, width of which do not exceed weld pool width [6, 7], was taken by the E.O. Paton

Electric Welding Institute for such surfaces being deposited.

Example of three-layer microplasma powder cladding of fragment of tip of blade airfoil (Figure 2) was used for expansion of concept on geometry and process dependencies in formation of narrow bead-on-plate for nickel heat-resistance alloys with limited weldability [8, 9]. Analysis of modes of cladding carried on procedure from work [10] shows that growth of cross-section size of deposited bead from JS32 alloy of 2–4 mm range at limited change of welding current (1–3 A) is accompanied by significant increase of heat input. In turn, more than 2 times increase of heat energy input during arc burning promotes for formation of microcracks in the deposited metal at further heat treatment based on homogenizing mode for JS26 and JS32 alloys.

It should be noted that mechanism of technological regulation of cross-section of deposited metal in cladding of 0.5–5.0 mm width narrow substrate is fragmentary studied [2, 3, 11]. Therefore, in order to form corresponding representations of aims and tasks of such regulation, it is initially reasonable to analyze predicted shape of deposited beads in the range of their relative width $B/\delta = 1-10$ and relative height $H/\delta \leq 4$. These indices characterize a set of sizes of bead cross-sections, which can be kept on considered narrow substrate without application of forming devices in process of microplasma and argon-arc cladding. Taking into account mentioned above the aim of the present work is:

- analysis of dependencies of distribution of deposited and base metal in possible bead cross-sections and formation of generalized criteria of their shape optimality, and

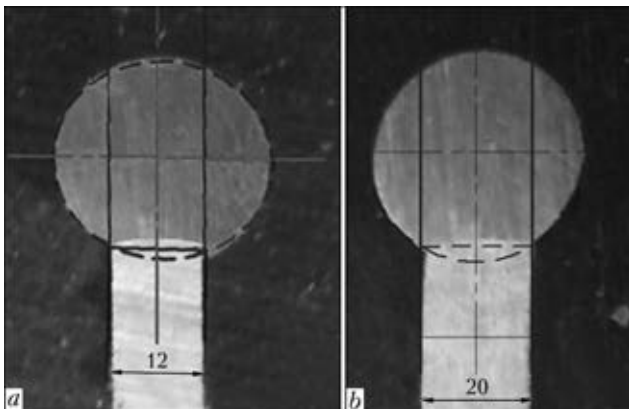


Figure 1. Contour of cross-section of beads deposited on narrow substrate of different width: *a* – ellipse; *b* – circumference

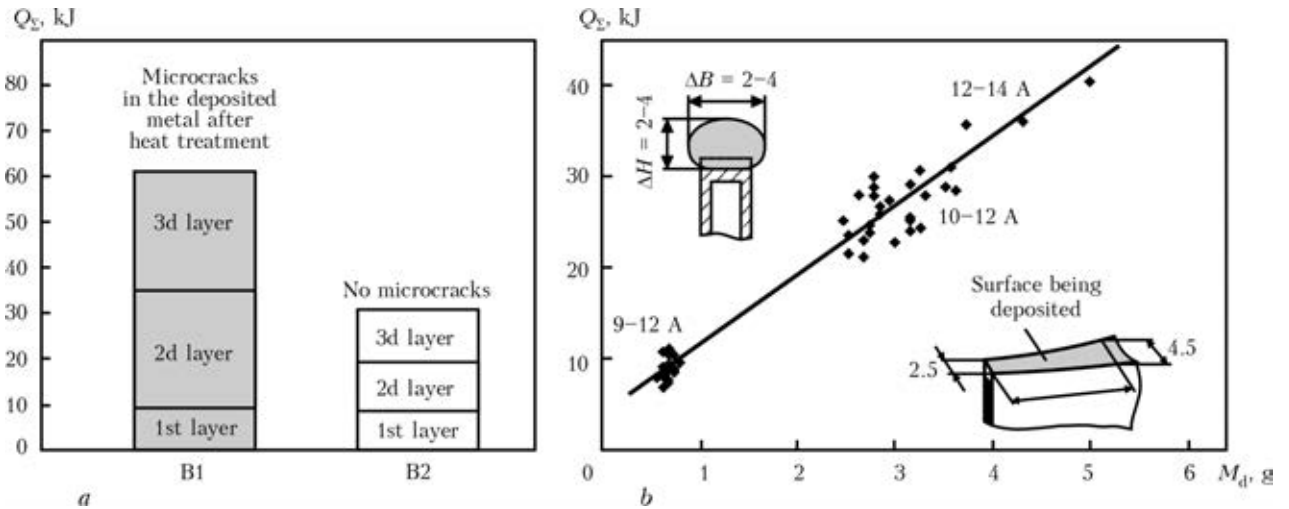


Figure 2. Tendency to microcrack formation in deposited metal JS32 at 3-layer microplasma powder cladding of tip of blade airfoil (a), and dependence of total heat input in anode Q_{Σ} on mass M_d of bead deposited per one layer (b)

• deriving of engineering dependencies to determine the relationship between the necessary height of deposited layer, bead size, mass of deposited metal and filler consumption, required for corresponding repair-reconstruction technologies.

Figure 3 and Table 1 give initial geometry indices of bead deposited on narrow substrate necessary for further analysis of its shape. Authors of the paper tried to approximate definitions of the most of them to ones traditionally accepted for bead-on-plate [12, 13]. Series of new definitions, i.e. effective bead height h , bead cross-section F_E , cross-section of deposited metal in bead F_{DP} , were implemented due to the necessity of study of size of rectangle with sides δ and $(h + h_{BM})$ inscribed in bead contour. The following assumptions were taken in analysis of bead cross-section (see Figure 3):

• bead contour is the part of circumference or ellipse;

• fusion line of base and deposited metals lies in AB segment;

• areas of corresponding ellipse or circumference and contour of bead cross-section differ per ΔF_1 segment value, which equals the area of bead upper reinforcement;

• molten base metal does not come out of the limits of narrow substrate and being localized in rectangle with δ and h_{BM} sides;

• after machining deposited metal has rectangular cross-section with δ and $h_{BM} + h$ sides.

Shape of beads was studied by means of full-scale modelling of technologically possible cross-sections at variation of δ , H , B parameters and determination of areas of its constituents (Figure 4) in the program of system for automatic computer-aided design of process documents Compass-3D V12. The following most probable laws of sequential change of geometric configuration corresponding to bead contour were considered: diameter of circumference increases (Figure 5, a), horizontal axis of ellipse expands up

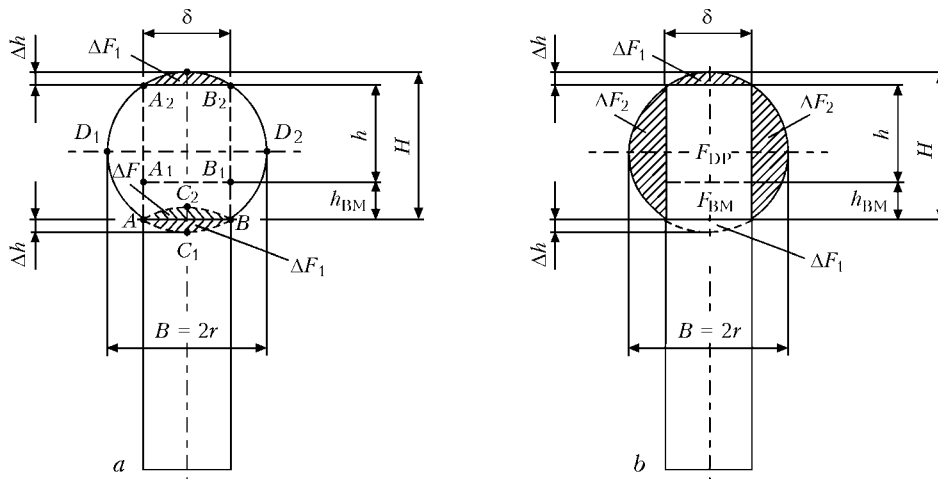


Figure 3. Basic indices of bead cross-section in single-layer cladding on narrow substrate (a) (designations see in Table 1), and (parts of the bead (b) removed in machining of deposited metal) (hatched)



Table 1. Main geometry indices of cross-section of bead deposited on narrow substrate

No.	Parameter	Designations according to Figure 3
1. Size		
1.1	Width of narrow substrate	δ
1.2	Bead width	B
1.3	Bead height	H
1.4	Depth of base metal penetration	h_{BM}
1.5	Effective height of deposited metal	h
1.6	Effective height of bead	$h_{BM} + h$
1.7	Thickness of bead side reinforcement	$\Delta p = 0.5(B - \delta)$
1.8	Height of bead upper reinforcement	$\Delta h = H - h - h_{BM}$
2. Relative size		
2.1	Relative width of bead	B/δ
2.2	Relative height of bead	H/δ
2.3	Relative depth of base metal penetration	$h_{BM}/(h_{BM} + h)$
2.4	Relative height of bead upper reinforcement	$\Delta h/(H + \Delta h)$
3. Contour		
3.1	Geometry figure corresponding to bead contour	Closed $AC_1BD_2CD_1$ curve
3.2	Perimeter of bead contour	Closed ABD_2CD_1 curve
4. Cross-section area		
4.1	Area of base metal penetration	$F_{BM} = h_{BM}\delta$
4.2	Effective area of deposited metal in bead	$F_{DP} = h\delta$
4.3	Effective bead section	$F_E = F_{BM} + F_{DP}$
4.4	Area of bead upper reinforcement	Segment ΔF_1
4.5	Area of bead side reinforcement	Segment ΔF_2
4.6	Area of deposited bead (limited by perimeter of bead contour)	$F_B = F_E + \Delta F_1 + 2\Delta F_2$
4.7	Area of geometry figure corresponding to bead contour	$F_{BCF} = F_E + 2\Delta F_1 + 2\Delta F_2$
5. Relationship of areas of elements in bead cross-section		
5.1	Portion of base metal	$\gamma_{BM} = F_{BM}/F_B$
5.2	Relative area of bead effective section	$\gamma_E = F_E/F_B$
5.3	Relative area of effective section of deposited metal	$\gamma_{ED} = F_{DP}/F_B$

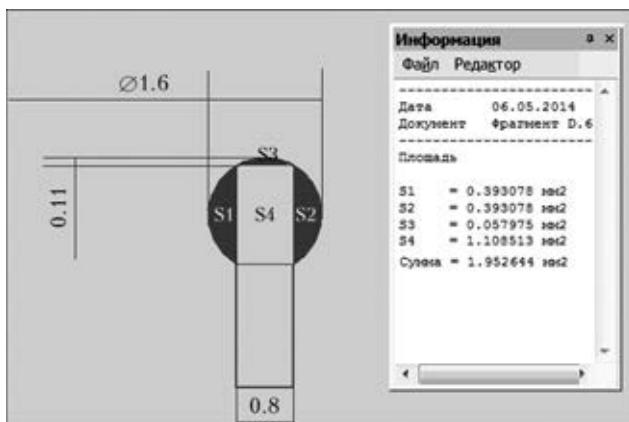


Figure 4. Example of determination of area of bead cross-section elements at their full-scale modelling in system of automated computer-aided design Compass-3D V12

to circumference (Figure 5, *b*), and vertical axis of ellipse stretches up to circumference (Figure 5, *c*).

Initially, full-scale modelling of technologically possible shapes of cross-section of single-layer deposited metal was carried out for narrow substrate of $\delta = 0.8, 1.5, 4$ and 6 mm in the ranges of bead width-to-height relationship of $B = (1-10)\delta$ and $H \leq 4\delta$. Amount of analyzed cross-sections made 40–50 pcs for each dimension type of width of narrow substrate. Obtained data array γ_E and B/δ was estimated on membership to general dependence $\gamma_E = f(B/\delta; \gamma_{BM} = 0)$ visually as well as using statistical criteria* [14], namely

* At $\gamma_E = f(B/\delta)$ division for series of linear sections.



Pearson (R), index of determination (R^2) and Fischer (F).

After that, determined geometry dependencies of bead shape were cross-checked for $\delta = 0.5, 2, 3, 5, 8$ and 10 mm by means of random sampling of bead width-to-height relationship in the same range. Amount of analyzed possible cross-sections made $10-15$ pcs for each additional dimension type of narrow substrate width.

Figure 6 shows collection of $\gamma_{DP} = f(B/\delta; \gamma_{BM})$ dependencies obtained as a result of processing of data of full-scale modelling of technologically possible cross-sections of deposited beads. $\gamma_{ED} < 0$ case corresponds to lowering of narrow substrate relatively to its initial level Z_1Z_2 , $\gamma_{ED} > 0$ – to rising. Approximation of aggregate of points B/δ and γ_{BM} by power function at which $\gamma_{ED} = 0$ at $B/\delta > 1.4$ allowed connecting condition of narrow substrate rising with one of the most important indices of cladding efficiency, i.e. portion of base metal in the deposited bead:

$$\gamma_{BM} < \gamma_E = \left(\frac{B}{\delta}\right)^{-0.866} \quad (1)$$

Thus, increase of rising efficiency of narrow substrate being deposited with expansion of relative bead width requires more rigid limitation of portion of base metal in it. It should also be noted that maximum $\gamma_E = 0.714$ values (see curve 1 in Figure 6) is observed for $B/\delta = 1.28$, and relative area of upper and side bead reinforcements is minimum at that. Beads with $B/\delta = 1.2-1.4$, for which $\gamma_E > 0.7$, can be assumed at some approximation as corresponding to criterion of maximum

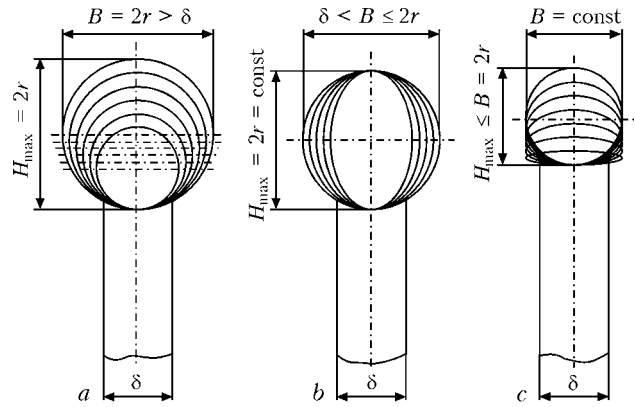


Figure 5. Typical changes of shape of bead cross-section at variation of parameters of mode of narrow substrate cladding of effective cross-section area. For $B/\delta = 1.4-10$, γ_E value in $0.12-0.70$ value range can be specified with the help of dependence (1).

Preliminary specification of portion of base metal is necessary for analysis of peculiarities of metal distribution between central part and periphery of the bead. Content of deposited γ_{ED} and base metal γ_{BM} in the central part of the bead is, respectively:

$$\gamma_{ED} = \gamma_E - \gamma_{BM}, \quad (2)$$

$$\gamma_{BM} = \frac{F_{BM}}{F_B} = \frac{h_{BM}\delta}{F_B}, \quad (3)$$

where, in the cross-section of deposited bead h_{BM} , F_{BM} are the depth and area of base metal penetration, and F_B is the bead area. F_B value can be calculated as

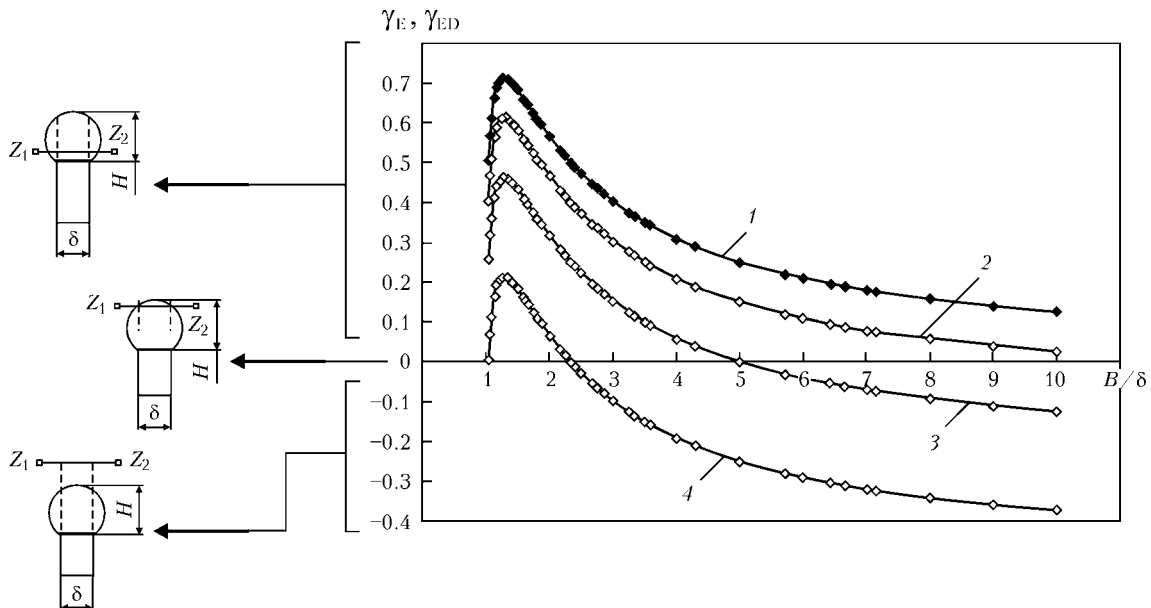


Figure 6. Dependence of relative area of effective bead section γ_E and relative area of effective section of deposited metal γ_{ED} on relative width of bead B/δ (based on data of statistical processing of full-scale modelling results): Z_1, Z_2 – level of narrow substrate before bead deposition; 1 – $\gamma_E = \gamma_{ED}$ at $\gamma_{BM} = 0$; 2 – γ_{ED} at $\gamma_{BM} = 0.1$; 3 – at $\gamma_{BM} = 0.25$; 4 – at $\gamma_{BM} = 0.5$

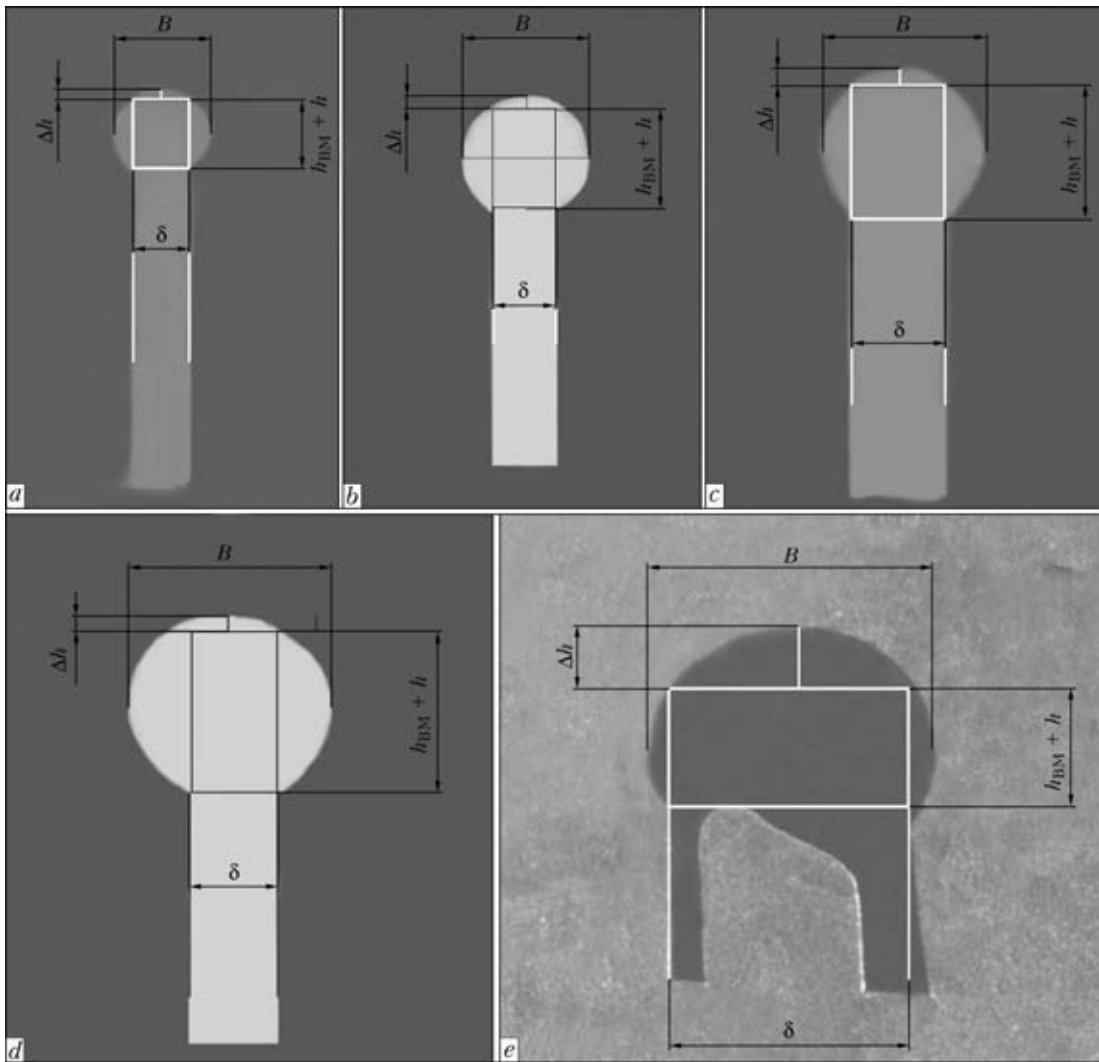


Figure 7. Scheme of measurements of sizes and view of cross-section contours of beads deposited on narrow substrate of different width (according to Table 2)

$$F_B = F_{BCF} - \Delta F_1 = 0.25\pi B(h_{BM} + h) - \Delta F_1, \quad (4)$$

where F_{BCF} is the area limited by figure of contour of bead cross-section (ellipse or circumference); Δh , ΔF_1 are the value and area of bead upper reinforcement, respectively. In turn, ΔF_1 value of circumference segment area (or in general case — ellipse) can be approximately calculated similar to area of upper reinforcement of butt weld [13]:

$$\Delta F_1 = 0.73\Delta h\delta. \quad (5)$$

Value of upper reinforcement of deposited bead Δh , which combines necessary height of deposited layer with necessary bead height, is to be determined for calculations on dependencies (1)–(5). Formulae for calculation of saggita of segment [15] can be used for figures in form of circumference, corresponding to bead contour, however, accurate calculation of Δh for figure in form of ellipse is complicated.

Processing of statistical data of full-scale modeling showed that given parameter can have the

Table 2. Comparison of calculation and actual value of bead upper reinforcement Δh deposited on narrow substrate of different width

Parameter	Figure 7, a		Figure 7, b		Figure 7, c		Figure 7, d		Figure 7, e	
	$\Delta = 1.2 \text{ mm}$		$\Delta = 1.2 \text{ mm}$		$\Delta = 2.0 \text{ mm}$		$\Delta = 2.0 \text{ mm}$		$\Delta = 5.0 \text{ mm}$	
	Calc.	Actual								
B , mm	–	2	–	2.40	–	3.32	–	4.52	–	6
B/δ	1.67	–	2	–	1.66	–	2.26	–	1.20	–
$h_{BM} + h$, mm	–	1.49	–	1.95	–	2.66	–	3.57	–	2.77
Δh , mm	0.20	0.23	0.16	0.20	0.36	0.43	0.30	0.22	1.06	1.20



most reasonable expression via relative height of bead upper reinforcement $\Delta h / (H + \Delta h)$. Indicted dependence is approximated to power function with high degree of certainty

$$\frac{\Delta h}{H + \Delta h} = 0.3215 \left(\frac{B}{\delta}\right)^{-2.161} \quad (6)$$

Taking into account that $H = h_{BM} + h + \Delta h$, the following expression for upper reinforcement of the deposited bead is received after series of transformations:

$$\Delta h = \frac{0.3215 \left(\frac{B}{\delta}\right)^{-2.161} (h_{BM} + h)}{1 - 0.6430 \left(\frac{B}{\delta}\right)^{-2.161}} \quad (7)$$

Numerical modelling data based on dependence (7) indicate that the value of bead upper reinforcement does not exceed 1 mm. Δh value can make several millimeters in the case of combination of $B/\delta > 2$ and $h_{BM} + h > 3-5$ mm that should be taken into account in selection of size of the deposited bead. It is determined (Figure 7, Table 2) that acceptable level of convergence of calculation (7) and experimental data is achieved for height of bead upper reinforcement Δh .

Substitution of expressions (4), (5), (7) in dependence (3) and some transformations provide for the following expression of portion of base metal γ_{BM} through relative penetration depth of base metal $h_{BM} / (h_{BM} + h)$ and relative bead width B/δ :

$$\gamma_{BM} = \frac{h_{BM}}{h_{BM} + h} \times \frac{\left[1 - 0.6430 \left(\frac{B}{\delta}\right)^{-2.161}\right]}{0.25\pi \left(\frac{B}{\delta}\right)^{-2.161} - 0.2347 \left(\frac{B}{\delta}\right)^{-2.161}} \quad (8)$$

Let us plot dependencies (1), (2), (8) on one diagram and estimate distribution of metal between effective bead section and its reinforcements at relative bead width more than 1.4 (Figure 8). Numerical modeling data show that content of base metal in the bead can make 2–22 % in area of optimum modes of cladding ($h_{BM} / (h_{BM} + h) = 0.1-0.3$). Efficiency of filling of bead central part by molten metal is sequentially reduced due to increase of area of side allowances at rise of B/δ relationship.

Due to the fact that portion of base metal in the deposited bead is limited, it is reasonable to extend concept of dependencies of consumption

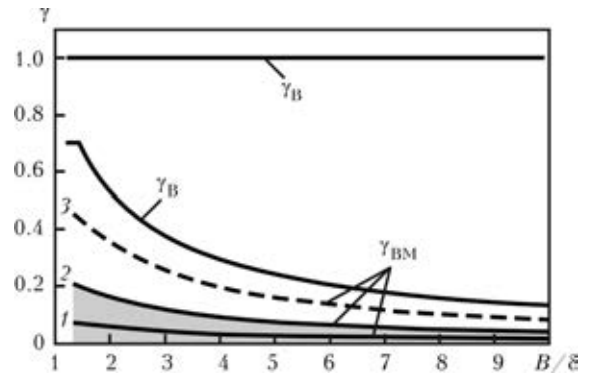


Figure 8. Balance of metal distribution in deposited bead depending on relative bead width: γ_B – whole metal; γ_E – portion of metal in bead effective section; γ_{BM} – portion of base metal corresponding to values of relative depth of penetration; 1 – $h_{BM} / (h + h_{BM}) = 0.1$; 2 – 0.33; 3 – 0.66 (area of filling corresponds to optimum cladding modes)

of filler metal in narrow substrate cladding. They are determined by direct and indirect filler loss.

The first type of loss is mainly provoked by distributed feed of disperse filler in the weld pool [3, 16]. The second one is due to «redistribution» of deposited metal from rectangle with δ and $(h + h_{BM})$ sides in area of upper and side reinforcements (see Figures 1 and 3). Limitation of cross-section areas ΔF_1 and ΔF_2 in the deposited bead is one of the important technological tasks for such type of deposition due to appropriateness of reduction of consumption of arc heat and costs on expensive filler for cladding of «excess» bead volume which is subsequently removed by machining.

The production practice showed that $\Delta p = 0.50-1.25$ mm thickness range of bead side reinforcement corresponds to optimum labor expenditures of further treatment. Verification of correspondence of criteria of optimum effective cross-section and optimum labor expenditures directed on treatment of bead deposited over $\delta = 0.5-10$ mm narrow substrate is represented in form of numerical solution (Table 3) of system of equations:

Table 3. Change of relative width of bead B/δ depending on width of narrow substrate δ at thickness of bead side reinforcement $\Delta p = 0.50-1.25$ mm

δ , mm	B/δ	δ , mm	B/δ
0.5	3–6	5	1.20–1.50
1.0	2–3.50	6	1.17–1.42
1.5	1.67–2.67	7	1.14–1.35
2.0	1.50–2.25	8	1.13–1.31
2.5	1.40–2	9	1.11–1.28
3.5	1.28–1.71	10	1.10–1.25

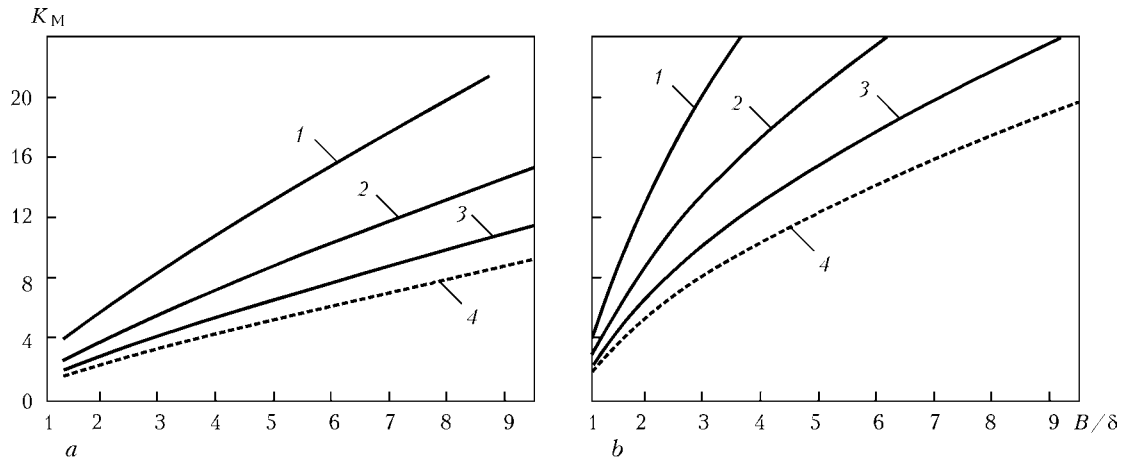


Figure 9. Numerical modelling of coefficient of filler specific consumption K_M depending on relative width of bead and relative depth of penetration: *a* – $h_{BM}/(h + h_{BM}) = 0.25$; *b* – 0.66 at CFU = 0.4 (1), 0.6 (2), 0.8 (3) and 1.0 (4)

$$\frac{B}{\delta} = \frac{\delta + 2\Delta p}{\delta}; \quad (9)$$

$$1.2 \leq B/\delta \leq 1.4. \quad (10)$$

It is well known fact that mass of deposited metal M_D can be determined based on cross-section area of deposited metal F_D , bead length L and material density ρ_M :

$$M_D = F_D L \rho_M. \quad (11)$$

Here

$$F_D = F_B - F_{BM} = F_B - h_{BM}\delta. \quad (12)$$

In turn, F_B area can be expressed through relative effective cross-section of bead γ_E :

$$F_B = \frac{F_E}{\gamma_E} = \frac{(h_{BM} + h)\delta}{\gamma_E}. \quad (13)$$

Taking into account (1) the following is received after some transformations:

$$F_B = (h_{BM} + h)\delta(B/\delta)^{0.866}. \quad (14)$$

Dependencies (11)–(14) allow estimating necessary mass of deposited metal for narrow substrate depending on required effective height of deposited metal h . A coefficient of specific consumption K_M , calculated considering dependencies (2) and (8), is appropriate for demonstration of dynamics of consumption of filler material in its reconstruction. It characterizes increase of total amount of filler in comparison with consumed for filling of bead central part:

$$K_M = CFU^{-1}(\gamma_{ED})^{-1}; \quad (17)$$

$$M_N = K_M M_0 N, \quad (18)$$

where CFU is the coefficient of filler use; M_0 is its consumption for rectangle with δ and h sides

in one part; N is the amount of parts recovered by cladding. The results of numerical modelling of K_M value (Figure 9) show significant dependence of filler consumption on width of narrow substrate, coefficient of filler use, relative width of bead and relative depth of penetration of base metal. Figure 9 also shows an appropriateness of development and realizing of additional block of process activities directed on rise of efficiency of disperse filler application (for microplasma powder cladding).

Thus, it is determined that generalized geometry criterion of shape of studied beads is their relative width. Its value of 1.2–1.4 provides for the maximum relationship of areas of central part and total bead cross-section area, namely approximately 0.7. The condition of rise of narrow substrate in process of single layer cladding is related with limitation of portion of base metal in the bead $\gamma_{BM} < \gamma_E = (B/\delta)^{-0.866}$. Portion of base metal for optimum cladding modes and depending on relative bead width should make 3–22 % of total bead volume. The possibility of combination of criteria of optimum bead shape and optimum machining allowance 0.50–1.25 mm depend on width of narrow substrate and can be complete for $\delta = 5$ –7 mm and partial for $2.5 \leq \delta < 5.0$ mm. Only sequential approximation to optimum distribution of metal between bead central part and its reinforcements is possible in the case of $\delta < 2.5$ mm narrow substrate at indicated machining allowance.

Obtained data on dependencies of shaping of cross-section of deposited metal and necessary filler consumption also indicate that optimizing the width of bead deposited on narrow substrate allows 10–40 % reduction of amount of «excess» deposited metal and, respectively, decrease amount of irrational heat input to the anode. This will have positive effect on weldability of



nickel heat-resistant alloys in cladding (particularly, multi-layer) on narrow substrate as well as allow significant limitation of consumption of filler material and labor expenditures of given repair-reconstruction technology.

Conclusions

Analysis is given to geometry dependencies of shaping of single layer bead on narrow substrate of 0.5–5.0 mm width and tasks are specified for process regulation of its shape during cladding in part concerning effective rising of narrow substrate, optimum effective cross-section area of the bead and acceptable side machining allowances.

Proposed are the formulae for estimation engineer calculations determining the relationship between required height of deposited layer, bead size, mass of deposited metal and filler consumption in narrow substrate cladding. They can be used in development of repair-reconstruction technologies for parts of aircraft gas-turbine engines.

1. Peremilovsky, I.A., Gejchenko, V.S., Frumin, I.I. (1976) Repair surfacing of aircraft engine turbine blades. *Avtomatich. Svarka*, **5**, 54–56.
2. Arzhakin, A.N., Stolyarov, I.I., Turov, A.V. (2003) Development of technology for repair of 8th stage blades of aircraft engine using automatic surfacing method. *Svarshchik*, **4**, 8–9.
3. Yarovitsyn, A.V., Yushchenko, K.A., Nakonechny, A.A. et al. (2009) Peculiarities of low-amperage argon-arc and microplasma powder cladding on narrow substrate. *The Paton Welding J.*, **6**, 31–35.
4. (2010) Technological Seminar of Deloro Stellite in Zaporozhie. *Ibid.*, **1**, 46–49.
5. Yushchenko, K.A., Savchenko, V.S., Yarovitsyn, A.V. et al. (2010) Development of the technology for repair microplasma powder cladding of flange platform faces of aircraft engine high-pressure turbine blades. *Ibid.*, **8**, 21–24.
6. Som, A.I., Gladky, P.V. (1984) Peculiarities of plasma cladding on narrow substrate. In: *New processes of surfacing, properties of deposited metal and transition zone*, 20–24. Kiev: Naukova Dumka.
7. Gladky, P.V., Pereplyotchikov, E.F., Ryabtsev, I.A. (2007) *Plasma cladding*. Kiev: Ekotekhnologiya.
8. Sorokin, L.I. (1997) Weldability of heat-resistant alloys used in aircraft gas-turbine engines. *Svarochn. Proizvodstvo*, **4**, 4–11.
9. Sorokin, L.I. (1999) Stresses and cracks in welding and heat treatment of heat-resistant nickel alloys. *Ibid.*, **12**, 11–17.
10. Yarovitsyn, A.V. (2015) Energy approach in analysis of microplasma powder surfacing modes. *The Paton Welding J.*, **5/6**, 14–21.
11. Gejkin, V.A., Martyshin, G.V., Sharonova, N.I. et al. (2011) About displacement of deposited bead in repair of labyrinth sealings by nonconsumable-electrode gas-shielded surfacing. *Svarochn. Proizvodstvo*, **3**, 27–30.
12. Petrov, G.L., Tumarev, A.S. (1967) *Theory of welding processes (with basics of physical chemistry)*. Moscow: Vysshaya Shkola.
13. Akulov, A.I., Belchuk, G.A., Demiantsevich, V.P. (1977) *Technology and equipment of fusion welding*. Moscow: Mashinostroenie.
14. Rozanov, Yu.A. (1989) *Theory of probability, random processes and mathematical statistics: Manual for higher school students*. 2nd ed. Moscow: Nauka.
15. Bronshitejn, I.N., Semendyaev, K.A. (1967) *Handbook on mathematics for engineers and higher school students*. 11th ed. Moscow: Nauka.
16. Yushchenko, K.A., Yarovitsyn, A.V., Yakovchuk, D.B. et al. (2013) Some techniques for reducing filler powder losses in microplasma cladding. *The Paton Welding J.*, **9**, 30–36.

Received 16.04.2015



EVALUATION OF SHAPE AND SIZES OF WELD POOL IN SURFACING USING COMBINED STRIP ELECTRODE

V.N. MATVIENKO, V.A. MAZUR and L.K. LESHCHINSKY

Priazovsky State Technical University

7 Universitetskaya Str., 87500, Mariupol, Ukraine. E-mail: matviyenkovn@mail.ru

Results of the calculation evaluation of shape and sizes of weld pool in submerged arc surfacing using combined strip electrode are presented. The mathematical model was used based on solution of nonlinear differential equation of heat conductivity considering the dependence on temperature of thermophysical properties of base metal. The calculated dependencies describing the process of heat spreading in the base metal during surfacing using combined strip electrode were obtained from the conditions of additive action of three sources — one middle strip and two side strips. With increase in heat input at the edges not only shape and sizes of the pool are changed, but also the non-uniformity of penetration increases. It is shown that due to the change in rotation angle of the side strips relative to the middle strip of combined electrode it is possible to influence the shape formation of weld pool and penetration depth. Adequacy of the developed model is confirmed by a well coincidence of the calculated data with the experiment. 10 Ref., 9 Figures.

Keywords: heat spreading, calculation of heating temperature, shape of weld pool, mathematical model, submerged arc surfacing, combined strip electrode, rotation angle of side strips, heat input at the pool edges, non-uniformity of penetration

The process of wide-layer surfacing using strip electrode is characterized by a lower penetration of the product and decrease in the volume of participation of material of the product in the deposited layer [1]. The dispersed heat input on the melting front of the base metal [2], as well as increased heat dissipation on the edges of the weld pool, characteristic for this process, contribute to the formation of defects — lacks of penetration at the edges, undercuts, and slag inclusions (Figure 1). Their appearance is greatly influenced by an outflow of molten metal from the side borders of the weld pool with formation of axial flow directed to the tail part of the pool. This is confirmed by a large convexity of the middle part of back wall of the crater formed in surfacing using strip electrode (Figure 2).

To eliminate the edge defects it is necessary to redistribute the heat and mass transfer across the width of the pool, to change the direction of

molten metal flows by improving the filling of the side areas of the pool with the molten metal. To achieve such changes the effect of magnetic field on the pool melt is used [3], as a result of which the flows are formed directed from the center to the edges of the pool and further along the edges to the tail part. At the same time, the shape of weld pool is changed, and on the back wall of the crater two convexities are formed. Similarly the shape of the pool is affected by using the strip electrode, profiled along the entire width, which allows improving the quality of bead formation, reducing the probability of edge defects arising [4]. Much wider possibilities of influencing the formation of weld pool and the conditions of wide bead formation belong to the process of surfacing using combined strip electrode, the use of which provides a strictly limited uniform penetration of the base metal and lack of defects in the fusion zone [5].

The design of combined strip electrode (Figure 3) is characterized by sizes of middle and side strips, feed speed of each strip, rotation angle α of side strips relatively to the middle one and



Figure 1. Defects of bead formation in surfacing using strip electrode: *a* — undercut; *b* — edge lack of penetration and slag inclusion



Figure 2. Shape of weld pool in surfacing using strip electrode of 50×0.5 mm

gap e between the strips. These characteristics of combined electrode affect melting conditions of the base metal, shape formation of weld pool and non-uniformity of penetration. The experimental study of these processes is quite difficult. At the same time, the numerical modeling of heat spreading process during fusion welding (surfacing) can not only reduce the labor intensity of the investigations, but also obtain new data for prediction of shape and sizes of the pool, composition, structure and properties of weld metal (deposited layer) [6, 7].

Therefore, in the present work for investigation of the shape and sizes of the weld pool in surfacing using the combined strip electrode the mathematical modeling method was applied combined with the experiments.

Mathematical modeling of heating and melting process of the base metal. Heat spreading in submerged arc surfacing using strip electrode is described by the equation of limiting condition of heating process of a semi-infinite body using the linear source of a finite width. The calculated values of sizes of penetration zone obtained during solving the linear differential equation of heat conductivity for a heat-conductive solid body with the thermophysical properties independent of temperature significantly differ from the experiment [2, 8].

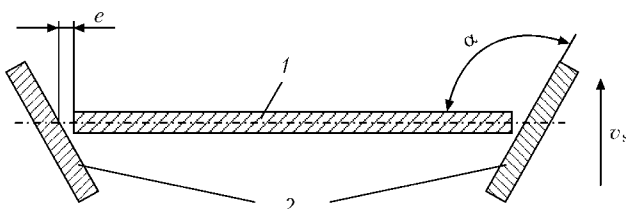


Figure 3. Design of combined strip electrode: 1 – middle strip; 2 – side strips

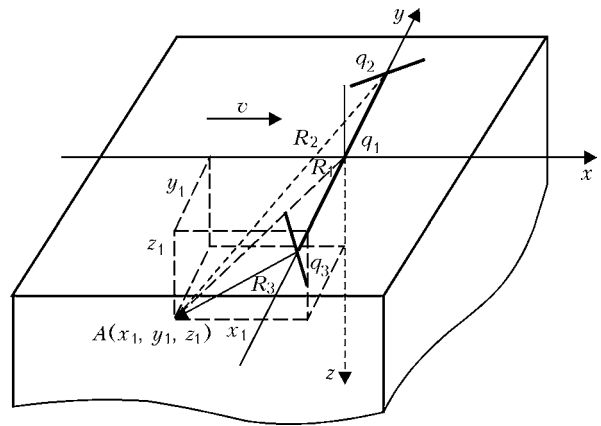


Figure 4. Calculation scheme of heating the body using three strips of combined electrode

The accuracy of calculations is significantly increased, if the thermophysical metal properties dependence on temperature is taken into account, which requires solution of nonlinear three-dimensional differential equation of heat conductivity. The numerical solution of the equation using the finite element method is used as the basis of the developed mathematical model [9]. Moreover, it was taken into account that before surfacing the temperature of all the points of the body is the same and equal to ambient temperature, during surfacing the power of heating source is completely consumed for heating the body and the heat flux at its edges is equal to zero. The use of software MSC.Patran-Nastran during modeling allowed obtaining not only the current temperature values but also the quantitative characteristics of thermal field in the area of heating and melting of the base metal.

The heating of the base metal using linear heat source [2] in the process of surfacing with combined strip electrode is determined by the combined action of three sources – middle q_1 and two side ones q_2 and q_3 (Figure 4). The heating temperature of metal from the effect of each of the strips of the combined electrode is calculated according to the dependence for the heat source of constant power moving along the surface of a semi-infinite body:

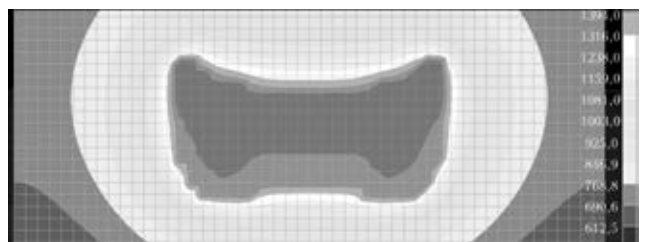


Figure 5. Model of thermal field of the body deposited surface for inclination angle of side strips $\alpha = 120^\circ$

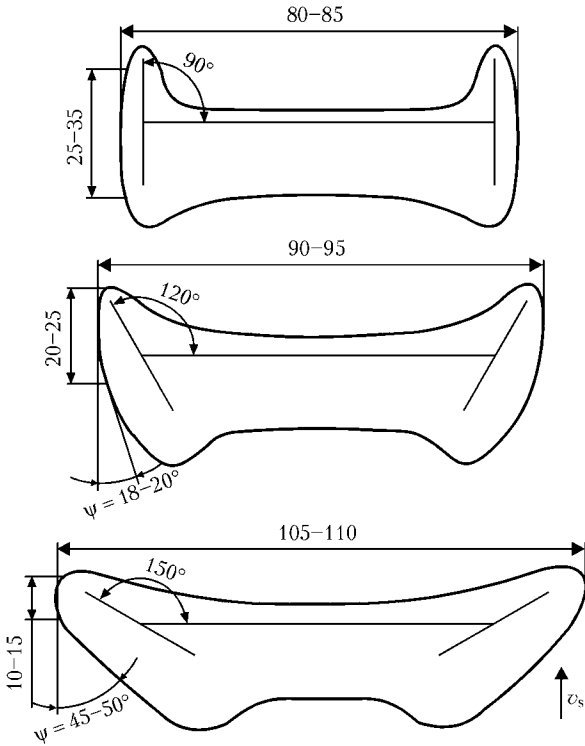


Figure 6. Modeling of shape and sizes of weld pool (boundaries of T_{melt} isotherm)

$$T_i(x, y, z) - T_0 = \frac{q}{2\pi B(b)} \int_0^{y_i} \left(\frac{1}{R_i} \right)^{\frac{v}{2a}} (x_i - R_i)$$

where $R_i = \sqrt{x_i^2 + y_i^2 + z_i^2}$.

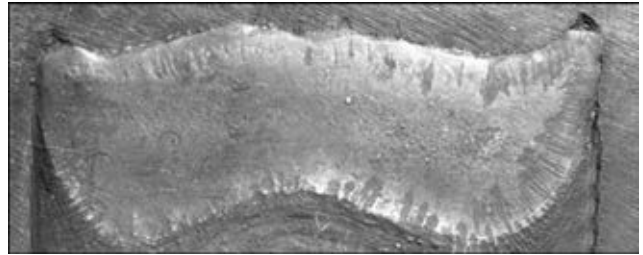


Figure 7. Shape of weld pool in surfacing using combined strip electrode at $\alpha = 120^\circ$

The calculations during modeling and experiments were carried out for the process of surfacing on the plates of steel St3 of 40 mm thickness using combined electrode of strips Sv-07Kh25N13 (middle strip was 75×0.5 mm, side strips were 25×0.7 mm), rotation angle of the side strips to the middle one $\alpha = 90-150^\circ$, gap between the strips $e = 0^{+5}$ mm. The parameters of surfacing under flux OF-10 were as follows: $I_s = 1300-1350$ A; $U_s = 30-32$ V; $v_s = 14$ m/h.

Modeling of thermal field of product to be deposited. To evaluate the shape and sizes of weld pool the models of thermal field and position of isotherm T_{melt} in the plane parallel to the surface being deposited were investigated (Figures 5 and 6). Moreover, it was taken into account that melting of the metal and formation of pool depends largely on rotation angle of the side strips relatively to the middle strip of the combined electrode. According to data of the preliminary experiments, the reduction in rotation

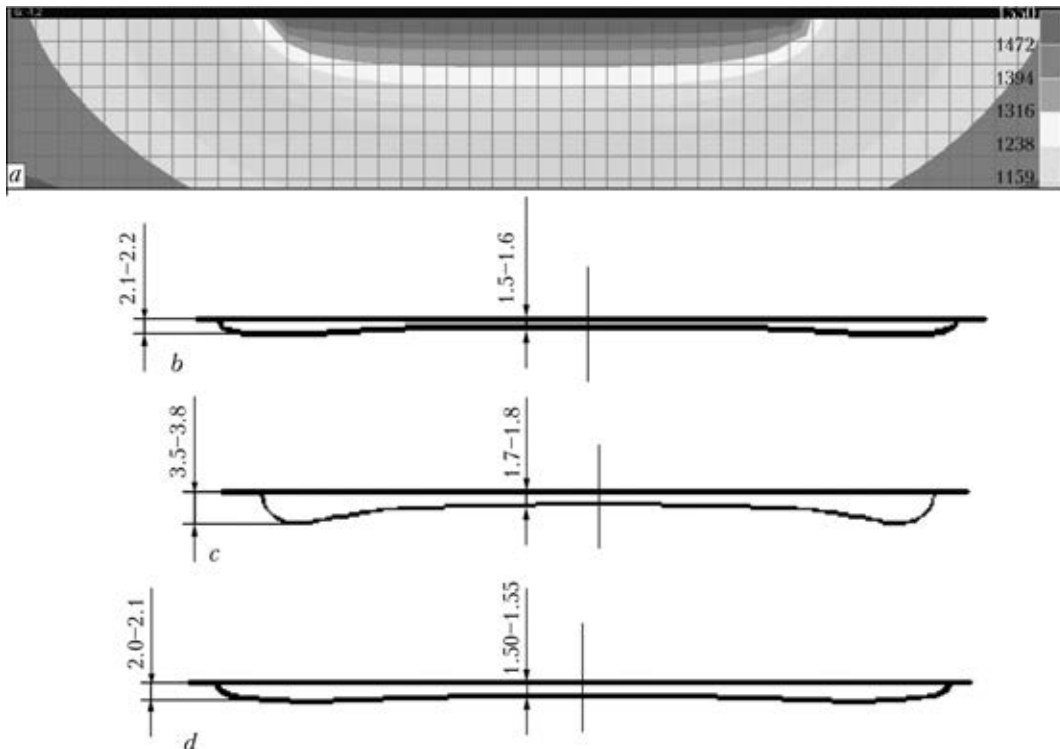


Figure 8. Model of thermal field (a) and boundary of isotherm T_{melt} (b-d) in the plane perpendicular to deposited surface at $\alpha = 120^\circ$ (a, b), 90° (c) and 150° (d)



angle $\alpha < 90^\circ$ results in deterioration of weld bead formation and increase in non-uniformity of penetration.

Therefore, in this study the results of computer modeling of thermal field for the values of rotation angle $\alpha > 90^\circ$ were considered. With increase in angle α from 90 to 150° (see Figure 6) the degree of heat input dispersion and electrode metal transfer to the weld pool is changed. This influences the position of the edge of isotherm T_{melt} , obtained in modeling allowing evaluating not only the change of shape of the pool, but also the length of areas B_{melt} of melting isotherm oriented along the longitudinal axis of the pool. This influences the filling and the time of existence of the melt at the pool edge. In addition, the geometry of the combined electrode depends on angle ψ , characterizing the deviation of isotherm T_{melt} from the areas, oriented along the longitudinal axis of the pool, and determining decrease in the width of the pool tail part relatively to the width of the melting front (see Figure 6). The adequacy of the results of modeling the shape and sizes of the weld pool is confirmed by the experimental data (Figure 7).

The influence of geometry of the combined strip electrode on the shape and sizes of the weld pool considered on the model, providing improvement of bead formation, was combined with the need in providing reliable uniform penetration of the base metal. Basing on this, the choice in modeling the optimal values of the rotation angle of the side strips of combined electrode was performed considering the restrictions of penetration depth at the edges. The concentration maximum of heat and mass transfer at the edges of the pool occurs when rotation angle of the side strips is $\alpha = 90^\circ$, which is accompanied by increase in penetration depth in these zones (Figure 8, c).

As is seen from the edge position of isotherm T_{melt} , the main part of the penetration area comprises the areas, removed from the center of the pool. With increase in angle α up to 150° the heat flow dispersion results in significant increase in the width of the pool and the non-uniformity of penetration decreases (Figure 9, d). The optimum high quality combination of bead formation and uniformity of penetration are achieved when $\alpha = 120^\circ$, which is revealed in modeling of the thermal field and the edge of isotherm T_{melt}

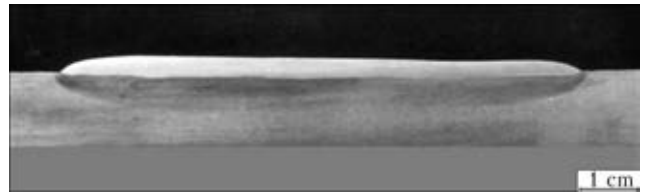


Figure 9. Macrosection of deposited bead cross-section at $\alpha = 120^\circ$

(Figure 8, a, b), and is also confirmed by macrostructure of the cross section of the weld bead (Figure 9).

In conclusion it can be noted that the accuracy of the calculated values of the temperature of heating the base metal and the position of boundary of the melting isotherm determining shape and sizes of weld pool in surfacing using combined strip electrode [10] is significantly increased in case of using thermophysical characteristics of metal, dependent on temperature, in calculations. This is confirmed by relevance of data, obtained during mathematical modeling, and the results of experiment.

1. Ryabtsev, I.A. (2005) High-efficiency wide-layer surfacing using electrode wires and strips (Review). *The Paton Welding J.*, **6**, 31–35.
2. Makhnenko, V.I., Kravtsov, T.G. (1976) *Heat processes in mechanized surfacing of parts of circular cylinders type*. Kiev: Naukova Dumka.
3. Nakano, S., Chiba, T., Ichihara, N. et al. (1982) *Horizontal electroslag welding process for surfacing*. Pat. 4309587 USA. Int. Cl. B23K 9/04. Publ. 1982.
4. Leshchinsky, L.K., Matvienko, V.N., Lavrik, V.P. (1985) Influence of electrode strip shape on quality of steel deposited layer. *Avtomatich. Svarka*, **9**, 60–62.
5. Matvienko, V.N., Leshchinsky, L.K., Egorov, V.A. et al. *Method of split strip electrode surfacing*. USSR author's cert. 1561348. Int. Cl. B23K 9/04. Publ. 03.01.90.
6. (2011) *ASM Handbook. Welding fundamentals and processes*, Vol. 6A.
7. Majstrenko, A.L., Nesterenkov, V.M., Dutka, V.A. et al. (2015) Modeling of heat processes for improvement of structure of metals and alloys by friction stir method. *The Paton Welding J.*, **1**, 2–10.
8. Belousov, Yu.V., Leshchinsky, L.K., Sologub, B.B. (1976) Selection of optimal shape of strip electrode for wide-layer surfacing. *Avtomatich. Svarka*, **12**, 24–28.
9. Samotugin, S.S., Nesterov, O.Yu., Mazur, V.A. et al. (2004) Mathematical description of heat propagation in complex shape tool under action of plasma heat source. *Vestnik IANU*, 101–107.
10. Matvienko, V.N., Leshchinsky, L.K., Mazur, V.A. (2014) Heating and melting of base metal in submerged arc surfacing with composite strip electrode. *Svarochn. Proizvodstvo*, **4**, 3–7.

Received 22.06.2015



COMPUTER INFORMATION-AND-MEASURING SYSTEM FOR INVESTIGATION OF ARC SURFACING PROCESSES

I.A. RYABTSEV, Yu.N. LANKIN, V.G. SOLOVIOV,
P.P. OSECHKOV, V.A. TISHCHENKO and A.G. TIKHOMIROV
E.O. Paton Electric Welding Institute, NASU
11 Bozhenko Str., 03680, Kiev, Ukraine. E-mail: office@paton.kiev.ua

On the basis of portable computer and advanced software the information-and-measuring system was developed, which is intended to investigate the peculiarities and next automation of the arc surfacing processes. In the surfacing installation equipped with the developed computer information-and-measuring system (CIMS) it is possible to carry out experimental investigation of the influence of surfacing method, diameter or cross section of the used electrode material on its welding and technological characteristics and quality of the deposited beads and layers formation with a high degree of accuracy and reliability. CIMS with accumulation of databases on technologies of arc surfacing of different parts can serve as a basis for creation of systems of automatic control of arc surfacing processes. 3 Ref., 1 Table, 4 Figures.

Keywords: *arc surfacing, arc surfacing automation, flux-cored wires, surfacing modes, surfacing technologies*

Due to its versatility the arc surfacing is used for restoration and strengthening of the parts of different configurations, sizes and mass. At the same time, during surfacing of parts (sheets) having a small thickness (less than 5 mm), because of the risk of burns-through it is necessary to use electrode wires of small diameters, high deposition rate and the lowest possible surfacing performance modes in current and voltage. However, it can reduce the stability and efficiency of surfacing process and deteriorate the formation of deposited beads. At the same time, if there is no danger of burns-through, then for improving the efficiency the maximum surfacing modes are used. As a result the penetration of base metal and its volume in the deposited metal are increased, which often leads to the need in performing the multi-layer surfacing.

In practice, in the production the solution of the problem of development of the technology and techniques for surfacing the specific part depends on the experience of a surfacing technologist which does not always leads to reaching the optimum result. To avoid the possible errors in development of surfacing technologies, a higher degree of automation and computerization of the development and control of arc surfacing processes is required.

The development of systems of automatic control of processes of arc surfacing of different parts requires consideration of many parameters. It should provide the possibility of selection of the type of electrode material (solid or flux-cored

wire, cold-rolled or flux-cored strip) and its sizes (diameter, cross section); surfacing method (submerged, open-arc or in shielding gases); presetting and maintaining the preset conditions and techniques of surfacing; marking of accidental or intentional deviations from the preset surfacing modes; memorization and subsequent use of optimum modes of surfacing the specific parts. The existing experience [1–3] shows that the modern level of development of computer science allows solving this problem.

If not to complicate the problem of development of automatic control systems for arc surfacing process by selection of chemical composition of the deposited metal, produced on the basis of the service conditions of the specific deposited part, then the approximate list of data necessary for development of such systems has the following form: surfacing voltage $U_s(t)$; surfacing current $I_s(t)$; diameter (cross section) of the electrode material; feed speed of the electrode material; deposition rate; surfacing heat input; stick-out of electrode wire (strip); geometric dimensions of deposited beads and overlapping of adjacent deposited beads; geometric dimensions of part and specimen being deposited; grade of welding wire (strip); grade of base metal; need in shielding gas and its composition; need in flux and its grade; need in preheating and post surfacing heat treatment; integrated indicator of quality of surfacing, taking into account the geometric dimensions and deposited metal formation, volume of base metal in the deposited metal, surfacing efficiency, character of molten electrode metal transfer and process running stability, etc.



The existing universal surfacing installations of type UMN-4, UMN-10, U-653, etc., as well as surfacing machines (installations) of type AD-231, A-1406, A-1412, are generally completed with the power sources of type VDU-506, VDU-1201, or VDU-1202, which are designed for surfacing currents of up to 500 and 1200 A, respectively. In this equipment the setting up of surfacing conditions as to voltage is produced using potentiometers in the control circuit of the power source and installation, and as to current it is made using the potentiometer of regulating the feed speed of the electrode wire in the control circuit of surfacing installation. Taking this fact into account, the setting up of necessary surfacing conditions as to current and voltage are performed by changing the position of the potentiometer for voltage adjustment P_u and the position of the potentiometer for adjustment of wire feed speed P_{vp} during surfacing of reference specimens.

For automatic determination of the potentiometers position (P_u and P_{vp}) in accordance with the preset mean values of surfacing current \bar{I}_s and voltage \bar{U}_s it is required to determine the mathematical dependencies $P_u = F_u[\bar{U}_s, \bar{I}_s]$ and $P_{vp} = F_{vp}[\bar{U}_s, \bar{I}_s]$. The functions F_u and F_{vp} refer to the specific current source and specific installation as well as to the specific setting up of the surfacing method and conditions. To obtain these functions it is necessary to gather the experimental database for each of the methods, types and modes of surfacing, for which the installation is intended.

To obtain these dependencies and filling up the computer database for the surfacing modes a series of experiments on surfacing using flux-cored wires with open arc, under flux and in shielding gases was carried out. The experiments were performed in universal surfacing installation U-653, equipped with rectifier VDU 506. It allows surfacing the plane parts and the parts such as rotation bodies.

The registration of surfacing current and voltage in these experiments was performed using the developed computer information-and-measuring system (CIMS). The digitalization and data entry of the primary converters into PC were performed using measuring voltage converter E14-140 of L-Card company with the built-in 14-discharge ADC. The registration of parameters was carried out at frequency of 1 kHz. The input data processing was performed using the specially developed software in the environment of Microsoft Visual Studio 2010. For analysis of the output system data the standard software was used, such as PowerGraph, MATLAB, etc. According to the data entered into the computer the current state of the investigated process (arc ignition, arc

breaks, short circuits of arc gap, arc burning periods) is identified automatically and the current and voltage parameters are calculated for the corresponding surfacing process.

In general, CIMS provides control and registration of the following surfacing process parameters: current values of surfacing voltage $U_s(t)$, current values of surfacing current $I_s(t)$, current values of arc voltage $U_a(t)$ and arc current $I_a(t)$; $U_a(t)$ and $I_a(t)$ at that were determined by excluding the voltage and current values from $U_s(t)$ and $I_s(t)$ in the time intervals of short circuits and arc breaks; average arc voltage \bar{U}_s and arc current \bar{I}_s during the surfacing period; entry of specifications for arc voltage $U_{a,sp}$ and arc current $I_{a,sp}$; manual entry and indication of $P_{u,sp}$ and $P_{vp,sp}$ values; indication of working area of the approximating functions (in \bar{U}_s and \bar{I}_s parameters), providing the accuracy of approximation of voltage ± 1 V and ± 10 A of current.

The main CIMS interface is shown in Figure 1, a. According to the results of surfacing the protocol of surfacing is formed (Figure 1, b). To the protocol all the necessary information is entered, which is later used for analysis, processing and formation of approximating functions.

To carry out the above mentioned experimental investigations 9 pilot batches of flux-cored wires of 1.8, 2.4 and 2.8 mm diameter were manufactured for surfacing under flux, with open arc and in shielding gases. The metal part of flux-cored wires charge was calculated in a way to provide producing of the deposited metal of the same type – 25Kh5FMS.

As the base metal the plates of steel St3 of 15 mm thickness were used. The pilot wires were used to perform surfacing of specimens in a wide range of surfacing conditions as to current and voltage. In the selected range of conditions the correlations between the position of potentiometers P_{vp} and P_u , and the average values of arc current \bar{I}_a and arc voltage \bar{U}_a were fixed, recorded by CIMS (see Figure 1).

In total, 9 series of experiments were carried out in the following ranges of surfacing conditions. In all the experiments the surfacing was performed at the same speed – 20 m/h.

- 19 experiments on open-arc surfacing using flux-cored wire of 1.8 mm diameter at current 160–260 A and voltage 22–29 V;
- 22 experiments on open-arc surfacing using flux-cored wire of 2.4 mm diameter at current 180–300 A and voltage 24–32 V;
- 34 experiments on open-arc surfacing using flux-cored wire of 2.8 mm diameter at current 200–300 A and voltage 24–32 V;
- 17 experiments on surfacing under flux AN-26 using flux-cored wire of 1.8 mm diameter at current 240–300 A and voltage 26–31 V;

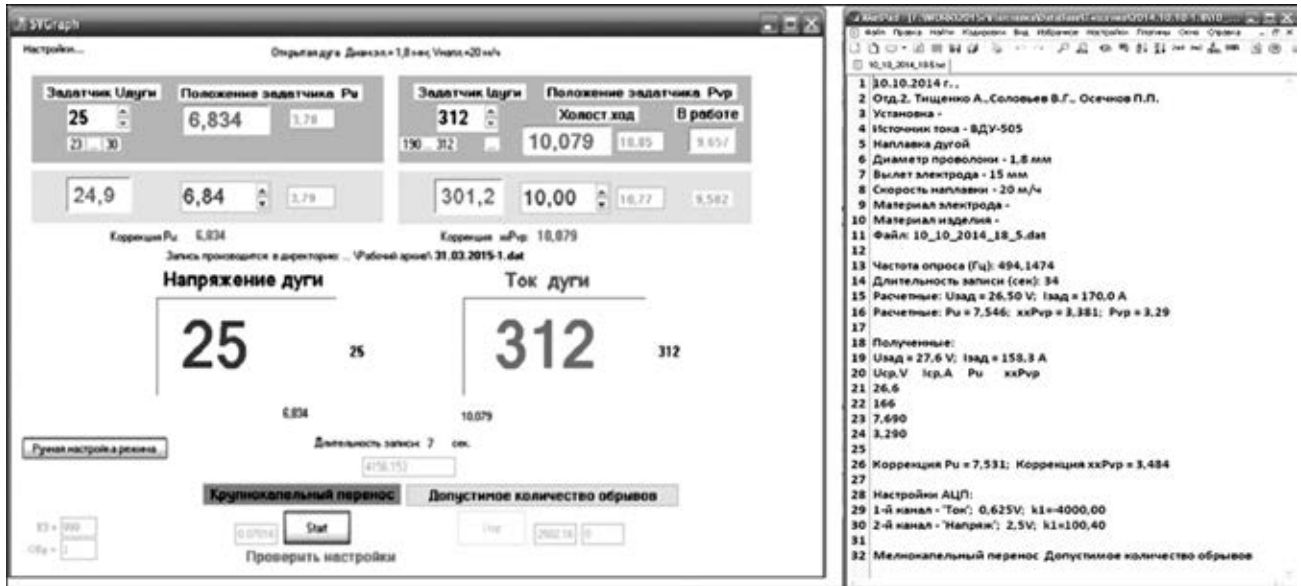


Figure 1. Basic interface of system for entry, monitoring and recording of surfacing parameters (a), and protocol of recording the results of experiment on surfacing (b)

Results of experiments on open-arc surfacing using self-shielding flux-cored wire PP-Np-25Kh5FMS of 1.8 mm diameter showing the dependencies between position of potentiometers of voltage controller P_u and controller of wire feed rate P_{vp} , and average values of voltage \bar{U}_a^* and current \bar{I}_a^* recorded by the system

Number of experiment	\bar{U}_a, V	\bar{I}_a, A	P_u	P_{vp}	Number of experiment	\bar{U}_a, V	\bar{I}_a, A	P_u	P_{vp}
1	27.6	179	7.69	3.29	14	23.8	193	6.42	5.01
2	25.6	182	7.26	3.49	15	23.4	177	6.01	5.52
3	26.5	206	7.54	3.38	16	26.5	251	7.77	5.49
4	27.6	177	7.69	3.41	17	25.7	144	7.01	3
5	25.2	233	7.41	4.27	18	23.4	156	5.61	5.03
6	25.8	210	7.41	4.27	19	23.7	158	6.32	3.74
7	27.8	211	7.91	4.23	20	25.0	160	6.95	3.74
8	25.9	285	7.77	5.81	21	26.1	214	7.51	4.51
9	22.7	265	6.92	6.14	22	23.9	174	6.33	3.90
10	24.0	240	7	4.76	23	28.8	217	8.16	4.39
11	23.1	197	6.44	4.76	24	23.7	200	6.82	5.16
12	24.9	256	7.41	5.49	25	22.8	219	6.33	5.61
13	24.0	176	6.42	4.53	26	24.0	285	7.32	5.61

* \bar{U}_a, \bar{I}_a – values of arc voltage $U_a(t)$ and arc current $I_a(t)$, respectively, averaged during the period of surfacing.

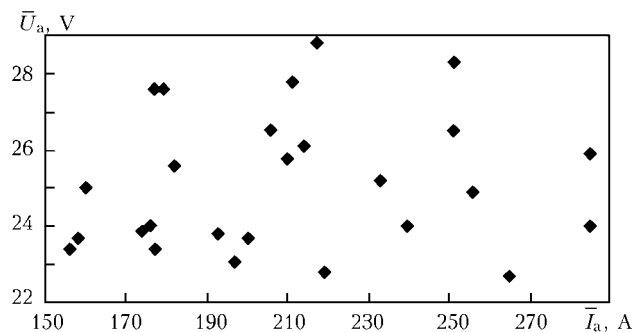


Figure 2. Area of used conditions during the experiments on open-arc surfacing using 1.8 mm flux-cored wire

- 25 experiments on surfacing under flux AN-26 using flux-cored wire of 2.4 mm diameter at current 220–400 A and voltage 22–32 V;
- 24 experiments on surfacing under flux AN-26 using flux-cored wire of 2.8 mm diameter at current 240–420 A and voltage 22–38 V;
- 14 experiments on surfacing in the mixture of shielding gases (Ar + 18 % CO₂) using flux-cored wire of 1.8 mm diameter at current 220–310 A and voltage 20–30 V;
- 12 experiments on surfacing in the mixture of shielding gases (Ar + 18 % CO₂) using flux-

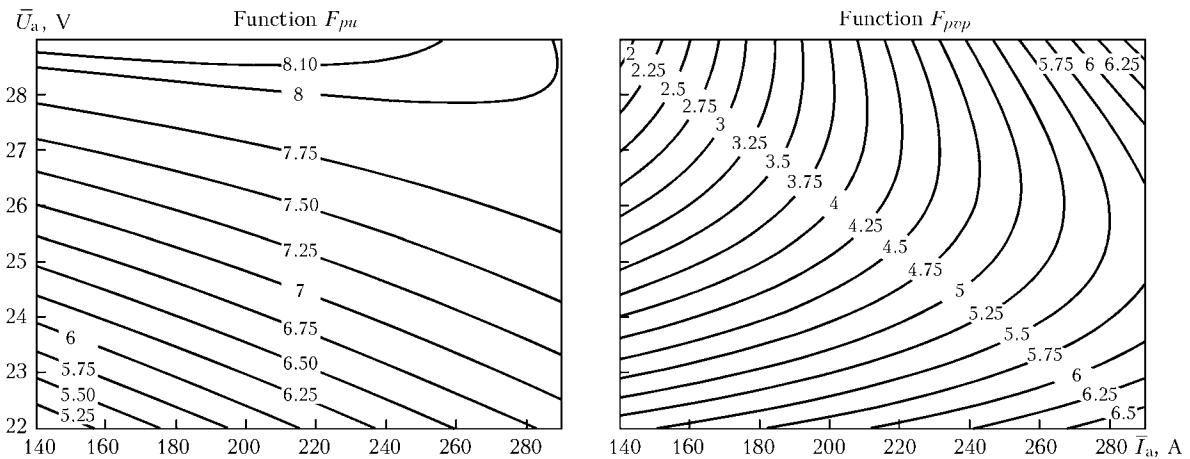


Figure 3. Diagrams of F_{pu} and F_{pvp} functions depending on average values of current and voltage in open-arc surfacing using self-shielding flux-cored wire of 1.8 mm diameter

cored wire of 2.4 mm diameter at current 210–440 A and voltage 22–40 V;

- 26 experiments on surfacing in the mixture of shielding gases (Ar + 18 % CO₂) using flux-cored wire of 2.8 mm diameter at current 180–340 A and voltage 22–40 V.

As an example in the Table the results of experiments are given obtained in open-arc surfacing using self-shielding flux-cored wire of 1.8 mm diameter, and in Figure 2 the area of used surfacing conditions is shown.

The regression analysis of the data given in the Table and in Figure 2 was carried out, basing on its results the diagrams of functions F_{pu} and F_{pvp} were plotted depending on the average values of arc current and voltage in open-arc surfacing using flux-cored wire of 1.8 mm diameter (Figure 3).

Figure 4 shows the area of conditions of open-arc surfacing using flux-cored wire of 1.8 mm diameter in coordinates \bar{I}_a/\bar{U}_a , wherein the approximation error during presetting the surfacing voltage and current does not exceed ± 1 V and ± 10 A, respectively.

As a result of all 9 series of experiments the similar dependencies between the position of corresponding potentiometers for adjustment of voltage and wire feed speed and calculated average values of arc current and arc voltage were obtained, recorded by CIMS in the process of surfacing of each of approximately 200 deposited beads.

Conclusions

1. On the basis of portable computer and advanced software the information-and-measuring system was developed intended to investigate the peculiarities of arc surfacing. CIMS with accumulation of databases on technologies of arc surfacing of different parts can serve as a basis for creation of systems of automatic control of arc surfacing processes.

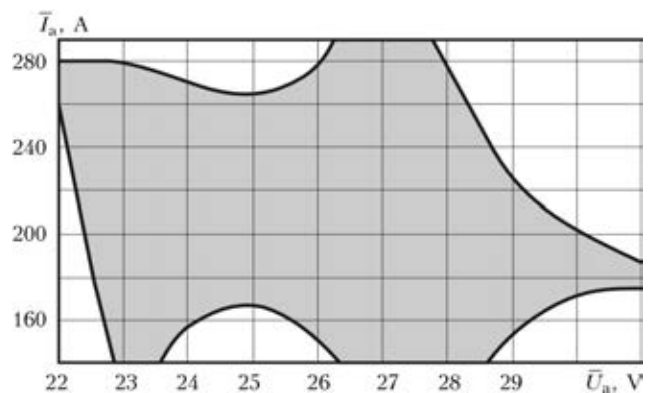


Figure 4. Range of open-arc surfacing modes with flux-cored wire of 1.8 mm diameter, where the approximation error in arc voltage and current during surfacing does not exceed ± 1 V and ± 10 A, respectively

2. According to the results of experimental investigations on surfacing using flux-cored wires, with open arc, in shielding gases and under flux, the dependencies between the position of the corresponding potentiometers for adjustment of voltage and wire feed speed and average values of arc current and voltage for surfacing were determined, preset by the surfacing technologist. This allows using the developed CIMS with a high degree of accuracy to establish the surfacing modes by arc current and voltage without surfacing of reference specimens.

1. Bocharnikov, I.V., Gladky, P.V., Demchenko, V.F. et al. (1992) Expert system «Surfacing». In: *Deposited metal. Composition, structure, properties*, 94–97. Kiev: PWI.
2. Demchenko, V.F., Kozlitina, S.S., Ryabtsev, I.A. (1998) Computer system of design of arc surfacing technology. *Avtomatich. Svarka*, **11**, 61–66.
3. Lankin, Yu.N., Ryabtsev, I.A., Soloviov, V.G. et al. (2014) Effect of electric parameters of arc surfacing using flux-cored wire on process stability and base metal penetration. *The Paton Welding J.*, **9**, 25–29.

Received 23.06.2015

EQUIPMENT FOR PREPARATION OF PIPE ENDS TO WELDING OF POSITION BUTT JOINTS OF PIPELINE

L.M. LOBANOV¹, N.M. MAKHLIN², V.K. SMOLYAKOV², V.E. VODOLAZSKY²,
V.E. POPOV² and A.A. SVIRIDENKO³

¹E.O. Paton Electric Welding Institute, NASU

11 Bozhenko Str., 03680, Kiev, Ukraine. E-mail: office@paton.kiev.ua

²SE «Research Engineering Center of Welding and Control

in Power Engineering of E.O. Paton Electric Welding Institute»

11 Bozhenko Str., 03680, Kiev, Ukraine. E-mail: electro@paton.kiev.ua

³Company CHEZARA

25 Odintsov Str., 14030, Chernigov, Ukraine. E-mail: mial@chezara.com

The results are given on developments of the PWI and its special sub-divisions in creation of domestic specimens of current equipment for preparation to welding of ends and edges of position butts of 14–159 mm diameter pipelines from austenite and pearlite class steels and high alloys in assembly, repair and modernization of power engineering objects, including power generating units of nuclear and heat electric plants, in chemical and power machine building, at enterprises of oil-and-gas complex and other branches of industry. Studied are the peculiarities of design of developed end facers for treatment of 14–76 mm diameter pipes with wall thickness up to 7 mm and pipe cutters for treatment of V- and U-groove edges of position butts in pipes of 76–159 mm diameter and up to 12 mm wall thickness and main constituents of this equipment. It is shown that developed domestic equipment, in comparison with foreign analogues, has a series of significant advantages allowing increasing total efficiency of machining and reducing time of personal staying in zone of influence of harmful environment factors. 26 Ref., 5 Tables, 6 Figures.

Keywords: nuclear power engineering, pipeline position butts, automatic orbital welding, machining, pneumatic drives, end facers, pipe cutters, supports, cutting tools

In the most cases, pipelines of power engineering objects, oil-and-gas complex and other branches of economy are the base elements of technological circuits which require performance of significant amount of welded joints. For example, assembly of one power generating unit of nuclear power plant (NPP) with water-moderated type reactor requires performance of not less than 120,000 pipeline welded joints, as a rule, in form of position butts. Functions, performed by pipelines of NPP power generating units, and their effect on life, safety and nuclear safety, complexity of their operation conditions provide for high requirements to quality, service properties and corrosion resistance of welded joints of such pipelines [1–5]. At that, the pipelines are subjected to effect (in the most cases simultaneous) of high temperatures, increased pressure, corrosion and radiation activity of heat carrier and other media, tightness in places of welding performance and limited access to this places. Majority of the similar requirements exist for pipelines in objects in other branches of economy.

Multiple researches and longstanding practice proved that fulfillment of these requirements is only possible under condition of providing of high quality in preparation for welding of pipe ends or edges for pipeline position butts by means of their machining with the help of special metal cutting equipment [3–8]. Earlier Ukraine did not have development and commercial production of such equipment. Therefore, up to the moment organizations and enterprises of nuclear power engineering and other branches of Ukrainian economy should use equipment of similar designation which comes into Ukraine only by means of import and can only partially fulfill Ukrainian consumers according to its properties. Besides, absence of domestic current equipment for preparation of pipeline position butts for welding is one of the main factors preventing wide-scale automation of welding operations at assembly, repair and updating of power engineering objects and other braches of Ukrainian economy.

Taking into account circumstances mentioned above, development of domestic technologies as well as creation and mastering of domestic industrial production of state-of-the-art equipment for preparation of pipeline position butts for welding is very relevant task.

Aim of the present work lies in studying some important peculiarities of the processes of machining for welding of pipe ends and edges of pipeline position butts and equipment for realizing these processes as well as representation of results of investigations, pilot-technical and pilot-design works, carried in 2013–2014 at the PWI together with REC WCPE in the following directions:

- determining and optimizing the requirements to processes on preparation for welding of position butts in NPP pipelines of 14–219 mm diameter and defining the optimum parameters and modes of machining of pipe ends of up to 4 mm wall thickness and V- and U-groove edges of welds in pipes with up to 12 mm wall thickness;
- development of construction solutions for equipment used in preparation for welding of position butts of 14–159 mm diameter pipelines and drawing up of technical documents for pilot samples of corresponding domestic equipment, arrangement of their production, manufacture, setting, finishing, testing and pilot-industrial inspection of these pilot specimens.

Investigations of peculiarities of processes on preparation for welding of position butts of 14–219 mm diameter NPP pipelines. Investigations and technological works covered the study of effect of accuracy of pipeline part edges preparation on welded joint quality. Structural components of such parts correspond to PN AE G-7-009-089 and OST 24.125.02–89 requirements. Besides, ranges of optimum modes of treatment by cutting were determined, which should provide correspondence of edge preparation and surfaces of pipeline parts to the requirements of normative documents acting in the field of nuclear power engineering of Ukraine.

Specimens of pipeline parts from 08Kh18N10T steel of 18, 38 and 57 mm nominal diameters and 2.5, 3.5 and 4 mm nominal wall thickness, respectively, as well as from steel 20 of 108, 159 and 219 mm nominal diameters and 5, 6.5 and 12 mm nominal wall thickness, respectively, were used for investigations. Edges of specimens of pipeline parts used for investigations were treated with the help of versatile turn-mill machine 1M61 and milling machine 6R82Sh.

Ends of specimens of pipeline parts from steel 08Kh18N10T were treated in such a way, applicable to S-39 welded joint, as to simulate deviation of specimen plane end from plane normal to longitudinal pipe axis. These are the conditions of non-regular gap and deviation of internal diameters of pipeline part, subjected to welding, from reference values, i.e. conditions of joining of parts with different wall thickness.

Table 1. Linear and angular dimensions of specimens of pipeline parts from 08Kh18N10T steel for simulation of non-regular gap

Nominal diameter \times pipe thickness ($D \times S$), mm	The largest value of non-regular gap δ , mm		
	0.3	0.5	0.7
	Angle of deviation of line normal to pipe longitudinal axis α , angle deg		
18 \times 2.5	1.23	1.72	2.88
38 \times 3.5	0.55	0.92	1.29
57 \times 4.0	0.36	0.60	0.84

Treatment of ends in specimens of pipeline parts from 08Kh18N10T steel for non-regular gap conditions in performance of S-39 type welded joint was carried out in accordance with Table 1.

Treatment of ends in specimens of pipeline parts from 08Kh18N10T steel for conditions of joining the parts with different wall thickness in performance of S-39 type welded joint was carried out in accordance with Table 2.

Treatment of groove edges in specimens of pipeline part from steel 20 for simulation of deviations of linear and angular dimensions, regulated by PN AE G-7-009-089 and OST 24.125.02–89 for S-42 type welded joint was performed in accordance with Figure 1 and Table 3. Skewness of bevel angles in samples of pipeline parts from steel 20 for simulation of deviations from reference values for pipes with nominal sizes 108 \times 5, 159 \times 6.5, 219 \times 12 mm made 4, 8 and 12 angle degree.

Control of linear and angular dimensions in process of treatment of specimens of pipeline parts from 08Kh18N10T steel and steel 20 was carried out with the help of standard measurement instrumentation, in particular, calipers ShTs-P-160 and ShTs-P-250 on GOST 166 (the largest measurement error ± 0.07 and 0.08 mm, respectively), indicator pipe wall thickness gauges S-10A and S-25 on GOST 11358 (the largest measurement error ± 0.02 and 0.10 mm, respectively), angle gauge with vernier UT mod. 127 of 0–180 angle degree measurement range on GOST 5378 and the largest measurement error ± 2 angle min, and set of probes No.3 [9].

Table 2. Linear dimensions of specimens of pipeline parts from 08Kh18N10T steel for simulation of joining conditions of pipe parts of different wall thickness

Nominal diameter \times wall thickness ($D \times S$), mm	Difference of internal diameters of parts (Δd) joined by welding, mm		
	0.01D	0.015D	0.02D
18 \times 2.5	0.18	0.27	0.36
38 \times 3.5	0.38	0.57	0.76
57 \times 4.0	0.57	0.86	1.14

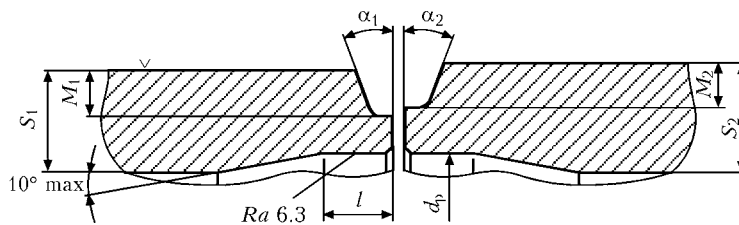


Figure 1. Scheme for edge groove preparation steel 20 of pipe with wall thickness from 5 to 12 mm for simulation of deviations of linear and angular dimensions of parts, subjected to welding, from reference values (conditions of skewness of bevel angles and conditions for joining of pipe parts with different root face) in S-42 type joint performance

Table 3. Linear dimensions of edge grooves preparation in specimens of pipeline parts from steel 20 for simulation of deviations from regulated values

Pipe nominal values ($D \times S$), mm	Edge groove preparation						
	Boring diameter d_b , mm		Wall thickness in place of boring, not less than	Root face ($S - M$) at $S_1 = S_2$, mm			
	Nominal value	The largest allowable deviation		$S_1 - M_1$	$S_2 = M_2$		
					$M_2 = M_1$	$M_2 = M_1 + 1$	$M_2 = M_1 + 1.5$
108 × 5.0	100	+0.23	2.7	$2.3^{+0.4}$	$2.3^{+0.4}$	$3.3^{+0.4}$	$3.8^{+0.4}$
159 × 6.5	149	+0.26	3.8	$2.7^{+0.3}$	$2.7^{+0.3}$	$3.7^{+0.3}$	$4.2^{+0.3}$
219 × 12.0	199	+0.30	8.8	$3.0^{-0.3}$	$3.0^{-0.3}$	$4.0^{-0.3}$	$4.5^{-0.3}$

Specimens of parts of 18 and 38 mm diameter pipelines treated in accordance with Tables 1–3 were subjected to automatic non-consumable argon-arc orbital welding (GTAW) by pressure molding method. ADTs 625 U3.1 automatic machine was used for GTAW of position butts of 18–42 mm diameter pipelines. Welding of specimens of parts of 57 mm diameter pipelines with 4 mm wall thickness by sequential penetration method was carried out applying ADTs 626 U3.1 automatic machine for GTAW of position butts of 42–76 mm diameter pipelines [10]. Specimens of parts of 108 and 159 mm nominal diameter pipelines from steel 20 were subjected to multi-pass GTAW with filler wire feed and oscillations of non-consumable electrode. At that ADTs 628 UKhL4 and ADTs 629 UKhL4 automatic machines were used for GTAW of position butts of 76–108 and 108–159 mm diameter pipelines, respectively [11]. Specimens of parts of pipelines with 219 mm diameter were put to multi-pass manual TIG welding with filler wire feed. At that ITs 617 U3.1 power source for TIG welding, power supply module MPS-101, welding current regulator RDG-201 U3.1 [12], ABITIG GRIPP26 torch (ABOCOR BINZEL company) with 3.15 mm diameter tungsten electrode of WT20 grade and Sv-08G2S 1.6 mm diameter filler wire were used.

Quality of welded joints in specimens of parts of 18–159 mm diameter pipelines was inspected by visually, radiographic and penetrant methods

[13]. The following is determined based on results of performance of several series of pilot welding:

- when performing S-39 type welded joints of 14–76 mm diameter pipe with wall thickness up to 4 mm, the deviations of plane of the ends subjected to treatment and further welding of parts should not exceed 1.23 angle degree of normal line relatively to longitudinal pipe axis for 18 × 25 pipes, 0.55 angle degree for 38 × 3.5 pipe, 0.36 angle degree for 57 × 4.0 pipe etc. However, in all cases they should be not more than 0.3 mm, since the deviations exceeding this value provide for high possibility of appearance of weld defects such as sagging, lack of penetration, edge lack of fusion, undercuts;

- deviations of internal diameters of parts, subjected to welding, from reference values in welding of S-39 type joints should not exceed $0.01D_{nom}$ value, where D_{nom} is the pipe nominal external diameter. Nonobservance of this requirement result in formation of such defects as violations of weld regulated shape, lack of penetration, edge lack of fusion, root concavities;

- skewness of groove bevel angles of specimens of pipeline parts in performance of S-42 type welded joints should not exceed 4 angle degree. Large values of skewness of bevel angles are characterizes by such solid defects as inadmissible failures in weld formation, lack of fusion of edges and separate beads, lack of penetration in final passes, sagging of weld part close to edge with overstated bevel angle, undercuts in facing weld;

• deviations of boring of internal diameters from reference values in welding of S-42 type joints should not exceed +0.23 mm for 108×5 pipe, +0.26 mm for 159×6.5 pipe, +0.3 mm for 219×12 pipe, and difference between both root faces should not exceed 0.5 mm, since pipeline part welds, in which root face of one of the edges deviates from root face of another more than per 0.5 mm, tend to such defects of root weld as failure of its regulated shape, lack of penetration, sagging of the weld from one of its side surfaces and concavities or lack of fusion from another. At that the defects of root weld are very rare and in some specimens they are not found at all in the case of application of welding modes with modulated current even at up to 0.75 mm difference between root face.

Investigations on determination of ranges of cutting optimum modes were also carried out in addition to analysis of the effect on welded joint quality of accuracy of preparation of pipeline part edges for welding. Necessity in such investigation is caused by peculiarities of corrosion-resistant steels of austenite class (for example, 08Kh18N10T grade), relating to base materials, which are used for NPP pipelines, as well as peculiarities of processes of their machining.

One of the main peculiarities of corrosion-resistant steels lies in the fact that their structure represents itself solid solution of austenite class with face-centered cubic lattice [14]. Austenite class steels are the most difficult for machining among the all types. This can be explained by series of factors, main of which is tendency of such steels to cold working, at that even insignificant deformations promote for strong metal hardening. In cutting treatment, high toughness of austenite class steels promotes for formation of long chips that also deteriorates treatment conditions. Low heat conductivity of corrosion-resistant steels stipulates elevated temperature in cutting zone and, as a result, activation of adhesion and diffusion processes as well as intensive bonding of contact surfaces and failure of tool working part.

Experimental and technological works on determination of optimum cutting modes were carried out in specimens of pipeline parts from 08Kh18N10T steel of 18, 38, 57, 108, 159 and 219 mm nominal diameter and 2.5, 3.5, 4, 5, 6.5 and 12 mm wall thickness. At that, the recommendations were used determined in the course of many-year investigations directed on machining of austenite class steels and available industrial experience of such treatment [14]. According to these recommendations, the optimum val-

Table 4. Optimum values of parameters of treatment modes for pipeline parts from 08Kh18N10T steel

Name of operation	Nominal dimensions of pipe ($D \times S$), mm	Values of parameters of cutting modes	
		Cutting rate, m/min	Feed for finish turning, mm/rev.
Trimming and cutting	18×2.5	10	0.05
Boring of internal diameter	38×3.5	12	0.06
	57×4.0	15	0.07
Bevel formation	108×5.0	10	0.08
Root face formation	159×6.5	15	0.10
Internal diameter boring	219×12.0	20	

ues of cutting speed are limited by a range from 10 to 40 m/min in the case of fine external longitudinal turning and undercutting of parts from 08Kh18N10T steel. At that, the values of correction factors K_m and K_{nv} make 0.8 and 0.9, respectively. The first one considers the effect of physical-mechanical properties of billet from corrosion-resistant steel on cutting rate, and the second takes into account the effect of surface condition of this billet on cutting rate. The recommended feed rates for precision turning of parts from heat-resistant and stainless steels using cutting tools with hard-alloy plates are from 0.04 to 0.12 mm/rev.

The results of investigations on determination of ranges of optimum modes for treatment by cutting of pipeline parts from 08Kh18N10T steel showed that the optimum cutting mode values should correspond to that given in Table 4.

Peculiarities of construction of new equipment for preparation of pipeline position butts for welding. Analysis of information on parameters, characteristics and design of the best foreign examples of equipment for treatment of ends and edges of pipeline parts subjected to welding, for example, produced by PROTEM, POLYSOUDE (France), ARC MACHINES (USA), ESAB, Atlas Copco (Sweden), Georg Fischer, DEPRAG (Germany), ISCAR (Israel), Petersburg Industrial Company (Russia), Aotai (China) [15–23 etc.] companies, showed that these analogues have the following disadvantages:

- mainly internal positioning, which promotes for certain difficulties in performance of mandatory on-line inspection of geometry parameters of pipe ends or edge groove preparation of pipeline position butts and significantly increasing amount and duration of preparatory and finishing operations and, respectively, duration of personal staying in zone of radioactive pollution;

- absence of some important options, necessary for fulfillment of the requirements of acting in Ukraine PN AE and other normative documents (for example, end facers of foreign production can't provide internal pipe boring);

- high price and significant service expenses.

Therefore, one of the main tasks in development of domestic equipment for machining of ends and edges of pipeline parts subjected to welding was development of models of equipment free from disadvantages typical for foreign analogues, but at the same time close to these analogues by weight.

Earlier carried investigations and production practice showed that achievement of high machining quality of pipe ends and groove edges of pipeline position butts, their assembly and further welding is possible under condition of positioning the mechanisms for treatment, assembly, alignment and welding over the pipe external surface [24]. Such a positioning makes a basis in construction of models of domestic equipment for preparation of pipeline position butts for welding, which are developed at the PWI together with REC WCPE.

Any device for machining of pipe ends or groove edges in pipeline position butts consists of such main parts as driver — electric or pneumatic drive unit, reduction gear, face plate with set on it support (supports), each of which is equipped with one or two tool holders and mechanism of cutting tool feed.

The driver is one of the most important and necessary assembly units of equipment for preparation of pipeline butts for welding. Construction of drivers for this equipment in form of pneumatic drives is seemed to be the most reasonable taking into account designation, peculiarities of such equipment and specific conditions of its operation at NPP.

Main characteristics of pneumoengine of manual pneumatic angle grinder IP 21230

Output shaft power, W	1300 ₋₁₃₀
Frequency of rotation of idle output shaft, rpm	6400 ₋₆₄₀
Specific air consumption, m ³ /min	1.5 ± 0.15
Compressed air pressure, MPa (kgf/cm ²)	0.63 (6.3)
Overall dimensions, not more than, mm:	
length	350
width	164
height	140
Weight, kg	not more 3.1

Pneumoengine is a basis of any pneumatic drive unit. The pneumoengines in comparison with drivers of other types have series of advantages, among which are significantly lower specific volume, size and weight than in electric engines with similar energy parameters (power etc.), capability of safe operation under condi-

tions of simultaneous effect of high temperature and humidity of environment, significant vibrations and knocks, indices of safety higher than in electric engines, fundamental possibility (in contrast to electric drives) to provide fulfillment of safety requirements in operation under dangerous and particularly dangerous conditions, lot easier and cheaper service maintenance.

Pneumoengines of vane type [25], having the largest widespread, are characterized by the highest safety. Turning moment of the latter is determined by vane surface area, which is subjected to compressed air pressure, and level of this pressure. This provides for the possibility for regulation of rate and turning moment of pneumoengine by means of change of pressure of air coming in it.

Typical peculiarities of vane type pneumoengines are the necessity in providing structural strength and rigidity of cylinder-body and high accuracy of treatment of its internal surfaces. It, from the one side, requires manufacture of body billet by forging or using other technologically complex forming methods and, from the other, obligatory application of not only high-frequency metal-working machines, but special technological fitting and non-standard devices for control of linear and angle dimensions, and fulfillment of the requirements on optimum profile and accuracy of manufacture of rotor vanes, on gaps between vane edges and body internal surfaces, and outlet port size. Indicated peculiarities of pneumoengine manufacture stipulate significant primary expenses for technological equipment and fitting as well as production preparation. It can be economically proved only under conditions of large-series or gross production. It should be also taken into account that there is no domestic production of pneumoengines up to the present moment.

Circumstances mentioned above and tendency to unification of main constituent parts of domestic equipment for machining of ends and edges of pipeline parts subjected to welding are taken into account. So, it is reasonable and economically relevant to use serial pneumoengines of finished models of pneumotools, in particular, imported from CIS countries or South-West Asia, for example, pneumoengine of manual pneumatic angle grinder IP 21230.

Providing real machining modes requires that a face-plate in equipment for preparation for welding of pipeline position butts with imbedded in it cutting tool should rotate at a rate significantly less in comparison with rotation rate of output shaft of pneumoengine. The latter can be achieved only by means of corresponding reduction. This

promotes for presence of special transmission-reduction gear in structure of equipment for preparation to welding of pipeline position butts.

There are reduction gears of different types, main of which are planetary, helical and worm. In comparison with other reduction gears, the planetary reduction gears are characterized by high efficiency, low inertia moment, capability to reproduction of large reduction ratios as well as the smallest size in relation to turning moment created by reduction gear [8, 26].

In addition to this, an important advantage of planetary reduction gear is the possibility of simple flange connection, positioning of reduction gear shaft in the center and free selection of spatial position. Mentioned advantages of planetary reduction gears predetermined selection of double straight-type reduction gear, specifically of this type in construction of domestic models of equipment for welding of pipeline position butts. At that, all developed models of end facers and pipe cutters use not only the same unified pneumodrive, but the same unified variant of planetary reduction gear.

Theoretical basics of designing of machine parts and mechanisms, experience of development and construction of equipment for metal treatment by cutting and taking in account properties of materials, being subjected to treatment in preparation for welding of pipeline parts, conditions of such treatment and requirements to processes of preparation of position butts in NPP pipelines of 14–159 mm diameter were used as a basis for development of kinematic schemes of pilot specimens of end facers TRTs 38 U3.1 (for pipes of 14–38 mm diameter and wall thickness to 5 mm) and TRTs 76 U3.1 (for pipes of 38–76 mm diameter and wall thickness to 7 mm), and pipe cutter TTTs 660 U3.1 (for pipelines of 108–159 mm diameter and wall thickness to 15 mm). At that, kinematic and power calculations for transmissions and mechanisms of face-plates of these end facers and pipe cutter, calculation of strength and life of elements of such transmissions and mechanisms as well as calculation of cutting force were carried out. It allowed selecting necessary materials.

Figure 2 shows kinematic scheme of the developed domestic end facers TRTs 38 U3.1 and TRTs 76 U3.1, and Figure 3 gives kinematic scheme of pipe cutter TTTs 660 U3.1.

Investigations and practice show that one of the main factors, limiting the possibility of pipeline part treatment in zones with environment increased aggressivity and allowable duration of production personal staying in such conditions,

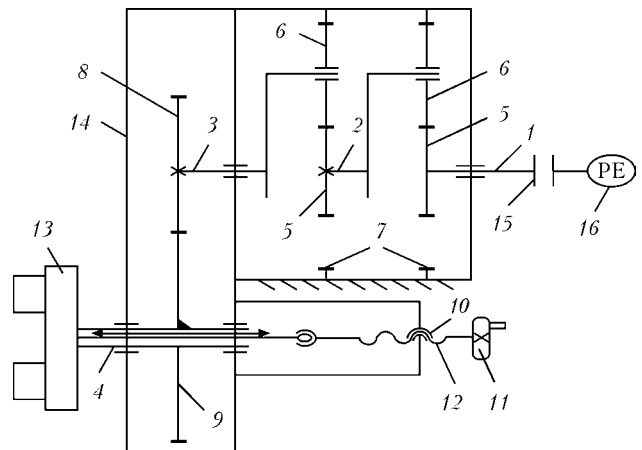


Figure 2. Kinematic scheme of pilot end facers: 1–4 – shafts of kinematic segments; 5–9 – gears of kinematic segments; 10 – nut; 11 – handwheel; 12 – feed screw; 13 – face-plate; 14 – body; 15 – socket; 16 – pneumoengine

is a time interval necessary for performance of cutting process itself as well as re-adjustment of cutting tool. Therefore, one of the ways for increase of efficiency of equipment for treatment of NPP pipeline parts lies in such a design of face-plate. It provides for possibility of simultaneous treatment of several surfaces due to presence in its structure of several cutting tool holders that promotes for maximum possible reduction of duration of cutting process and re-adjustment of cutting tool. Based on this, the technical solutions were proposed. According to them two diametrical supports are installed on face-plate of each of end facers that provides for the possibility of simultaneous treatment of pipe ends with

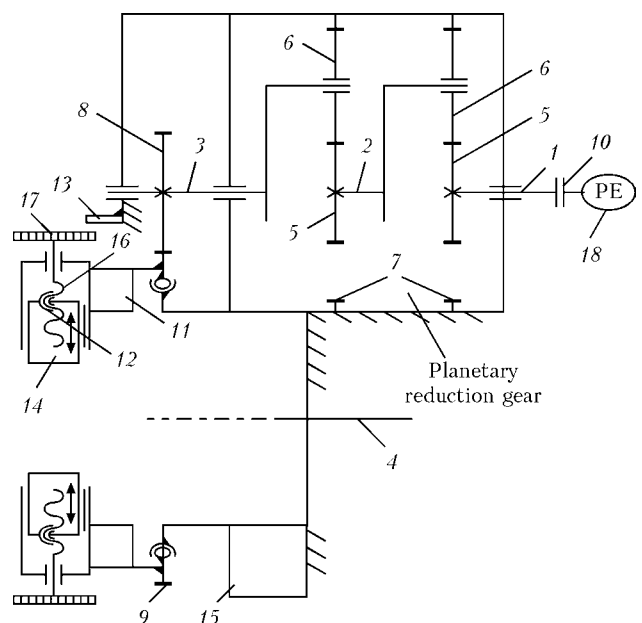


Figure 3. Kinematic scheme of developed pipe cutter: 1–4 – shafts of kinematic segments; 5–9 – gears of kinematic segments; 10 – socket; 11 – face-plate; 12 – nut; 13 – turn lock; 14 – support; 15 – body; 16 – feed screw; 17 – tooth wheel; 18 – pneumoengine

the help of four cutting tools. At that facing of pipe, formation of external and internal faces and internal pipe boring are carried out simultaneously in one pass.

Similar approaches are typical for designing the structure of split pipe cutter, the face-plate of which is proposed to be made in form of turret head with two transverse supports and one bored. It allows for combining the work of several cutting tools of different configuration, for example, one cutting tool can be fixed in each of two transverse supports, or cutting off tool in one transverse support and straight turning tool in other, besides this cutter can be set for performance of external face. It should also be noted that simultaneous application of two supports with set in it cutting tools allow significantly increasing safety of equipment due to balancing of banding strains, which inevitably appear in process of cutting and having negative effect on kinematic segment elements. The latter consists of output shaft of reduction gear and gear drive from reduction gear to face-plate.

Assemblies of reverse feed of TRTs 38 U3.1 and TRTs 76 U3.1 end facers providing manual feed are made according the same construction diagram. It provides for possibility of movement in any of two possible directions of face-plate of end facers together with cutting tools set in its slides (tool holders) by means of interaction of rod of feed

assembly with face-plate rod. TTTs 660 U3.1 pipe cutter includes automatic feeding of cutting tools with the help of feed screw, on which tooth wheel of «star» type is installed. After face-plate has made one complete revolution, the tooth wheel moves for one tooth and is fixed in this position with the help of spring-loaded ball. As a result corresponding rotary motion of feed screw takes place, and, based on this, translational motion of the slider with cutting tool set on face-plate per one step of automatic feed. The condition for rotation of «star» type tooth wheel of transverse support per only one tooth from previous fixed position to the next is provided with the help of rotation lock, which is rigidly fixed to one of the stationary pipe cutter bodies.

Carried investigations on peculiarities of processes of preparation for welding of pipeline position butts and industrial experience determined that machining accuracy of pipe ends and groove edges of pipeline position butts, as well as cleanliness of treated surfaces, mainly depend on accuracy and reproducibility of alignment of end faces and pipe cutters on treated pipes. Analysis of possible structural solutions in equipment for preparation for welding showed that invariance of initial external positioning of models of this equipment (mainly end facers) is achieved in the case if their structure provides for presence of self-alignment mechanism. Following from this, technical solution* was proposed in process of development of domestic equipment for preparation to welding of pipeline position butts. According to it assembly for treatment of ends and edges consists of stationary head, including mechanism for positioning on pipe external surface, and stationary body with inside face-plate containing tool holders. Due to the presence of (at least two) fast-acting spring-loaded locks, for example of lever type, the stationary positioning mechanism has the possibility of fast connection with stationary body of the head or disconnection from this body. Besides, the head also includes a self-alignment mechanism, for example of collet type, which has rigid connection coaxial with longitudinal axis of treated pipe and longitudinal axis of positioning mechanics. Figure 4 shows the structural scheme of end facer built using proposed solution.

Company CHEZARA (Chernigov, Ukraine), based on technical documents developed by PWI REC WCPE, produced the pilot specimens of

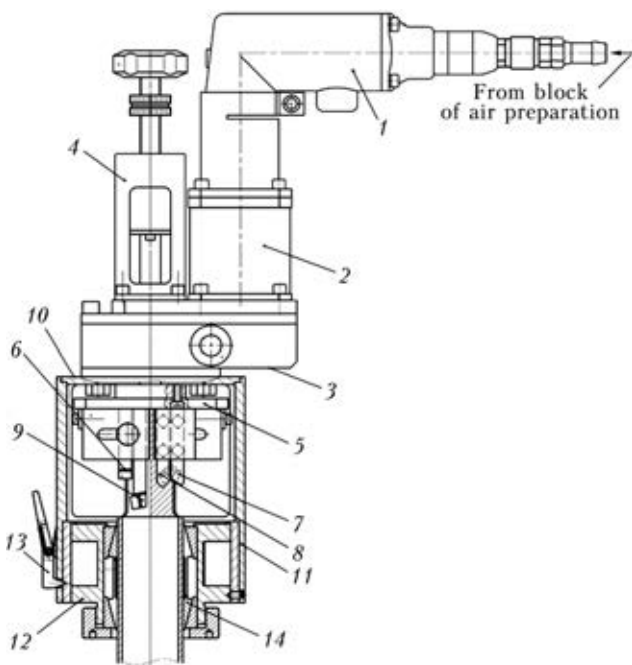


Figure 4. Structural scheme of end facer with self-alignment: 1 – drive unit (pneumoengine); 2 – reduction gear; 3 – stationary body; 4 – feeder; 5 – face-plate; 6–9 – side-facing and straight turning tools (for formation of inner and outer faces, respectively); 10 – head; 11 – stationary body of head; 12 – positioning mechanism; 13 – fast spring-loaded locks; 14 – self-alignment mechanism

* Lobanov L.M., Smolyakov V.K., Vodolazsky V.E., Makhlin N.M. Portable device for treatment of ends and edges of pipes at their preparation for welding. Pat. appl. UA 201503704 of 20.04.2015. Int. Cl. B23K 9/235 (2006.01).

Table 5. Main parameters and characteristics of pilot specimens of end facers and pipe cutter, and their analogues

Parameter or characteristic	Model				
	TRTs 38 U3.1	TRTs 76 U3.1	TTTs 660 U3.1	Mangust-2T (Russia)	PROTEM PUS40 (France)
Smallest outer diameter of treated pipe, mm	14	38	108	45	43
Largest outer diameter of treated pipe, mm	38	76	159	120	219
Largest wall thickness of treated pipe, mm	5	7	15	5	16
Length of boring of internal diameter of treated pipe, mm, not less than	10	15	20	No boring option	
Positioning	On pipe outer surface			Inner	
Method of cutting tool feed	Manual	Manual	Automatic	Manual	Manual
Cutting tool feed, mm/rev., not more than	0.20	0.15	0.10	0.20	0.20
Nominal frequency of face-plate rotation, rpm	110	100	60	70	25
Consumption of compressed air at idle running, m ³ /min, not more than	1.5	1.5	1.5	1.7	1.6
Overall dimension, mm, not more than	350×140×170	370×160×175	520×500×435	470×400×120	400×246×246
Weight with drive unit, kg, not more than	9.5	12.6	19.3	9.5	16.0

**Figure 5.** General view of pilot samples of TRTs 38 U3.1 and TRTs 76 U3.1 (on the left) end facers

end facers TRTs 38 U3.1 and TRTs 76 U3.1, and pipe cutter TTTs 660 U3.1, general view of which are given in Figures 5 and 6. Manufactured pilot specimens of equipment for preparation for welding of pipeline position butts were subjected to thorough investigations, including general-theoretical and functional ones. Technological investigations were carried out by REC WCPE together with specialists of «Atomremontservice» of «Energoatom». Table 5 gives the results of investigations carried with pilot specimens of end facers and pipe cutter, their parameters and characteristics.

Conclusions

1. Considered are the issues of effect on quality of welded joints of accuracy in preparation for welding of edges of parts of position butts in 14–159 mm diameter NPP pipelines from austenite and pearlite class steels. Ranges of optimum modes for treatment of ends and edges of these pipelines were determined as well as pecu-

**Figure 6.** General view of pilot specimen of TTTs 660 U3.1 pipe cutter

liarities of construction of equipment for preparation to welding of pipeline position butts were considered, and pilot specimens of such domestic equipment were manufactured and tested.

2. Results of testing of pilot specimens of end facers TRTs 38 U3.1 and TRTs 76 U3.1 and pipe cutter TTTs 660 U3.1 indicate that in comparison with the best foreign specimens of equipment for preparation to manual or automatic welding of parts of pipe position butts they can provide for:

- expansion of technological capabilities of equipment for preparation to welding of parts of position butts in steel pipelines;
- increase of efficiency of the processes of machining of steel pipeline position butts due to simplification of conditions for testing of internal geometry dimensions of treated pipes;
- simplification and reduction of prices on servicing of equipment for preparation for weld-



ing of parts of steel pipeline position butts due to maximum possible application in this equipment of domestic spare parts and materials and significant improvement of its reparability;

- not less than 1.5–2 times reduction of prime cost of these products;
- increase of quality and accuracy of preparation for welding, including automated one, of steel pipeline position butts.

Mentioned advantages of developed domestic equipment mainly relate to end facers and are received due to technical solutions concerning their positioning over external surfaces of treated pipes, providing the possibility of simultaneous facing, formation of external and internal faces and boring of inner diameter of these pipes as well as fast connection/disconnection of stationary mechanism for positioning of operating head with its stationary body.

3. Development, manufacture and testing of above-mentioned pilot specimens of end facers and pipe cutter and further mastering of their commercial production create backgrounds necessary for equipping the assembly and repair subdivisions and enterprises from power and other branches by state-of-the-art domestic equipment for preparation for welding of parts of steel pipeline position butts. This provides for elimination of one of the main factors preventing wide-spread implementation of finished as well as novel domestic technologies of automatic welding of pipeline position butts.

1. Cameron, I.R. (1987) *Nuclear reactors*. Moscow: Energoatomizdat.
2. (1990) *PN AE G-7-008-89*: Rules of arrangement and safety service of equipment and piping of nuclear power plants. Moscow: Energoatomizdat.
3. (1991) *PN AE G-7-009-90, PN AE G-7-010-90*: Equipment and piping of nuclear power plants. Welding and surfacing. Fundamentals. Moscow: Energoatomizdat.
4. Roshchin, V.V., Khavanov, V.A., Akulov, L.I. et al. (2002) Welding in mounting of equipment and metal structures of reactor plants. In: *Welding in nuclear*

industry and power engineering: Transact. of NIKIMT, Vol. 1, 81–118. Moscow: IzdatAT.

5. Grinenko, V.I., Roshchin, V.V., Khavanov, V.A. et al. (2008) To problem of automation of welding of mounting joints of nuclear power plant piping. *Tekhnologiya Mashinostroeniya*, **8**, 48–51.
6. Belkin, S.A., Shefel, V.V. (1985) Automatic argon-arc welding in mounting of nuclear power plant piping. *Energet. Stroitelstvo*, **11**, 43–46.
7. Bukarov, V.A. (2002) Technology of automatic arc shielded-gas welding. In: *Welding in nuclear industry and power engineering*: Transact. of NIKIMT, Vol. 1, 149–210. Moscow: IzdatAT.
8. Volkov, V.A. (2000) Special cutting equipment. *Tekhnologiya Mashinostroeniya*, **5**, 6–10.
9. Troitsky, V.A. (2012) *Visual and measuring control of metal structures and constructions*. Kiev: Feniks.
10. Makhlin, N.M., Korotynsky, A.E., Bogdanovsky, V.A. et al. (2011) Single- and multioperator systems for automatic welding of position butt joints of nuclear power plant piping. *The Paton Welding J.*, **11**, 28–36.
11. Makhlin, N.M., Korotynsky, O.E., Svyrydenko, A.O. (2013) Hardware and software complex for automatic welding of position butts of nuclear power plant piping. *Nauka ta Innovatsii*, **9(6)**, 31–45.
12. Makhlin, N.M., Korotynsky, A.E., Bogdanovsky, V.A. et al. (2004) Electronic controllers of welding current for multioperator welding systems. *Svarochn. Proizvodstvo*, **5**, 13–18.
13. Troitsky, V.A. (2006) *Compendium on quality control of welded joints*. Kiev: Feniks.
14. *Reference book of technologist-mechanician*, Vol. 2. Ed. by A.M. Dalsky et al. Moscow: Mashinostroenie-1.
15. <http://www.protem.fr/>
16. <http://www.polysoude.com/>
17. <http://www.arcmachines.com/>
18. <http://www.esab.com/>
19. <http://www.atlascopco.com>
20. <http://www.georgfischer.com>
21. <http://www.deprag.com>
22. <http://www.iscar.com>
23. <http://www.pkfppk.ru/>
24. Belousov, A.N., Chernyshov, G.G. (1977) Some problems of pipe butts preparation to welding. *Svarochn. Proizvodstvo*, **4**, 39–41.
25. <http://www.immerservice.ru/privod/pnevmodvigateli/>
26. Chernavsky, S.A., Snesarev, G.A., Kozintsev, B.S. et al. (1984) *Design of mechanical transmissions*: Manual for high technical schools. Moscow: Mashinostroenie.

Received 18.06.2015

AUTOVACUUM BRAZING IN REPAIR OF COPPER PANELS OF MCCB MOULDS

G.M. GRIGORENKO, A.L. PUZRIN, M.G. ATROSHENKO,
M.A. POLESHCHUK, A.V. SHEVTSOV and I.A. MOSSOKOVSKAYA

E.O. Paton Electric Welding Institute, NASU
11 Bozhenko Str., 03680, Kiev, Ukraine. E-mail: office@paton.kiev.ua

Using models the possibility of repair of worn-out flat panels of machines of continuous casting of billets (MCCB) moulds by autovacuum brazing of restoration copper layer was tested. The brazed joint was produced between two copper plates without defects in the form of pores and cracks. The tensile strength of copper brazed joint for separation between layers was investigated, and also the bend tests were performed. Thermal resistance of the brazed joint was evaluated. The obtained results allow the method of autovacuum brazing to be recommended for repair of flat panels of the moulds. 12 Ref., 6 Figures.

Keywords: *MCCB moulds, restoration repair, autovacuum brazing, seams, metallography, mechanical properties, thermal resistance*

At present the main amount of the melted steel is undergone casting in the machines of continuous casting of billets (MCCB). The molten steel is poured into special devices: water-cooled moulds, the inner cavity of which has a section, corresponding to the section of the future billet. Walls of the moulds, faced inwards, are manufactured of copper. Due to intensive dissipation of heat by the cooling water the molten metal is solidified on the inner wall of the mould. At the same time, steel crust, making an external surface of the billet being melted, is formed around the entire perimeter of its cavity. During the process of the billet withdrawal the hard steel crust is moved along the mould copper wall, thus leading to the non-uniform wear of the latter and formation of different long defects on it [1].

These defects are formed more intensively in melting out of rectangular-section billets in MCCB of a radial type. Moulds for melting of these billets are assembled of separate flat panels with a working wall of copper, alloyed by a small amount of silver or chromium. Area of some of them can reach one square meter [2].

For removal of defects the copper walls of mould panels should be subjected to periodical machining. The thinning of walls after multiple treatments causes the hazard of damage of water-cooling channels and coming out of order of the whole mould. Therefore, the task of restoration of the initial sizes of copper walls of the flat panels is urgent.

Electric arc surfacing of worn-out copper walls does not allow solving this problem as far

as at a local heating of large copper plates, possessing high heat conductivity, their non-admissible distortion, incapable to correction, is occurred [3].

A procedure was developed for deposition of a restoration layer of copper on copper plate by using the method of friction stir welding [4]. This method is rather efficient in repair of separate regions of mould walls, but its application on large surfaces requires also the additional measures for reducing distortion of the plates being repaired.

It is possible to avoid distortion of the mould walls by brazing-on of copper sheet of a required thickness to them over the entire surface. In this case the heating and cooling of the product occur uniformly in the whole volume, not causing its deformation.

To provide the effective operation of the MCCB mould with repaired copper walls, it is necessary to minimize an additional heat resistance during the brazing process, which is introduced by brazing alloy layer into the coefficient of heat transfer from the molten steel to the cooling water through a multilayer wall. This coefficient will be minimum at keeping the following conditions: it is necessary to have a defectless layer of a minimum thickness over all the surface of copper sheets being joined, and heat conductivity coefficient of the brazing alloy should be close to the appropriate copper coefficient.

Among all the known types of brazing the most quality joint of large-area surfaces is produced by the method of autovacuum brazing (AVB). The AVB technology is based on a spontaneous cleaning of metal surfaces from oxide films, forming an air-tight gap, and next its fill-

ing with a molten brazing alloy during the product heating for brazing. This process occurs due to diffusion of oxygen from the air-tight gap through an oxide film inside the hot metal. Here, an autonomous vacuum is formed in the gap. The fracture of oxide films in air-tight gap is started after reaching the vacuum of a definite degree. Time of cleaning of metal surfaces from oxide films can be significantly reduced by degassing of the air-tight gap before heating [5].

Using this method in industry under the conditions of «Azovmash» plant, the steel bimetal billets of up to 4 m² area are successfully manufactured [6]. However, there is no information in literature about AVB application for joining of copper sheets between each other.

The aim of the present work was in experimental verification of the possibility of producing the quality joint of copper sheets by AVB and application of this method for restoration of sizes of MCCB mould copper walls.

To guarantee the brazing quality at any region of joining of large-area flat products it is rational to use the AVB diagram at a horizontal position of the product being brazed. Here, brazing alloy in the form of a foil should be placed beforehand between the copper sheets over the whole area of contact. Experimental works were carried out by brazing of 80 × 80 mm packets.

The packets, prepared for brazing, were mounted into special cassettes, creating a closed volume (Figure 1). Material for manufacture of cassettes was a thin steel sheet, which at the brazing temperature provided the compression of the packet at atmospheric pressure uniformly over the entire surface. The packets were made of three layers: base metal simulating the mould wall, restoration layer and brazing alloy between

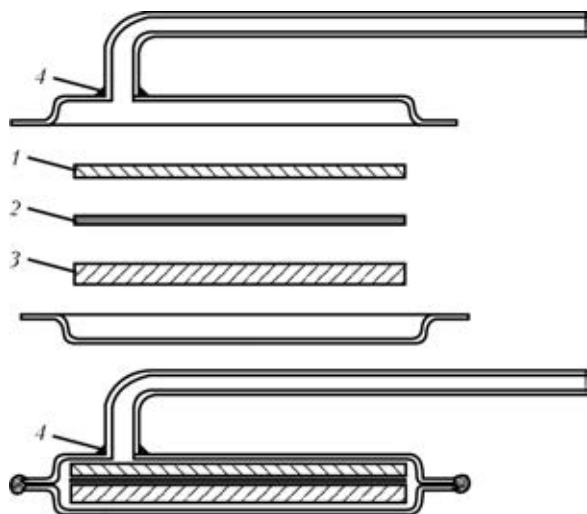


Figure 1. Assembly of cassette for AVB of specimens: 1 – restoration layer; 2 – brazing alloy; 3 – base metal; 4 – technological welds

them. As a base metal the 7 mm thick copper of M-1 grade was used, and the restoration layer of copper of the same grade had 2 mm thickness. The brazing alloy was a 0.2 mm thick foil, placed in two layers.

The filled cassettes were welded around the perimeter by argon-arc welding with a vacuum-tight weld. The branch pipe was welded-in to the cassette for degassing. The prepared cassettes were placed on the table in a muffle furnace, the branch pipe was taken outside, a forevacuum pump equipped with a manovacuummeter was connected to it.

Before brazing the rarefaction of $5 \cdot 10^{-2}$ mm Hg was created inside the cassette and the valve was shut. The furnace was heated up to the required temperature of brazing with 30 min isothermal holding. Cassettes were cooled together with the furnace. During the whole brazing process the rarefaction inside the cassette was controlled by a manovacuummeter. The brazed packets were cut into specimens for metallographic examinations and mechanical tests.

To select the optimum chemical composition of the brazing alloy, taking into account its temperature of melting and coefficient of heat conductivity, the experiments were carried out by using the foil of two different grades: brass L63 (brazing temperature is 950–960 °C) often used for copper brazing, and beryllium bronze BrB2 (temperature of melting is 1030–1040 °C) having a coefficient of heat conductivity close to that of copper.

During metallographic examinations of non-etched brazed joints on the specimens with brass L63 brazing alloy over the entire length of the seam [7] the elongated pores of length from 100 up to 330 μm and width from 20 up to 50 μm, located close to the seam middle, are observed. There are cracks between some pores (Figure 2, a). The formation of pores in the joint brazed using L63 alloy is explained by zinc evaporation during brazing [8]. The zinc evaporation is confirmed by increase in indications of the manovacuummeter at increase of the furnace temperature above 500 °C. At the same time, the place of joining of base metal and restoration layer is almost invisible, pores and cracks are absent on the non-etched section with BrB2 brazing alloy (Figure 2, b).

Figure 3 shows structures of brazed joints, revealed by etching in 50 % solution of nitric acid. On the specimen with L63 brazing alloy (Figure 3, a) there are common grains of seam with base metal and restoration layer. Thickness of brazing alloy layer is approximately 250 μm,

microhardness is 740–800 MPa. On the specimen, brazed with BrB2 alloy (Figure 3, *b*), the layer of brazing alloy of 90 μm thickness was observed having common grains with base metal on separate regions. On both sides of the seam, as well as in the seam itself, the non-metallic inclusions of a rounded shape of 5–60 μm size were observed. Microhardness of the brazing alloy layer is 1080 MPa, while that of base metal and restoration layer is 740 MPa. The smooth change in microhardness can be explained by the diffusion of beryllium of the brazing alloy inside the copper. The base metal and restoration layer of all the specimens have the structure, typical of the annealed copper.

Information about structure and sizes of the brazing alloy layer and diffusion zones, obtained during metallographic examinations, can be used for determination of their thermal resistance and evaluation of its contribution into coefficient of heat transfer from the molten metal to the cooling water through a multilayer wall of the mould. The thermal resistance of this wall R_{Σ} consists of a sum of resistances of layers included into it, each of which is determined by a quotient from division of layer thickness d (m) by coefficient of heat conductivity of its material λ ($\text{W}/(\text{m}\cdot^{\circ}\text{C})$). As applied to the copper wall of the mould, restored by brazing, the value of thermal resistance is determined by the following expression:

$$R_{\Sigma} = R_m + R_s + R_z = d_m/\lambda_m + d_s/\lambda_s + d_z/\lambda_z \text{ (}^{\circ}\text{C}\cdot\text{m}^2/\text{W}),$$

where R_m , R_s , R_z is the total thermal resistance of all the layers, respectively; $\lambda_m = 393 \text{ W}/(\text{m}\cdot^{\circ}\text{C})$; coefficient of heat conductivity of L63 brazing alloy layer is $\lambda = 105$, for BrB2 $\lambda = 352 \text{ W}/(\text{m}\cdot^{\circ}\text{C})$; R_z is the total thermal resistance of the diffusion zones, the heat conductivity of which can be accepted averaged between those of copper and brazing alloy [9].

The coefficients of heat conductivity of materials, used by us as brazing alloys, are the values of one order with coefficient of heat conductivity of copper. At the same time, the thicknesses of layer of the brazing alloy and diffusion zones, measured in tens or hundreds of microns, are by two-three orders lower than the total thick of copper layers, measured in tens of millimeters. Thus, the thermal resistance of the interlayer of brazing alloy and diffusion zones will be by the same two-three orders lower than the resistance of copper layers. Therefore, when calculating the thermal resistance of the restored copper wall of the mould the additional resistance, created by

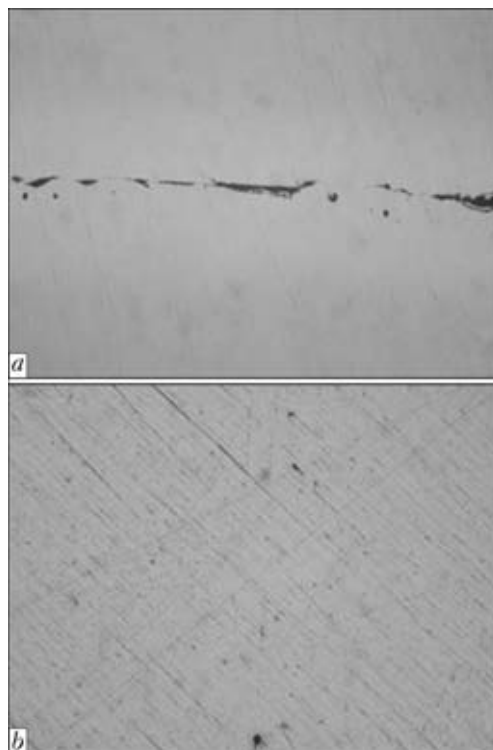


Figure 2. Structure ($\times 200$) of non-etched specimens after AVB of copper: *a* – L63; *b* – BrB2 brazing alloy

defectless brazed joint, produced by AVB method, can be not taken into account.

At the same time, the defects in the interlayer of the brazing alloy in the form of pores, cracks, and lack of brazing in particular, can create definite disturbances to the heat flow through a multilayer wall. At concentration of such defects in

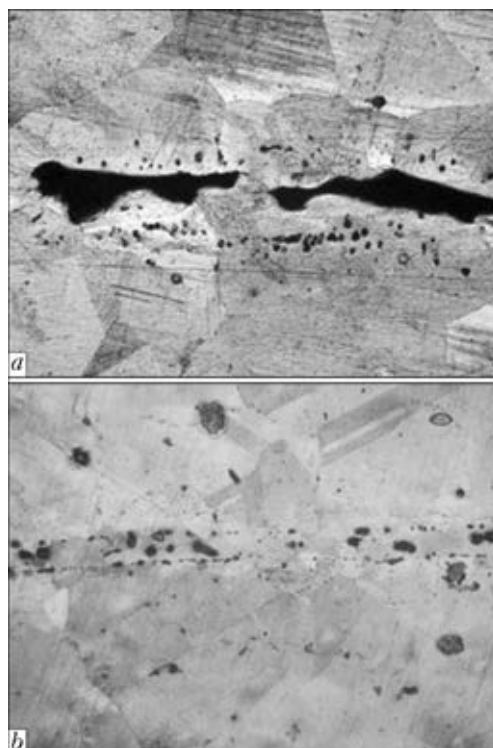


Figure 3. Structure ($\times 200$) of copper joints produced by AVB method: *a* – L63; *b* – BrB2 brazing alloy

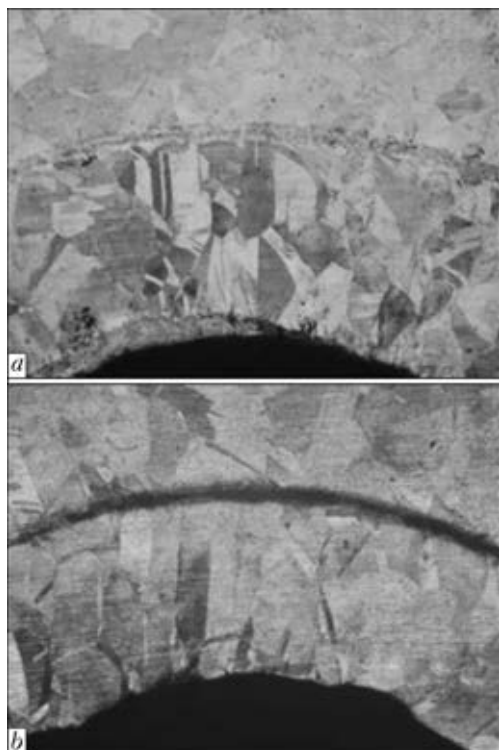


Figure 4. Microsections ($\times 25$) of bending places of brazed joints: *a* – L63; *b* – BrB2 brazing alloy

local area of the brazed joint a remarkable reduction in heat dissipation from the restoration layer may occur and, as a consequence, the increase in its temperature at this place. At a definite value of the heat flow from the molten metal to the mould multilayer wall the growth in temperature of the restoration layer can lead to its deformation at that place and even to separation from the base metal. Thus, during the restoration repair of copper walls of the moulds it is necessary to provide technologically defect-free brazing.

During operation of the mould with copper walls, repaired by AVB method, the seam, connecting the base metal and restoration layer, should have the strength, preventing the separation of the latter in effect of forces of shear and bending. In addition, to decrease the wear the surface of the restored layer should have the hard-

ness close to that of copper surface before the repair. The specimens were tested for separation of the restoration layer and bending of the brazed joint, and also the microhardness of surface of the restoration layer after brazing was measured.

For bending test across the entire surface of the brazed joint the special specimens of 80×10 mm size were cut out, which were bent for 90° angle by restoration layer inside. Separations of the restoration layer from the base metal on the specimens using brazing alloys L63 and BrB2 were not observed (Figure 4).

The mechanical properties of the produced brazed joints were evaluated by the tensile pull strength between the layers. The tests like those are not regulated by the GOST, therefore, they were performed using scheme, presented in Figure 5, *a*, on specimens, the sizes of which are indicated in Figure 5, *b* [10].

For verification and comparison of results, obtained according to the above-mentioned scheme, the monolithic specimens of the same sizes manufactured from the same copper sheet, which was used for brazing, were tested. The tensile pull strength of the monolithic specimen was 450 MPa, that corresponds to that of the wrought copper M1 [11]. Thus, the scheme of tests, used by us, can be considered acceptable.

The average value of tensile pull strength of specimens, brazed by brass L63, was 240 MPa, and that of specimens brazed by bronze BrB2 was 530 MPa. The lower value of the tensile pull strength of specimens brazed by L63, as compared with monolithic specimens, is explained by the pores presence in the seam. At the same time, the higher values of tensile pull strength, obtained in brazing of copper by bronze BrB2, can be explained by the absence of defects in the brazed joint, having the common grains with copper, and also by the presence of diffusion zone, hardened by beryllium, in the copper.

By analyzing the results of metallographic investigations, mechanical tests and evaluation of

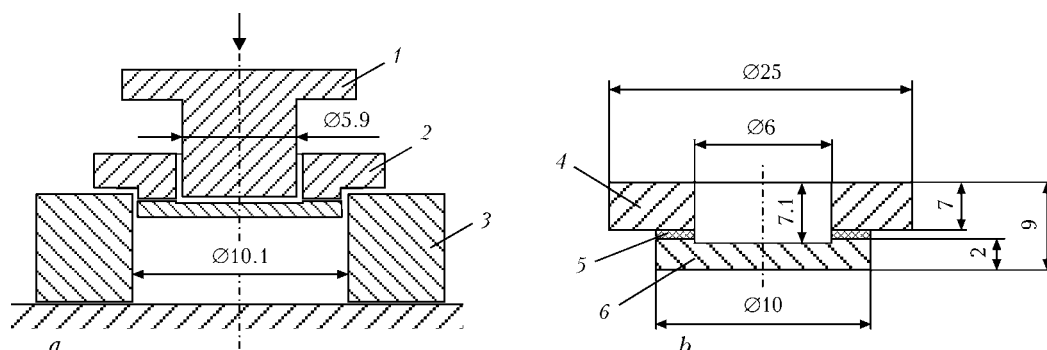


Figure 5. Scheme of pull tests (*a*) of brazed joint specimen (*b*): 1 – punch; 2 – specimen; 3 – matrix; 4 – base metal; 5 – seam; 6 – restoration layer

values of thermal interlayer of brazing alloys it is possible to recommend the brazing alloy of beryllium bronze BrB2 in the form of foil for restoration repair by AVB method of flat panels of the MCCB moulds.

Due to change in copper structure during heating for brazing, the hardness of base metal and restoration layer before and after AVB were determined. The initial values of copper hardness were in the ranges of 579–606 MPa, that corresponds to the hardness of the wrought and annealed copper [11]. After AVB the copper hardness decreased negligibly to 530–550 MPa.

The resistance of MCCB moulds, consisting of flat copper panels, does not often exceed 100 melts [2], while the resistance of moulds with protective coating – thin layer of material having the higher strength, is 10 times increased [12]. In this connection it is desirable to deposit the protective coating on the copper surface faced inside the mould. This coating may be a thin stainless steel sheet, brazed-on to the restoration layer of copper. The prior experience (Figure 6) shows a feasibility of producing for single heating the multilayer brazed joint, including restoration layer of copper and wear-resistant coating of thin stainless steel sheet.

Conclusion

It was shown experimentally that AVB method can be applied for producing the quality joint of copper sheets of large area in plane and is challenging in repair of panels of MCCB moulds. The defect-free brazed joints with high mechanical characteristics were produced by AVB method using foil of bronze BrB2 as the brazing alloy. Due to small thickness of the interlayer and high heat conductivity of the brazing alloy, its thermal resistance can be neglected at thermal design of the mould. The possibility of deposition of the protective coating simultaneously with deposi-

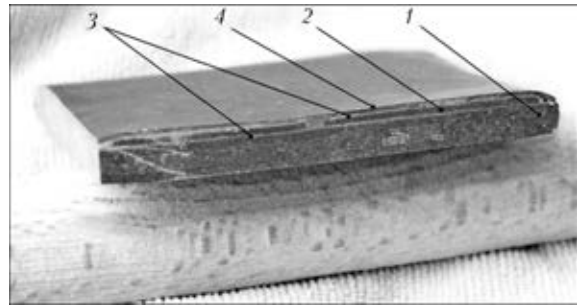


Figure 6. Multilayer joint produced per one heating by AVB method: 1 – base layer; 2 – restoration layer; 3 – seams; 4 – wear-resistant coating

tion of the restoration layer in the mould repair is shown experimentally.

1. Evteev, D.P., Kolybalov, I.N. (1984) *Continuous casting of steel*. Moscow: Metallurgiya.
2. Markushin, A.A., Kuklev, A.V., Ajzin, Yu.M. et al. (2005) *Radial slab mold with slot channels and nickel coating of walls*, 38–41. Moscow: Metallurg.
3. Abramovich, V.R. (1988) *Fusion welding of copper and alloys on its base*. Moscow: Mashinostroenie.
4. Nikityuk, Yu.N., Grigorenko, G.M., Zelenin, V.I. et al. (2013) Technology of reconditioning repair of slab molds of MCCB with friction stir welding method. *Sovr. Elektrometallurgiya*, **3**, 51–55.
5. Puzrin, L.G., Bojko, G.A., Atroshenko, M.G. (1975) *Autovacuum brazing*. Kiev: Znanie.
6. Puzrin, L.G., Atroshenko, M.G., Peshcherin, I.G. et al. (1984) Autovacuum brazing of ultra-thick wall vessels of up to hundred tons mass. In: *Problems of welding and special electrometallurgy*, 76–77. Kiev: PWI.
7. GOST 17325–79: Soldering and tinning. Main terms.
8. (1975) *Reference book on soldering*. Ed. by S.N. Lotsmanov et al. Moscow: Mashinostroenie.
9. Yong, H. (1979) *Basic formulae and data on heat exchange for engineers*. Moscow: Atomizdat.
10. Mardyan, M.G., Ryabchikov, E.A., Epshtejn, G.N. (1979) Procedure for determination of cohesive strength of bimetal layers. *Zavod. Laboratoriya*, **8**, 757–759.
11. Keloglu, Yu.P., Zakhariyevich, K.M., Kartashevskaya, M.A. (1977) *Metals and alloys*: Refer. Book.
12. Masato, T. (2009) Molds of machines of continuous steel casting of Mashima Kosan. In: *Proc. of Int. Sci.-Pract. Seminar on Electrocladding and Thermal Spraying* (Ekaterinburg, 2009), 1–19.

Received 16.04.2015

MANUFACTURING LARGE-SIZED BEDS BY CONSUMABLE-NOZZLE ELECTROSLAG WELDING

K.P. SHAPOVALOV¹, V.A. BELINSKY¹, S.N. KOSINOV¹, S.N. LITVINENKO¹,
K.A. YUSHCHENKO², I.I. LYCHKO² and S.M. KOZULIN²

¹Company «NKMZ»

4 Ordzhonikidzhe Str., Kramatorsk, Donetsk reg., Ukraine

²E.O. Paton Electric Welding Institute, NASU

11 Bozhenko Str., 03680, Kiev, Ukraine. E-mail: office@paton.kiev.ua

PWI in collaboration with Novo-Kramatorsk Machine-Building Works (NKMZ company) continues improving electroslag welding technology. This work provides a description of the technology of consumable-nozzle electroslag welding in manufacture of large-sized beds with butts of 420–460 × 2200–2380 and 940–1120 × 1040–1250 mm cross-section. Machine time shortening almost 2 times was achieved. Welded joints of large-sized cast-welded billets of beds for high-capacity mills are characterized by high quality. 8 Ref., 5 Figures.

Keywords: *electroslag welding, consumable nozzle, large-sized beds, heating, intermediate tempering, machine time reduction*

Electroslag welding (ESW) of large-sized metal billets is the most effective and widely applied welding process in manufacturing load-carrying elements of high-capacity machines and installations of mining, metallurgical and other sectors of heavy mechanical engineering [1]. First examples of manufacturing such metal structures of bed type in cast-welded variant were successfully implemented already at the start of ESW introduction at Novo-Kramatorsk Machine-Building Works (NKMZ) [2]. Scale breaker bed was made of four elements (St25L steel, 470 mm thickness of edges being welded) joined by ESW with wire electrodes. Butt joints were welded by one multielectrode machine of A-395 type in a certain sequence. After welding the bed plate was subjected to total high-temperature treatment

(HTT) (normalizing with tempering). Further on technology and technique of fabrication of metal structures of this type was improved in the directions of application of consumable nozzle (CN) ESW process and method of metered counteraction to welding deformations [3, 4].

In NKMZ welding production the high engineering level of manufacturing cast-welded or roll-welded massive parts is ensured, primarily, due to availability of modern welding equipment and required technological fixtures [5, 6], as well as application of high-efficient technological measures developed on the basis of electroslag process investigations [7].

Welded beds are designed to have an O-shape, consisting of individual elements connected predominantly by CN ESW. Bed of 50–62 t weight, consisting of two elements, was welded by one common weld by the schematic shown in Figure 1. Welding of beds of 205–270 t weight,

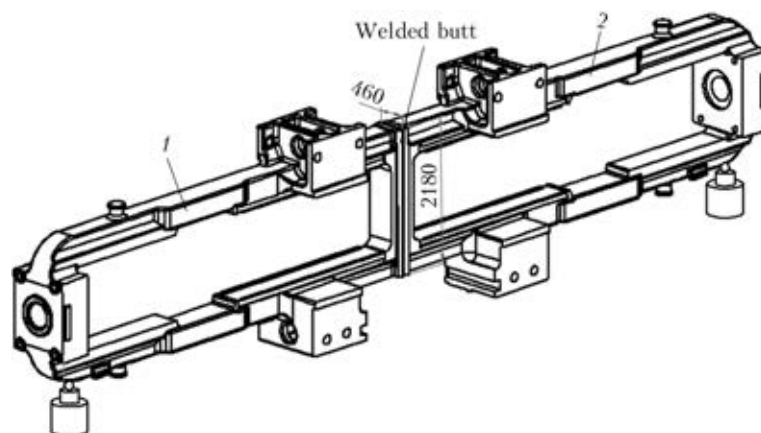


Figure 1. Schematic of assembly of bed elements for single-weld welding: 1 – left; 2 – right element

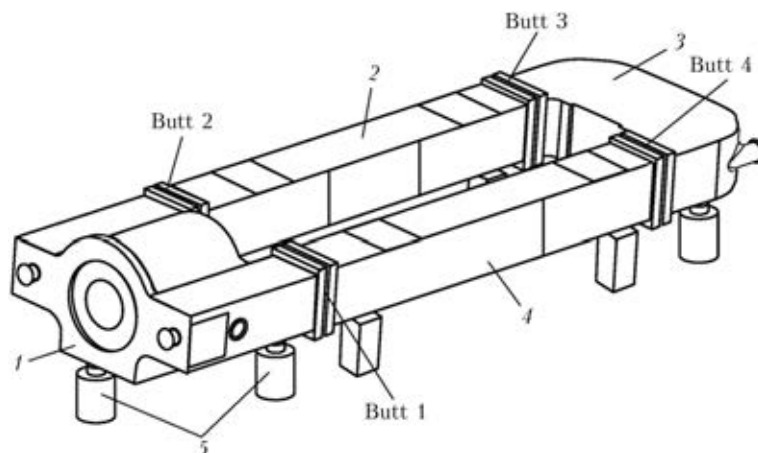


Figure 2. Schematic of assembly of bed elements with four welds: 1 – lower part; 2, 4 – middle inserts; 3 – upper part; 5 – supports

consisting of four elements, is usually performed in two steps: on two symmetrically located butts simultaneously (Figure 2).

Equipment available in the assembly-welding section and creative improvement of earlier developed technological measures at realization of specific CN ESW technologies for shop conditions and product range enabled organizing efficient production of such welded metal structures.

Modern technology and technique for CN ESW of cast-welded beds of different modifications of mill stands was successfully implemented in G.Z. Voloshkevich shop section of thick metal ESW in manufacture of rolling equipment within the framework of a number of large-scale projects on reconstruction of plate mills «2800» of Alchevsk, «2850» of Asha, «2500» of Magnitogorsk Metal Works and at construction of «4300» mill in the town of Rourkela, India.

Guarantee of electroslag process running without forced shutdowns, continuous monitoring of the main parameters of welding mode and subsequent HTT provides the required quality of welded joint metal, and precise allowance for

anticipated deformations ensures high accuracy of geometrical dimensions of bed structure after welding and, hence, minimum allowances for final machining. Continuous monitoring of welding modes is indicative of high reliability of maintaining and monitoring the selected parameters: not a single case of forced shutdown of the welding process has been recorded. Displacement of elements being welded was determined by measurement of the distance between center marks made on the base on top and bottom of the butts at 200 mm on both sides. Proceeding from the results of ultrasonic testing of welded joint metal conducted after HTT, all the beds were found to be fit for further processing.

Unique performance characteristics of the machine for CN ESW of thick metal [5, 6] enabled welding of butt joints of two separate beds (Figure 3) by the schematic in Figure 1 and of two butt joints of the same bed (Figure 4) by the schematic in Figure 2 simultaneously, thus reducing machine time of welding practically 2 times. Altogether four beds were made by the schematic in Figure 1 (butts of 420–460 × 2200–

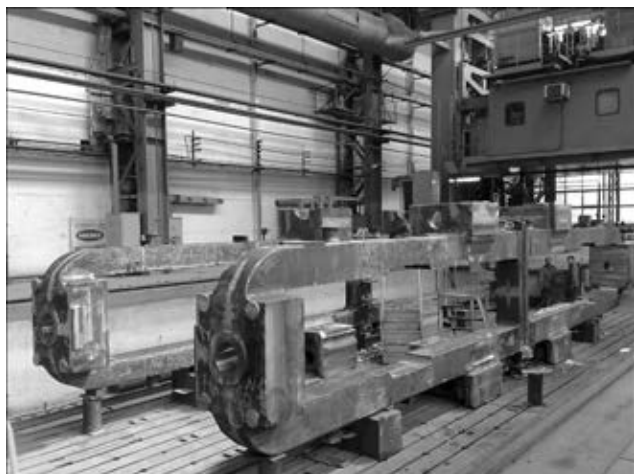


Figure 3. Simultaneous welding of two beds by the schematic in Figure 1 (work in progress)



Figure 4. Electroslag welding of two welds by the schematic in Figure 2 (work in progress)

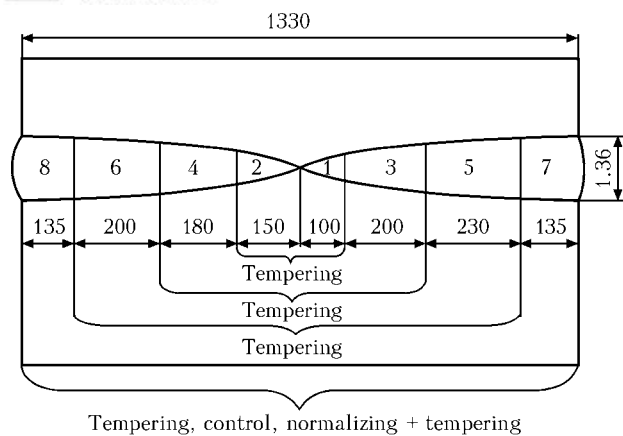


Figure 5. Sequence of groove filling in the butt and heat treatment of welds in manufacture of the bed with application of automatic SAW [8]

2380 mm cross-section) and 14 beds – by the schematic in Figure 2 (butts of 940–1120 × 1040–1250 mm cross-section). Duration of assembly-welding operations for variant of bed with one weld was 4 days, and for the bed with four welds it was 6 days.

In recent years, some specialists sometimes have had doubts about the priority of ESW application in manufacturing thick metal structures, referring to other welding processes as, for instance, narrow-gap automatic arc welding (AAW) or electron beam welding. Indeed, these processes allow welding up rather large thicknesses, but they are so far applied most often as an exception.

For comparison, we will give some data on manufacturing of a bed of «5000» mill with application of narrow-gap AAW. Bed elements were joined by six welds: a) four welds with butt cross-section of 1060 × 1060 mm; b) two welds of 1060 × 1330 mm cross-section [8]. Butt joint shape and sequence of weld filling are shown in Figure 5. Welding up of four welds (a) was performed simultaneously by four ESAB welding machines, and then welding up of two welds was performed (b). Technology of butt filling with welding wire envisaged the following: preheating and concurrent heating of each butt up to 150–200 °C (at ESW only heating of the butt beginning is performed); successive deposition of

welds in the gap individual sections; bed turning over to fill the opposite section; intermediate tempering of each two opposite sections (see Figure 5) at 580–600 °C. Welds were made with application of a special high-capacity turnover; device for preheating and concurrent heating; other fixture elements to ensure the bed geometrical parameters; immediate intermediate tempering after welding each two opposite sections. Technology of narrow-gap AAW does not have any advantages over ESW in any of the production cycle parameters. For instance, amount of deposited metal for six welds is equal to more than 7000 kg (2300 kg at ESW), while machine time is incomparable at all.

Thus, technique and technology of production of cast-welded large-sized billets for beds of high-capacity rolling mills, based on scientifically grounded application of CN ESW techniques, enables the plant to produce high-efficient competitive products.

1. (1980) *Electroslag welding and cladding*. Ed. by B.E. Paton. Moscow: Mashinostroenie.
2. Sterenbogen, Yu.A., Pogorelov, V.S. (1956) Electroslag welding of body of scale breaker. *Avtomatich. Svarka*, 4, 108–114.
3. Paton, B.E., Dudko, D.A., Yushchenko, K.A. et al. (1987) Electroslag welding: Results, problems and prospects of development. *Ibid.*, 5, 32–42.
4. Sushchuk-Slyusarenko, I.I., Lychko, I.I., Koval, I.M. et al. (1968) Producing exact sizes of large-dimensioned bodies in electroslag welding. *Ibid.*, 11, 55–58.
5. Nevidomsky, V.A., Krasilnikov, S.G., Panin, A.D. et al. (2002) New machine for electroslag welding of large parts at JSC «NKMBF». *The Paton Welding J.*, 2, 49–51.
6. Litvinenko, S.N., Shapovalov, K.P., Savchenko, I.S. et al. (2013) Systems of process control and monitoring of conditions – the important factors of quality assurance in electroslag welding of thick metal. *Ibid.*, 12, 39–41.
7. Yushchenko, K.A., Lychko, I.I., Sushchuk-Slyusarenko, I.I. (1999) Effective techniques of electroslag welding and prospects for their application in welding production. In: *Welding and Surfacing Rev.*, Vol. 12, 1–108.
8. Karzov, G.P., Galyatkin, S.N., Varovin, A.Ya. et al. (2009) Automatic submerged-arc welding of elements of superthick structures. *Voprosy Materialovedeniya*, 3, 357–371.

Received 28.05.2015

NOISE CHARACTERISTICS DURING WELDING IN ARGON-CONTAINING SHIELDING GASES

O.G. LEVCHENKO¹, V.A. KULESHOV¹ and A.Yu. ARLAMOV²

¹E.O. Paton Electric Welding Institute, NASU

11 Bozhenko Str., 03680, Kiev, Ukraine. E-mail: office@paton.kiev.ua

²NTUU «Kyiv Polytechnic Institute»

6/2 Dashavskaya Str., 03056, Kiev, Ukraine

The aim of this work was to measure the characteristics of acoustic noise at the workplace during manual TIG welding in argon and semiautomatic welding in Ar + CO₂. Welding was carried out inside the welding metal cabin of 1.8 m height, 2.0 m width and 2.4 m depth. The noise parameters were measured using the integrated sound level meter of the first class of accuracy. The point of measurement at the welder's workplace was located at the distance of 0.55 m from welding arc. A single measurement was conducted for about 60 s at the running ventilation unit. It was established that in TIG welding the value of equivalent sound level at the welder's workplace in the wide range of rated values of current $I = 45\text{--}210$ A does not exceed 64 dBA, that is significantly lower than the sanitary-hygienic standard of 80 dBA and is comparable with the level of 57 dBA of the background noise. In semiautomatic welding in Ar + CO₂ the noise level at the welder's workplace in the range of rated values of current $I = 80\text{--}250$ A exceeds MAL and reaches 96 dBA. The limit of safe working area as to noise was established at the distance of 2 m from the place of welding. The data of this work can be used for sanitary-hygienic assessment of noise episodes of specific welding processes in shielding gases. 6 Ref., 3 Tables, 5 Figures.

Keywords: *welding in shielding gas, argon, mixture of Ar + CO₂, acoustic noise, characteristics*

In this paper, which is a continuation of work [1], the results of investigations of noise characteristics at the welder's workplace are given during welding in shielding gases, namely in manual TIG welding and semiautomatic welding.

Manual TIG welding. Welding was performed in the KEMPPPI OY argon-arc DC welding machine Master 2200 (Finland) inside the welding metal cabin of 1.8 m height, 2 m width and 2.4 m depth. The steel (St3) plates of 12 mm thickness being welded were placed on the table and welded in argon using tungsten electrode of 2.4 mm diameter.

The noise parameters were measured using the «Bruel & Kjaer» integrated sound level meter (model 2230) of the first class of accuracy, whose functional and technical characteristics meet the requirements of interstate standard GOST 17187–2010 [2]. The measuring point was situated at the arm's length distance (0.55 m) from the welding arc.

The noise measuring at a typical workplace was conducted in accordance with the requirements of DSN 3.3.6.037–99 [3]. In all the measurements the noise levels with frequency correction A (general noise level) were recorded, which are required for sanitary-hygienic assessment: equivalent noise level L_{eq} , maximum $L_{op\ max}$ and minimum $L_{op\ min}$ sound pressure levels.

A single measurement was carried out for about 60 s at the operating ventilation unit. The characteristics of background noise L_{back} produced by the auxiliary equipment (current generator, ventilation unit) and other sources of noise located in welding shop, are the following, dBA: $L_{eq} = 56.5$; $L_{op\ max} = 72.7$; $L_{op\ min} = 53.3$.

The data on the noise values generated during welding at the welder's workplace in the range of rated welding current values of 45–210 A, are given in Table 1.

Let us define the noise value L_w generated directly by welding process. The value of the measured noise L_{meas} consists of two parts: background noise L_{back} and welding noise L_w . Using the principle of additivity of noise energy flows (intensities) at the point of measurement, it can be shown [4] that L_w value is determined by expression

$$L_w = L_{back} + 10 \lg (10^{(L_{meas} - L_{back})/10} - 1). \quad (1)$$

Hence, it follows that if the value of measured noise is significantly higher than the value of background noise, as far as the difference $L_{meas} - L_{back} \geq 10$, then it can be assumed with a high degree of accuracy (within the measurement error

Table 1. Noise level L_{meas} measured at the welder's workplace

I_w , A	L_{eq} , dBA	$L_{op\ max}$, dBA	$L_{op\ min}$, dBA
45	59.6	71.6	54.9
100	60.2	65.4	57.2
150	63.1	68.2	57.5
210	65.9	80.0	57.2

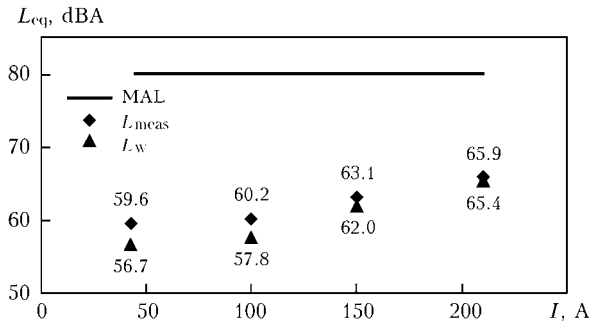


Figure 1. Dependence of noise levels L_{meas} and L_w on welding current at the welder's workplace

of ± 1 dB) that $L_{meas} \approx L_w$. As far as in this case this condition is not fulfilled, let us calculate the L_w value according to formula (1), using the data from Table 1. The noise level L_w at the welder's workplace at $I_w = 45$ A corresponds to 56.7, at 100 A – 57.8, at 150 A – 62.0 and at 210 A – 65.4 dBA.

Graphically, the values of L_{eq} are given in Figure 1.

It can be seen that the noise, produced by welding process, is much lower than the maximum admissible level (MAL) equal to 80 dBA [3]. The noise naturally decreases at decrease in current as the release of energy in the air drops also.

A negligible change in the noise level was observed in a rather wide range of changes in rated values of current: the growth in current by 4.7 times caused the noise amplification only by 12 %. The contribution of background noise to the general noise generation increases at decrease in welding current and is comparable to the value of welding noise. Thus, TIG welding does not require the carrying out of protective anti-noise measurements.

Semiautomatic welding in Ar + CO₂. Semiautomatic welding of steel (St3) plates of 4 mm thickness was carried out in the mixture of Ar + 18 % CO₂ using copper-plated wire Sv-08G2S of 1.2 mm diameter. In welding the «Lincoln Electric» inverter Invertec V350-PRO (USA) was used. The equipment for wire feed was «Lincoln Electric» LP-72.

The conditions of welding and measurement procedure were similar to those used in the previous case. The data measurements of the values

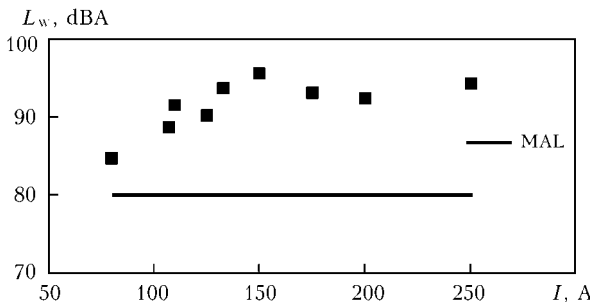


Figure 2. Level of welding noise at the workplace during semiautomatic welding in Ar + CO₂ mixture

Table 2. Measured noise level L_{meas} and calculated values of welding noise L_w at the welder's workplace

I_w, A	L_{meas}, dBA			L_w, dBA
	L_{eq}	$(L_{op})_{max}$	$(L_{op})_{min}$	L_{eq}
80	84.9	91.9	75.6	84.7
107	88.7	93.6	81.6	88.6
110	91.5	96.0	84.2	91.5
125	90.2	95.6	85.6	90.1
133	93.6	96.5	88.6	93.6
150	95.5	98.6	81.8	95.5
175	93.1	97.4	78.0	93.1
200	92.4	97.1	76.2	92.4
250	94.2	98.0	75.6	94.2

L_{meas} and L_w are given in Table 2. The level of background noise L_{back} at the welder's workplace is the following, dBA: $L_{eq} = 71.1$; $L_{op\ max} = 84.7$; $L_{op\ min} = 64.1$.

Graphically, the data of measurement values are given in Figure 2.

The measurement results show a significant excess in the MAL value, especially at the intensive welding modes. At the same time, two areas of dependence of the noise level on welding current are observed, qualitatively different from each other. At low currents in the range of 80–150 A the noise is amplified, but at further growth of welding current the noise level falls. This is explained by decrease in the level of acoustic emission due to reduction of arc length observed at high values of current during «submerged arc» welding mode [5].

Let us note the linear character of the dependence in the area of noise level growth, which is indicated by a sufficiently high square value of linear correlation $R^2 = 0.9$ (Figure 3). In the specified range a negligible noise amplification of approximately by 11 % is recorded at twice increase in current.

To determine the safe working area as to its noise level for the auxiliary personnel, the measurements of noise level at different distances from the source of noise were carried out. The data of noise level measurements at the distance from welding arc of 1, 1.5 and 2 m are given in Table 3.

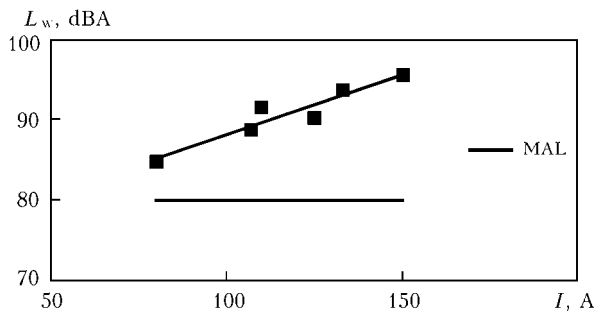


Figure 3. Level of welding noise at the workplace during semiautomatic welding in Ar + CO₂ in the linear region of noise growth

Table 3. Noise level L_{meas} at various distance from the welding arc

$I_w, \text{ A}$	$L_{\text{meas}}, \text{ dBA}$		
	L_{eq}	$L_{\text{op max}}$	$L_{\text{op min}}$
1 m			
80	83.3	92.9	74.6
107	84.8	92.0	81.7
125	85.7	92.0	84.7
133	86.1	92.7	85.2
1.5 m			
80	81.3	90.8	72.0
107	81.9	91.4	71.7
125	82.3	91.7	72.4
133	82.2	91.6	72.9
2 m			
80	78.1	87.5	70.8
107	78.6	87.9	70.5
125	79.1	88.1	71.4
133	79.0	88.0	71.8

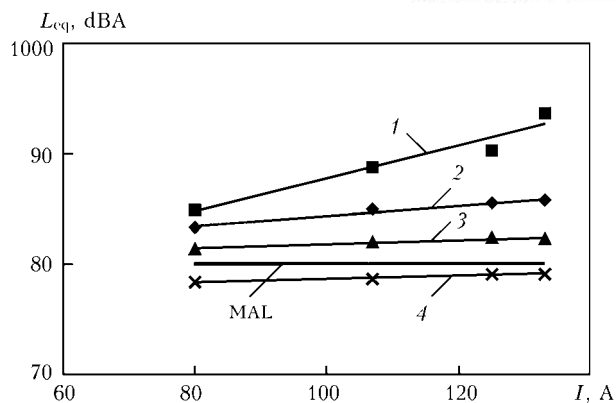
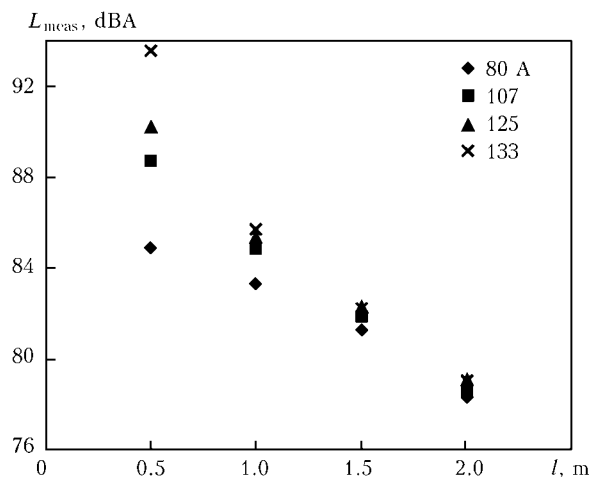
Using the means of data analysis MS Excel, it can be shown that the obtained data are well approximated by linear dependencies, which is confirmed by rather high square values of linear correlation R^2 lying in the range of 0.92–0.97. Let us note that linear dependence between the noise level and the value of welding current is also characteristic for manual arc welding using coated electrodes [1]. Graphically, the measurements data and their linear trends are illustrated in Figure 4. At removal from the welding place the noise level is reduced and already at the distance of 2 m its value is getting lower than MAL. Thus, the limit of the safe working area as to noise is in the range of distances from welding arc of 1.5–2.0 m.

At large distances from the source of noise the measured values of noise level slightly depend on welding mode and, in fact, due to scattering of sound waves the noise level is reduced down to background level (Figure 5).

As the level of noise, generated at the workplace, is much higher than MAL, it is necessary to use protective anti-noise measurements to reduce the impact of noise on welder [6], for example, to provide him with appropriate means of individual protection, or to reduce his working hours, according to [3]. We should also note that the personnel staying close to the place of such welding works (but not closer than 2 m) does not require protection.

Conclusions

1. In manual TIG welding the noise level at the welder's workplace in the wide range of rated values of welding current (45–210 A) does not exceed 64 dBA, which is much lower than the

**Figure 4.** Levels of measured noise during semiautomatic welding in shielding gas at distance of 0.55 (1), 1.0 (2), 1.5 (3) and 2.0 (4) m from the welding place**Figure 5.** Dependence of noise L_{meas} on distance from the welding arc at different values of current

established sanitary-hygienic standard (MAL = 80 dBA) and is comparable to the background noise level of 57 dBA.

2. In semiautomatic welding in Ar + CO₂ the noise level at the welder's workplace in the range of rated values of current (80–250 A) exceeds MAL and reaches 96 dBA. With increase in welding current from 80 to 150 A the noise is amplified, and the further increase in current leads to damping of noise due to immersion of arc into the weld pool. The working area safe as to noise is at distance of 1.5–2.0 m from the welding arc.

- Levchenko, O.G., Kuleshov, V.A., Arlamov, A.Yu. (2014) Sanitary-hygienic evaluation of noise in manual arc welding with covered electrodes. *The Paton Welding J.*, **9**, 45–48.
- GOST 17187–2010: Noise dosimeters. Pt 1: Technical requirements. Introd. 01.07.2012.
- DSN 3.3.6.037–99: Sanitary norms of industrial noise, ultrasound and infrasound. Introd. 01.12.1999.
- Grinchenko, V.T., Vovk, Sh.V., Matsipura, V.T. (2007) *Principles of acoustics*. Kyiv: Naukova Dumka.
- Volchenko, V.N., Yampolsky, V.M., Vinokurov, V.A. et al. (1988) *Theory of welding processes*. Moscow: Vysshaya Shkola.
- Levchenko, O.G., Kuleshov, V.A. (2013) Industrial noises. Pt 3. *Svarshchik*, **4**, 34–39.

Received 13.05.2015

PATON PUBLISHING HOUSE

www.patonpublishinghouse.com

SUBSCRIPTION

The Paton
WELDING JOURNAL

**АВТОМАТИЧЕСКАЯ
СВАРКА**

«The Paton Welding Journal» is Published Monthly Since 2000 in English, ISSN 0957-798X.

«Avtomaticheskaya Svarka» Journal (Automatic Welding) is Published Monthly Since 1948 in Russian, ISSN 005-111X.

«The Paton Welding Journal» is Cover-to-Cover Translation of Avtomaticheskaya Svarka» Journal into English.

If You are interested in making subscription directly via Editorial Board, fill, please, the coupon and send application by Fax or E-mail.

The cost of annual subscription via Editorial Board is \$348 for «The Paton Welding Journal» and \$180 for «Avtomaticheskaya Svarka» Journal.

«The Paton Welding Journal» can be also subscribed worldwide from catalogues subscription agency EBSO.

SUBSCRIPTION COUPON

Address for journal delivery _____

Term of subscription since _____

20

till _____

20

Name, initials _____

Affiliation _____

Position _____

Tel., Fax, E-mail _____

We offer the subscription all issues of the Journal in pdf format, starting from 2009.

The archives for 2009–2012 are free of charge on www.patonpublishinghouse.com site.



ADVERTISEMENT

in «Avtomaticheskaya Svarka» and «The Paton Welding Journal»

External cover, fully-colored:

First page of cover
(190×190 mm) – \$700
Second page of cover
(200×290 mm) – \$550
Third page of cover
(200×290 mm) – \$500
Fourth page of cover
(200×290 mm) – \$600

Internal cover, fully-colored:

First/second/third/fourth page
of cover (200×290 mm) – \$400

Internal insert:

Fully-colored (200×290 mm) –
\$340
Fully-colored (double page A3)
(400×290 mm) – \$500

• Article in the form of advertising
is 50 % of the cost of advertising
area

• When the sum of advertising con-
tracts exceeds \$1001, a flexible sys-
tem of discounts is envisaged

**Size of journal after cutting is
200×290 mm**

Editorial Board of Journal «Avtomaticheskaya Svarka» and «The Paton Welding Journal»

E.O. Paton Electric Welding Institute of the NAS of Ukraine

International Association «Welding»

11, Bozhenko Str., 03680, Kyiv, Ukraine

Tel.: (38044) 200 60 16, 200 82 77; Fax: (38044) 200 82 77, 200 81 45

E-mail: journal@paton.kiev.ua; www.patonpublishinghouse.com